D01 Award E17PC00011

BSEE Oil Spill Preparedness Division: Improved Oil Recovery Efficiency Sensor – Final Report

Prepared by:
Battelle Memorial Institute
505 King Avenue
Columbus, Ohio 43201-2696

Technical POC:
Slawomir Winecki, Ph.D.
E-mail: wineckis@battelle.org
Phone: (614) 424 – 4154
Battelle OPP204256

Submitted to:
U.S. Department of the Interior
Bureau of Safety and Environmental Enforcement
Acquisition Operations Branch
45600 Woodland Road, Mailstop VAE-AMD
Sterling, VA 20166-9216
Attn: Charles Cernat
Phone: 703-787-1339
Email: Charles.Cernat@bsee.gov

September 2018

BAA Solicitation E16PS00116

.

Table of Contents

List of Tables

Page

List of Figures

Page

1. Executive Summary

In this project, Battelle developed a novel sensor configuration capable of measuring oil content of oil-water mixtures and emulsions based on saline water, such as seawater. The sensor combines two measurement principles: (1) a dielectric measurement, and (2) an eddy currents loss measurement. The dielectric measurement is used for high oil content mixtures/emulsions that are of water-in-oil type, therefore have relatively low electrical conductivity. For this type of mixture/emulsion, the dielectric sensor provides a reliable measure of oil content. The eddy current measurement is used for low oil content mixtures/emulsions that are of oil-in-water type and have high electrical conductivity. For this type of mixture/emulsion, the eddy current measurement allows for a reliable measurement of oil content. Combination of both sensors allows for unambiguous measurement of oil content for a broad range of oil-water mixtures including mixtures of crude oils and/or mixtures with saline water. The sensor geometry provides a relatively uniform sensitivity across a pipe cross section, which allows for use of open pipes of broad diameter range, without any mixing or homogenizing devices. The sensor was demonstrated to provide a reliable oil content for broad ranges including pure water and pure oil. The device works at different water salinities and for different oil and crude types and is insensitive to oil-water dispersion state. Battelle filled a provisional patent application describing the novel sensor [1].

The sensor developed in this project could be used to help responders to more efficiently recover oil during a response operation. Currently, responders do not have a method for knowing in real time how much water they are collecting with their oil. Collecting a large amount of water means that temporary storage will be more quickly consumed and require the responder to halt recovery to offload recovered fluids. This sensor will provide information to allow responders to make informed decisions during recovery. For example, if a responder has collected oil within a boom but is recovering mostly water while skimming, the responder may decide to stop the skimmer, continue to collect in the boom, and begin recovery again when more oil is contained within the boomed area.

More generally, the sensor can be applied to any application where oil-water mixtures need to be evaluated for oil content or, equivalently, for water cut, and where high-water salinity prevents use of traditional sensors. Possible applications include oil and gas industrial settings where highly saline brines are used, and oil content needs to be measured.

2. Summary of Project Activities

The project started with laboratory tests of a dielectric sensor operating at 80-90 MHz, which is higher frequency than traditionally used for this type of device. The testing was performed using two types of refined oils (Hydrocal 300 and Calsol) and two types of crude oils (Hoops and Pacific Energy A-38), all provided by BSEE. Solutions of a Red Sea salt were used to simulate seawater with salinities up to 4 wt%. The dielectric sensor was found to be affected by high water conductivity and proved to be effective only for low-conductivity water-in-oil mixtures with high (60-70 vol% or higher) oil content. This sensor was not effective for high-conductivity oil-in-water mixtures with lower oil content. Attempts to improve this measurement at different frequencies (40 and 270 MHz) were not successful. This indicated that the dielectric sensor alone, while used with seawater-based oil-water mixtures, is not capable of providing the oil

fraction measurement for the entire range of oil concentration and that a different measurement principle is needed.

Once it became clear that the dielectric sensor would not work with highly conductive oil-in-water seawater-based mixtures, project focus shifted to the combination of dielectric and eddy current measurements. The eddy current effect which is well-known and used in many fields of engineering had to be adopted to the oil recovery sensor requirements. This required selection of a testing frequency which enables measurements in a required range of electrical conductivities and provided penetration depth consistent with sensor size. A model which links oil content with an eddy current signal was developed and validated experimentally. Tests of the combined dielectric and eddy currents sensor proved to be highly successful. The eddy currents measurement provided reliable oil content information for high conductivity oil-in-water mixtures, and effectively supplemented the dielectric measurement. A combination of the dielectric sensor, operating at 40 MHz, and the eddy current sensor, operating at 22 MHz, was tested with the same four oils as used in the dielectric sensor tests and water at three salinity levels, 2, 3, and 4 wt%. The two measurements combined with an algorithm which first determined the type of mixture being detected and then calculated the oil content based on the appropriate sensor signal provided reliable oil fraction measurement for the entire range of oil concentrations, all four oil types, and all salinities used. A correlation coefficient between the measured and true oil fraction was above 0.98. An average error of measurement was about 3% while the maximum error was about 10%. This level of accuracy is sufficient for the oil recovery operations.

Application of relatively high testing frequencies, in the multi-MHz range, and the use of standing wave ratio (SWR) analyzers to carry out the measurements were two important outcomes of this project. High frequencies, especially frequencies above 1-10 MHz, minimize concerns of electrode polarization and oil-water polarization effects. Elimination of these effects makes the measurement more reliable and less sensitive to oil-water dispersion. The use of SWR analyzers for both the dielectric and eddy currents measurements greatly simplifies development of sensor electronics and reduces its cost. SWR analyzers are widely used for testing of radio antennas and are easily available from multiple manufacturers at low cost. The sensor's controller can be realized using two SWR analyzers to carry out both measurements and an on-board computer to carry out algorithm calculations and communications.

The main project deliverable was the sensor prototype constructed as a flow through pipe, 4" nominal diameter, combining both the sensing cavity and the electronic controller. A laptop computer, connected with the sensor through an ethernet network cable, provided user interface with both sensor controls and a measured oil fraction readout. The sensor prototype was calibrated and tested at Battelle using mixtures of two oils (Hydrocal refined oil and Hoops crude) and water with 1-5 wt% salinity. These tests demonstrated the same level of accuracy, about 3 % average and about 10% maximum error, as seen previously in the pre-prototype tests.

The culmination of the project was the prototype sensor testing at BSEE's Ohmsett facility in Leonardo, New Jersey, which was carried out on June 4-8, 2018. These tests provided realistic and independent sensor evaluation including higher flows and more precise oil fraction measurements as compared to tests carried out at Battelle. The Ohmsett tests were carried out using two oils (Hydrocal and diesel) and two water salinities (1.55 and 3.60 wt%). The test demonstrated excellent correlation between the true and measured oil fractions (correlation coefficient above 0.96), average error about 7% and maximum error about 21%. Although the errors observed during Ohmsett tests were about twice larger than errors seen in laboratory tests, they still meet the requirements of the oil recovery operations.

The experimental setup at Ohmsett was prone to mixing air into the liquid streams which affected the tests since the current version of the sensor interprets entrained air as oil. Although this effect can be easily eliminated in future tests, a more prudent approach is to realize that a significant amount of air is frequently present during oil recovery operations and the sensor should account for this. Since significant presence of air in oil recovery streams, frequently described as “pumping empty”, and significant oil-water separation, are realities of oil recovery operations, it makes sense to develop a sensor which can handle these conditions. Development of a sensor with such capabilities will be the focus of the second phase of this project; see section 9.2 on page 30 for a more detailed description how this will be addressed.

The project activities included limited modeling to provide better understanding of the experimental results and to provide modeling tools that were used in the design of the prototype sensor. Two types of models were developed: an impedance model based on the complex impedance method, implemented using the MATLAB simulation package, and a finite elements model using COMSOL Multiphysics® software. The complex impedance model confirmed the experimental findings, mainly the high sensitivity of the dielectric sensor to seawater conductivity. The COMSOL Multiphysics models helped to understand details of sensor geometry, for both sensors, especially the specifics of sensor electrode sizes and placement. The modeling will be used more extensively during the next phase of development, as the sensor response to separated oil-water and entrained air will optimized using modeling.

3. Sensor Description

3.1 Traditional Dielectric Sensor

Use of a dielectric sensor to measure water content in oil-water mixtures, gas-water mixtures, and moisture levels in solids is well known and widely practiced [2-5]. The principle of measurement is the large value of water’s relative dielectric constant (permittivity) which is about 80. This value is much greater than the dielectric constant of gases (close to 1), organic liquids (like oils and crudes) as well as solids (about 3-5). These dielectric sensors are constructed as capacitors that contain a cavity filled with tested materials. The cavity can be either a flow through or a batch type device. The sensor detects changes in electrical capacitance, caused by different water content, by a direct capacitance measurement, or often by detection of a frequency shift of a resonance circuit, which includes the sensing cavity capacitance.

In principle, dielectric sensor could be used for off-shore oil recovery applications. However, the dielectric measurement is not reliable when the mixture being measured is highly electrically conductive, for instance seawater or any highly saline water found in industrial or oil and gas applications. In practice, dielectric sensors operating with seawater are capable of measuring oil content only for low conductivity, water-in-oil mixtures or emulsions that contain a minimum of 60-70% oil.

Figure 1 presents a design of a dielectric sensor which uses a dielectric sensing cavity formed by two metal electrodes attached to the outside of opposite sides of the pipe containing tested fluid. These electrodes are connected with two external electronic components, a capacitor and an inductor. The cavity capacitance and the two external components form a resonance circuit with resonance frequency depending on the capacitance and inductance of components. Battelle used dielectric sensors designed to operate in the 40-270 MHz range. A secondary pickup coil was installed in the proximity of the first coil and connected to a radio frequency SWR (standing wave radio) analyzer. Our laboratory tests used two SWR analyzers AA-170 and AA1400, while the sensor prototype used the AA-30 analyzers, all produced by Rig Expert.

The choice of the SWR analyzer is not critical for the sensor's operation. A distance between the two coils was adjusted to provide the optimal sharpness of the resonance peak.

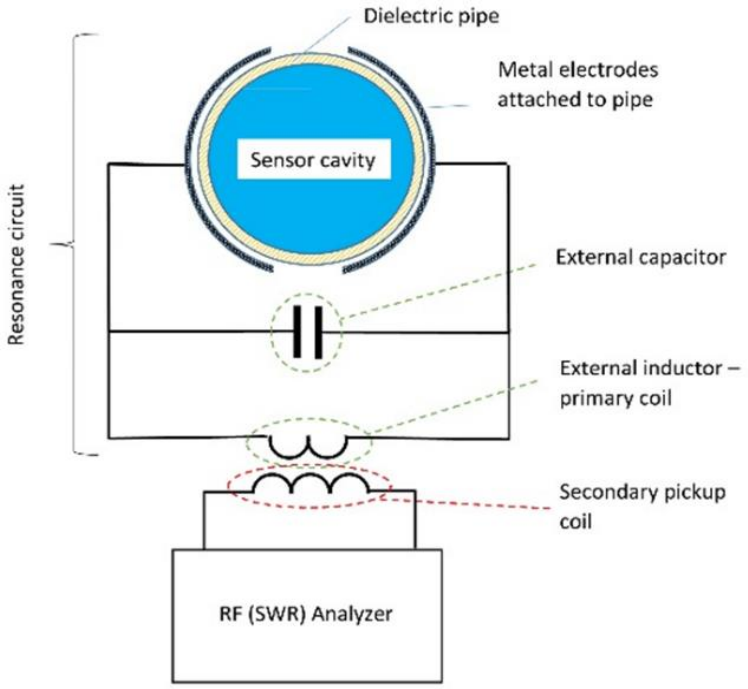

Figure 1. The equivalent circuit of the dielectric sensor together with external components used during testing.

The challenge of the dielectric measurement arises with materials that are highly electrically conductive, for instance seawater or any highly saline water used in industrial or oil and gas applications [2-5]. The high conductivity of the tested material manifests itself in the dielectric sensor as a low resistance connected in parallel with the cavity's capacitance which effectively shortens the cavity. This challenge cannot be solved by modifying sensor shape or size since the relative contribution of the cavity's capacitance and resistance is geometry-independent. Theoretically, the relative resistance contribution can be reduced by increasing the frequency of the dielectric measurement, since the capacitance contribution is increased at higher frequencies, while the resistive contribution remains constant [6-8]. However, frequency increase causes reduction of skin depth, which determines the extent of penetration of electromagnetic waves into the tested mixture. This decrease in skin depth penetration makes a sensor sensitive only to areas close to its electrodes, which may be a small fraction of overall sensor volume, especially for larger sensors. Due to high salinity of typical seawater, the conductivity effect is severe enough to prevent successful development of dielectric sensors that are effective in a marine environment. In the case of oil-water sensors operating with seawater, traditional dielectric sensors are capable of measuring oil content only for low conductivity, water-in-oil mixtures or emulsions that contain at least 60-70% of oil.

3.2 Eddy Currents Sensor

The failure of the dielectric measurement to be effective for the entire range of oil content values indicates that an alternative approach to test highly conductive oil-in-water mixtures is needed. One of the approaches is to use an electric conductivity measurement for oil-in-water mixtures

in combination with the dielectric measurement applied to water-in-oil mixtures, as described in the U.S. patent [9]. This patent discloses a strong, near logarithmic, dependence of conductivity with water cut in the oil-in-water mixture regime, which can be readily inverted to calculate oil fraction for these emulsions. Measurement of electrical conductivity is not trivial since it requires direct contact between metal electrodes and tested mixture. Such contact invites challenges associated with electrode polarization effects, electrode oxidation, and/or electrode erosion.

Battelle's approach uses an eddy current measurement which is effective for oil-in-water mixtures, while free of the conductivity measurement drawbacks. The eddy current effect is observed in all conductive materials that are exposed to changing magnetic fields. The eddy currents are actual electrical currents that cause two effects: (1) they have the orientation and intensity that tends to cancel the external magnetic field that generates them, and (2) they cause energy losses due to heat generation in the conductive media. In fact, the eddy currents are responsible for the finite skin depth penetration of electromagnetic waves in conductive media. Energy losses due to eddy currents allow for measurement of this effect by means of a resonance circuit. If the inductor generating the eddy current effect is a part of resonance circuit, eddy current energy losses in the tested material will cause losses in the resonance circuit. These losses will cause broadening and height reduction of a resonance peak, both easily measurable effects.

Figure 2 presents a diagram of the eddy currents measurement. An inductor is attached to the sensor cavity in a way which exposes the tested oil-water mixture to its magnetic field. The preferable form of the inductor is a coil wound around the pipe, as shown in the figure, since it ensures the most uniform sensitivity across the entire pipe's cross section. An alternative inductor design would be a differently arranged coil(s) attached to a side of the cavity pipe that accomplishes similar exposure to magnetic field. Preferably, the coils are not in direct electrical contact with the tested fluid since this would introduce direct conductivity effects and all problems with conductivity measurement listed above.

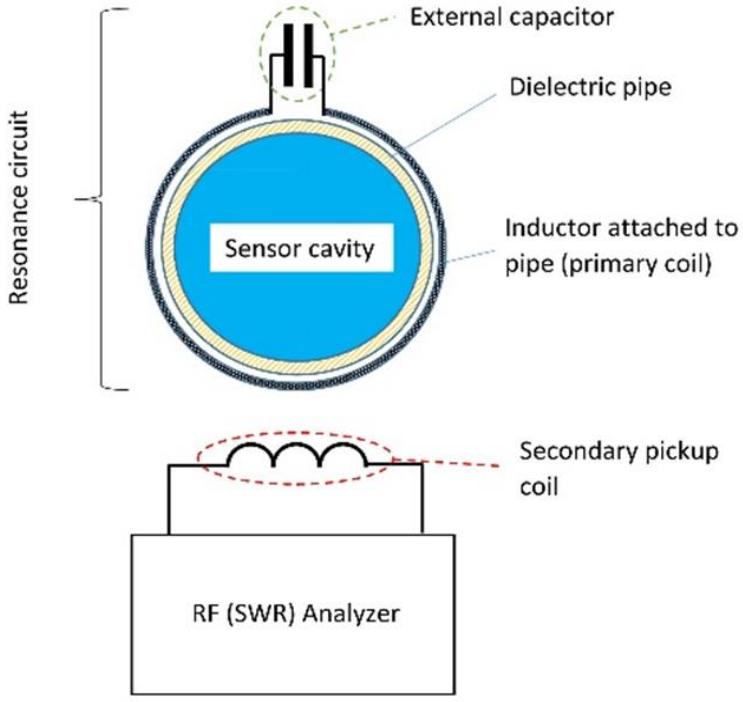

Figure 2. The equivalent circuit of the eddy current sensor together with external components used during testing.

The inductor is connected to an external capacitor to form a resonance circuit. Battelle tests used eddy currents sensors operating in 20-40 MHz frequency range which provided appropriate eddy currents measurement sensitivity for the 3-4" pipe diameter and 1-5% water salinities. A secondary coil, connected to the SWR analyzer, was placed in the proximity of the primary coil. For convenience, the secondary coil was also constructed as a single copper wire loop wound around the pipe. Similarly, as it was the case for the dielectric measurement, the coupling between both coils was critical to achieve a narrow and intense resonance peak.

The sensor which combines both measurement principles allows for an unambiguous measurement of oil content for a broad range of oil-water mixtures in the entire oil concentration range from pure oil to pure water. The dielectric measurement can be used for high oil content mixtures/emulsions that are of water-in-oil type, therefore have relatively low electrical conductivity. The eddy current measurement is used for low oil content mixtures/emulsions that are of oil-in-water type and have high electrical conductivity.

4. Demonstration of Sensor Performance in Laboratory

4.1 Experimental Setup and Approach

The tests with oil-water mixtures were carried out using the testing setup shown in Figure 3. The setup consisted of two acrylic 3-inch schedule 40 pipes, connected in a loop with PVC fittings.

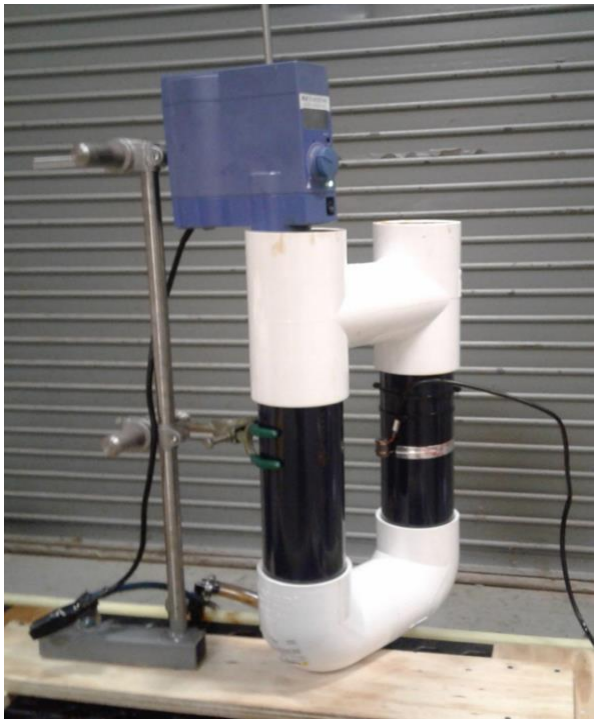

Figure 3. Experimental setup for testing oil-water mixtures at different mixing and flow conditions.

One of the pipes was used as the dielectric sensor cavity. Mixing and recirculation of the oil-water mixtures was realized using a 2.5-inch diameter propeller, shown in Figure 4, placed in the second pipe. Since the propeller and its shaft were made of stainless steel, it was essential to keep these components outside of the sensor to avoid interference with the measurements. The propeller was powered by a variable speed drive shown at the top of Figure 3. The propeller forced an upward movement of the mixture, causing a downward flow in the sensor cavity.

Figure 4. Impeller used to force oil-water mixture flow.

The tests carried out with different oils demonstrated that this experimental setup was capable of generating different degrees of oil-water dispersions. These dispersions included relatively coarse mixtures that readily separate once mixing ceases, and stable emulsions that remain stable for hours. The coarse, rapidly-separating mixtures were formed at low impeller speeds (500-700 RPM), especially if the oil content was below 40-60%. Higher impeller speeds (800-1000 RPM) and mixtures with high oil above 60-70% produced emulsions that were, in some cases, stable over several hours.

Four types of oil were used, two refined and two crudes, that covered a wide range of viscosities that may be encountered in real oil recovery situations. Table 1 lists the oils and their viscosities. All viscosities presented were measured at Battelle using a TA Instrument AR 2000EX rheometer.

Table 1: Oils used for testing in Task 1.

Oil	Type	Viscosity at 20°C (poise)
Hydrocal 300	refined	1.54
Calsol	refined	16.8
Hoops	crude	0.1
Pacific Energy A-38	crude	28.6

The goal of this project was to develop a sensor which can be used for a broad range of off-shore oil recovery applications where water may have different salinities. Table 2 lists salinities for several geographic locations [10]. Different seas have different salinity levels ranging from 1.0 wt% for the Baltic Sea up to 4.1 wt% for the Red Sea. The major oceans are interconnected and have salinity of 3.5 wt%.

Table 2: Sea water salinities for different geographic locations.

Sea	Salinity (wt%)
Pacific Ocean	3.5
Atlantic Ocean	3.5
Mediterranean Sea	3.8
Red Sea	4.1
Black Sea	1.3-2.3
Baltic Sea	1.0
Beaufort Sea	2.8-3.2

Based on the values in Table 2, tests were performed using three salinity levels in the 2-4 wt%. All saline water was prepared using the Red Sea salt shown in Figure 5. This type of salt contains mostly sodium chloride with additional salts common in sea water and it is frequently used for preparation of simulated sea water.

Figure 5. Red Sea salt used for preparation of simulated saline water.

4.2 Tests of Dielectric Sensor

Figure 6 shows a typical response of the dielectric sensor for oil-water mixtures with different oil content and with significant water salinity (2 wt% and above). The resonance frequency versus oil content curve has two distinctive regions. Most of the frequency shift occurs over the 80-100% oil-content range, which corresponds to low conductivity water-in-oil emulsions. The remaining range of oil concentrations, 0-80%, which corresponds to high conductivity oil-in-water emulsions, produces much smaller changes in resonance frequency. This type of sensor response is problematic since it does not lead to a reliable inverted expression, which can be used to calculate oil content as a function of measured resonance frequency. Furthermore, this type of frequency response is common for commercially available dielectric sensors.

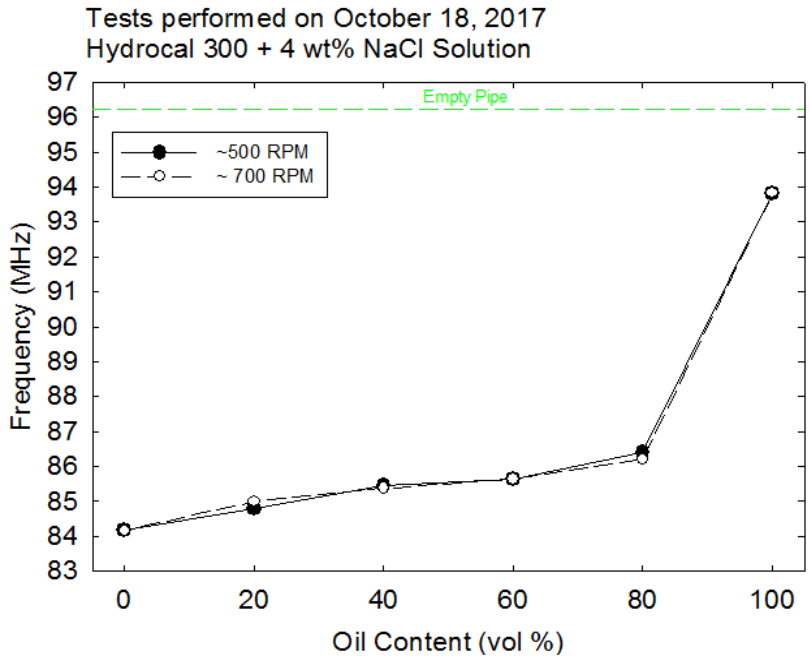

Figure 6. Dielectric sensor response for different levels of oil content measured at intermediate frequencies around 90 MHz.

An attempt was made to improve the sensor function by increasing the sensor's operational frequency. Figure 7 shows the result of tests carried out in the 230-255 MHz range. It is apparent that this increased frequency range does not improve the response of the dielectric sensor.

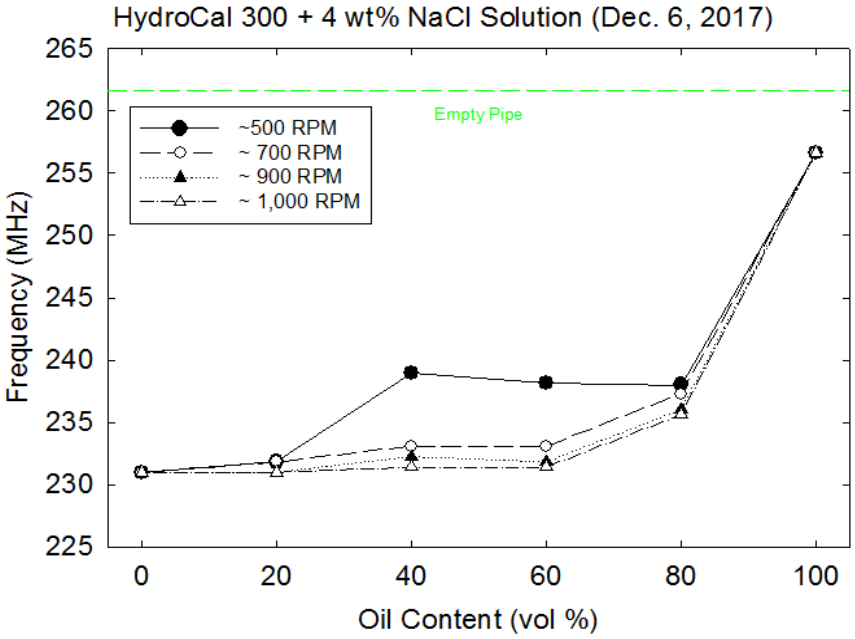

Figure 7. Dielectric sensor response for different levels of oil content measured at higher frequencies (230-260 MHz).

The dielectric sensor response was tested with all combinations of four oils (listed in Table 1) and water at three salinities, tap water, 2wt%, and 4wt% Red Sea salt solutions. The complete data is given in section 10.1 of this report. This data demonstrates that the dielectric measurement, if applied to mixtures based on saline water, is only capable of providing a reliable oil water content measurement for water-in-oil mixtures with high oil content. This finding redirected Battelle's efforts towards an alternative approach, which combines the dielectric and eddy currents measurements.

4.3 Tests of Eddy Currents Sensor

The eddy current measurement was performed for the same range of oil-water mixtures as used in the dielectric measurements. The primary measurement recorded during the eddy currents test was the height of a resonance peak. The resonance frequency was also recorded, however, it remained constant for all mixtures as well as for an empty pipe measurement. Figure 8 shows the evolution of the eddy current resonance peak with changing oil content. The eddy current signal, measured as a peak's height, is progressively reduced, and its width increased, with decreasing oil content.

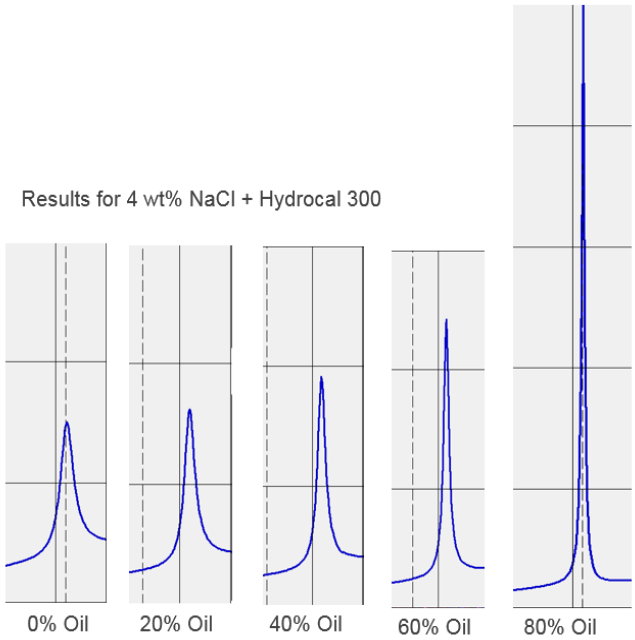

Figure 8 Typical peak height change observed for the eddy current sensor filled with different oil content mixtures.

The peak height dependence on oil content, for two 2 and 4 wt% water salinities, is shown in Figure 9. The peak height increases monotonically with oil content up to 70% and is independent of the mixer speed. The peak height dependence on oil content is quite strong considering that the decibel scale is logarithmic. One important feature of the eddy current measurement is its dependence on water salinity. Consistent with the physics of the eddy current effect, lower water salinity and/or higher oil content cause smaller mixture conductivity, which is responsible for larger height of the resonance peak. This means that the oil content measurement must account for water salinity. This can be realized by calibration of the sensor performed with pure water at given salinity or by directly entering the salinity calibration values into the sensor.

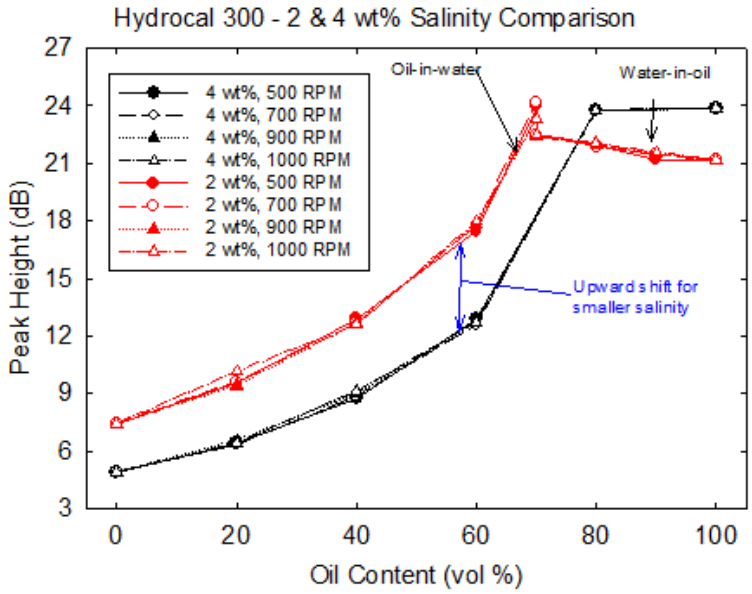

Figure 9. Eddy current peak height as a function of oil content and mixer speed, plotted for two water salinities.

Comparison of the results shown in Figures 6, 7 and 9, indicates that the dielectric and the eddy current measurements are complementary, and that if used in conjunction in a singular sensing device they can provide a reliable oil content measurement for the entire range of oil-water mixtures.

The dielectric and eddy current sensor responses were tested with all combinations of four oils, listed in Table 1, and three salinities, 2 wt%, 3 wt%, and 4 wt%. The complete data are given in Section 10.2 of this report. The data demonstrate that the combination of both testing methods provides a promising approach to measuring oil content in oil-water mixtures for a broad range of oils and seawater salinities.

5. Sensor Algorithm

An algorithm based on the combination of the dielectric and eddy current measurements must consist of three parts as outlined in Figure 10. First, the algorithm must detect what type of mixture is in the sensor. Then, one of the two measurement signals should be used to calculate the oil content.

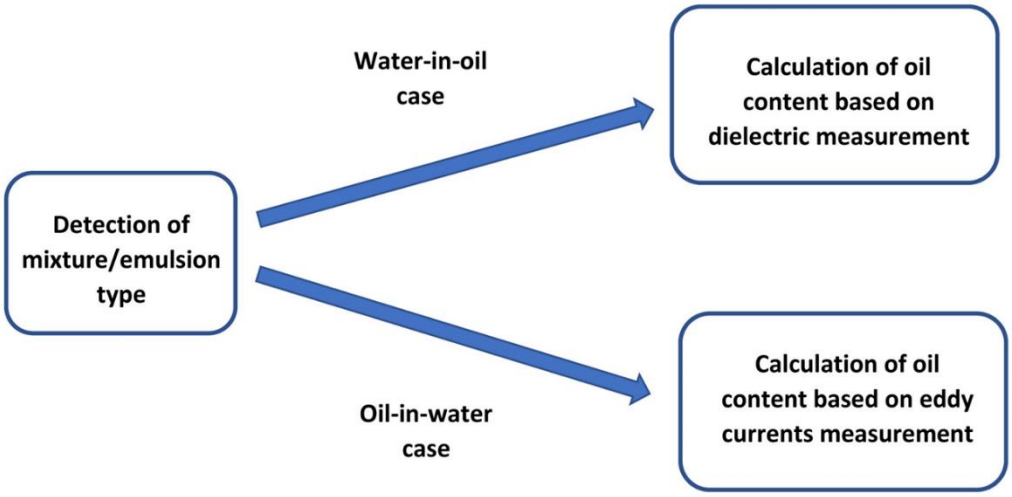

Figure 10. The three parts of the oil content measurement algorithm.

5.1 Detection of Mixture Type

Detection of the mixture type can be based on the resonance frequency obtained in the dielectric measurement. This is illustrated in Figure 11, which shows two typical results of the dielectric measurement for two types of oil. In both cases, frequencies falling in the bottom part of the overall frequency range correspond the oil-in-water mixtures, while higher frequencies correspond to the water-in-oil mixtures. Close examination of data collected for all combinations of oils and salinities indicated that a threshold of 35% correctly determines the type of mixture in all tested cases.

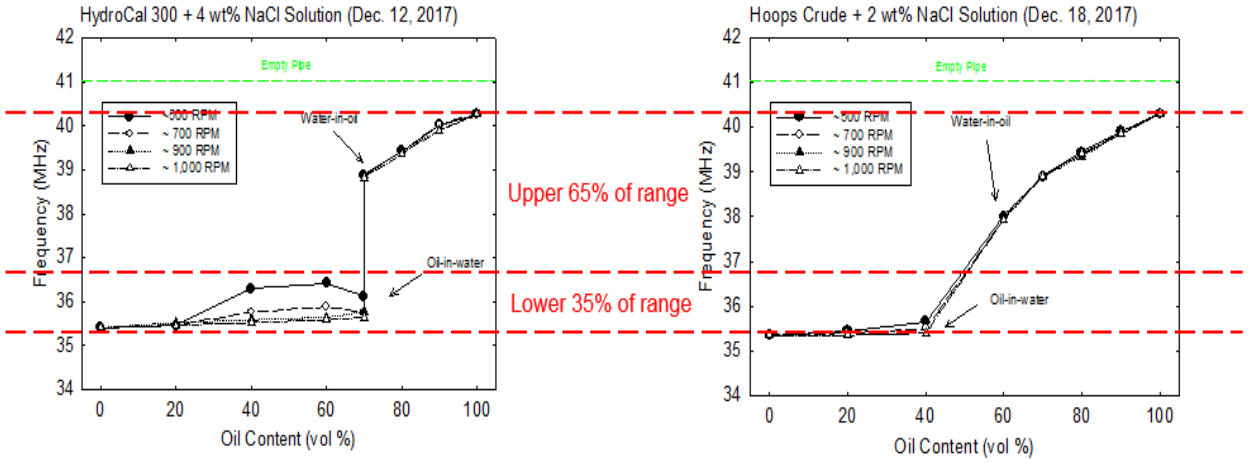

Figure 11. The principle of using the dielectric measurement resonance frequency to determine the type of mixture.

5.2 The Dielectric Part of the Algorithm

The oil content for water-in-oil mixtures can be expressed as a function of the resonance frequency shift measured by the dielectric detector. The frequency shift should be measured with respect to the frequency measured with pure oil of the same type as expected for the mixture (see Figure 12). In practice, this frequency should be recorded during detector calibration or carried out prior to testing. The pure oil calibration frequency is expected to change slightly for different oils due to differences in their dielectric permittivity constants. Smaller frequency changes may be caused by aging of the sensor materials and components, particularly aging of the sensor's pipe and/or external capacitor and inductor. A pure oil calibration performed before testing will account for these effects.

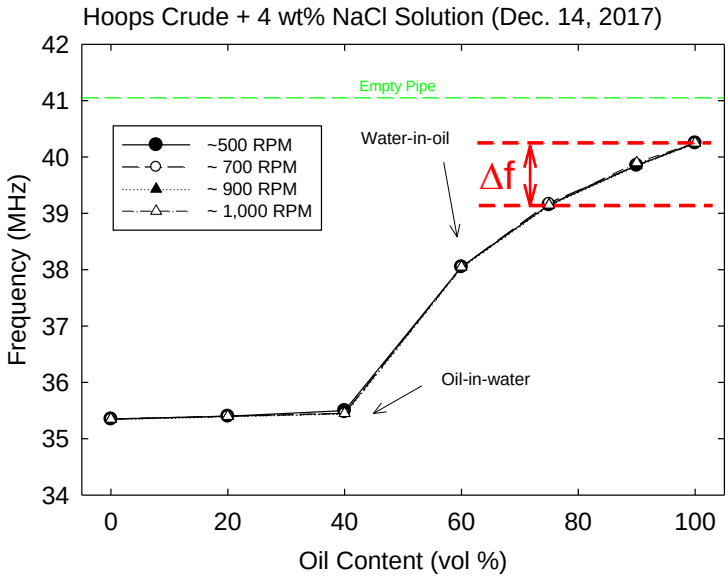

Figure 12. The shift of the dielectric sensor resonance frequency which can be used for oil content measurement.

Once the dielectric frequency shift is obtained it can be used to calculate the oil content. Figure 13 shows the oil fraction as a function of the frequency shift for all tested oil and salinity combinations. As shown, the experimental data follow a common curve, which can be approximated by a simple quadratic expression. This result is consistent with the physics of the dielectric measurement which predicts that, for low-conductivity water-in-oil mixtures, the frequency shift will be essentially independent of the water salinity and of the type of oil. The relative independence of oil type is the result of the fact that all common hydrocarbons have relative permittivity in the single-digit range.

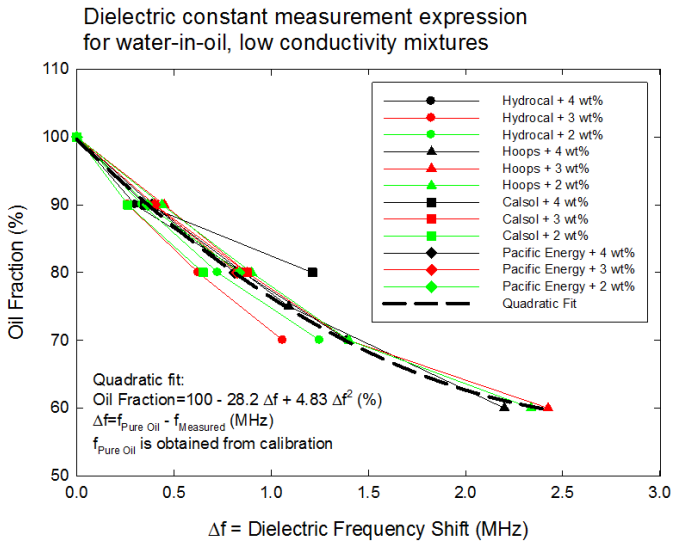

Figure 13. Oil content plotted as a function of a frequency shift measured by the dielectric method.

5.3 The Eddy Currents Part of the Algorithm

Calculation of the oil content for high conductivity oil-in-water mixtures can be realized based on the eddy current peak size. As it was discussed above, the eddy current measurement is affected by water salinity; however, this effect can be approximated by a simple vertical shift on the logarithmic decibel scale shown in Figure 9. This approximation allows for expressing the oil content as a function of the normalized eddy current peak size, parameter P, shown in Figure 14. In practice, the peak height for pure saline water should be recorded during detector calibration or carried out prior to testing.

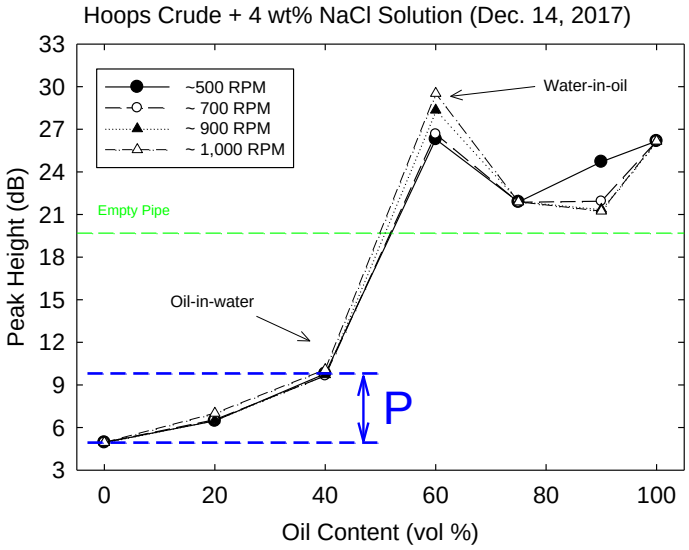

Figure 14. The relative change of eddy current peak height normalized to the pure saline water calibration point.

Figure 15 presents the oil fraction plotted as a function of the normalized eddy current peak size for all tested combinations of oil type and salinity. Again, the experimental data follow one common curve, which can be approximated by a simple cubic expression. It should be noted that this figure indicates some residual dependence on water salinity, mainly lower salinity produces larger normalized peak size. This effect was not included in the algorithm since it has only moderate effect on the error of the measurement.

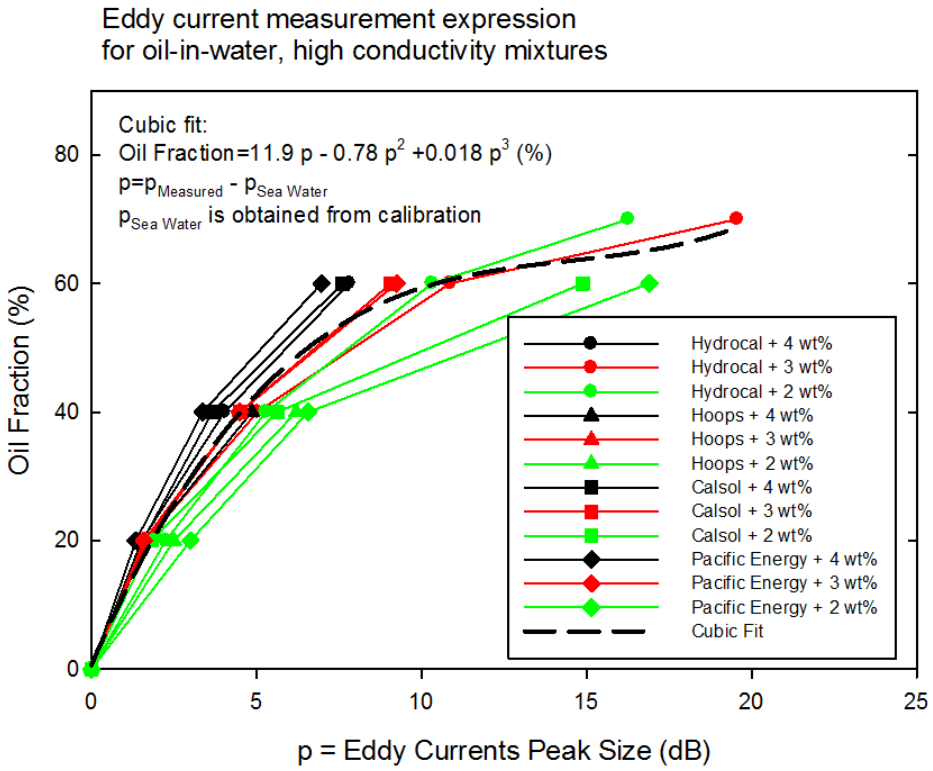

Figure 15. Oil content plotted as a function of the normalized eddy current peak size.

It is known that temperature has a significant effect on water conductivity [11]. To account for this effect, the actual sensor measures temperature, and its algorithm uses this information to correct the eddy current calculations. This correction is applied to the calibration measurement with pure saline water and the actual mixture measurements. In contrast, the dielectric measurement is affected by temperature to a much smaller extent.

5.4 Application of the Algorithm to Experimental Data

The algorithm described above was applied to all the data collected with four types of oil and three salinities. The algorithm followed the scheme shown in Figure 10 and used the two expressions given in Figures 13 and 15.

Figure 16 shows the comparison between true oil fraction and oil fraction obtained from the algorithm. The agreement is excellent across the entire range of oil-water mixtures. The overall correlation coefficient for all data shown is over 99%. It should be noted that, due to the pure oil and pure water calibrations used, the data indicate a perfect agreement for all measurements carried out with pure oil and with pure saline water, oil content 100% and 0%, respectively.

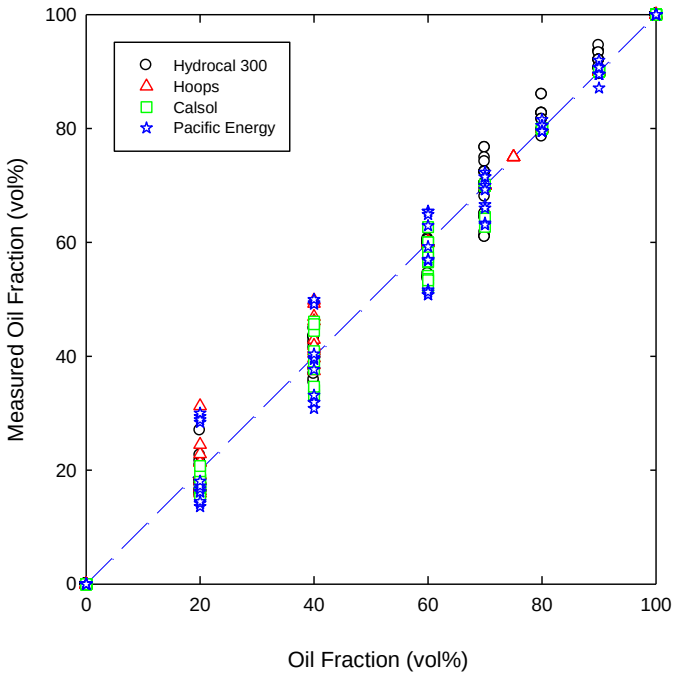

Figure 16. Correlation between measured and true oil fractions.

Figure 17 shows the error of measurement defined as a difference between measured and true oil fraction. The average error of measurement is below 3%, while the maximum errors are about 12% (positive side) and about 10% (negative side), both measured in units of oil fraction. This level of accuracy is expected to be improved in the final sensor implementation; however, it is already quite acceptable for oil recovery operations.

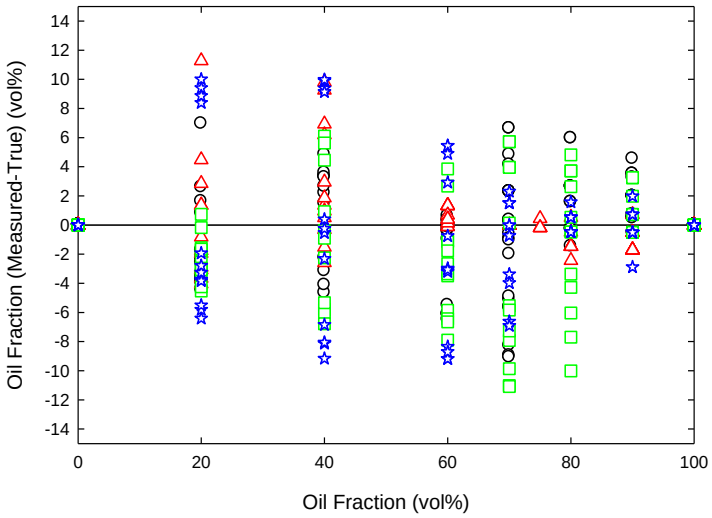

Figure 17. Distribution of errors for the oil content measurement.

6. Sensor Modeling

Limited modeling using the complex impedance method and the COMSOL Multiphysics software was performed as a part of the project. Results from both types of models are described in the sections below.

6.1 MATLAB Modeling

The complex impedance approach is a standard method to model alternating current (AC) electronic circuits [7, 12, 13]. Figure 18 presents an equivalent circuit of the dielectric sensor, which includes the sensing cavity, the capacitances of the pipe walls, the external capacitor and the external inductor. The sensor cavity was modeled as a capacitor and resistor, connected in parallel. The capacitance and resistance values were modeled using oil and seawater permittivity and conductivity and a flat cavity geometry with dimensions simulating a pipe. The wall and external capacitors were assumed to be ideal elements without losses. The external inductor was modeled as inductance and resistance in series, with the inductance and resistance values calculated using copper properties and coil dimensions. The model calculations were carried out in MATLAB.

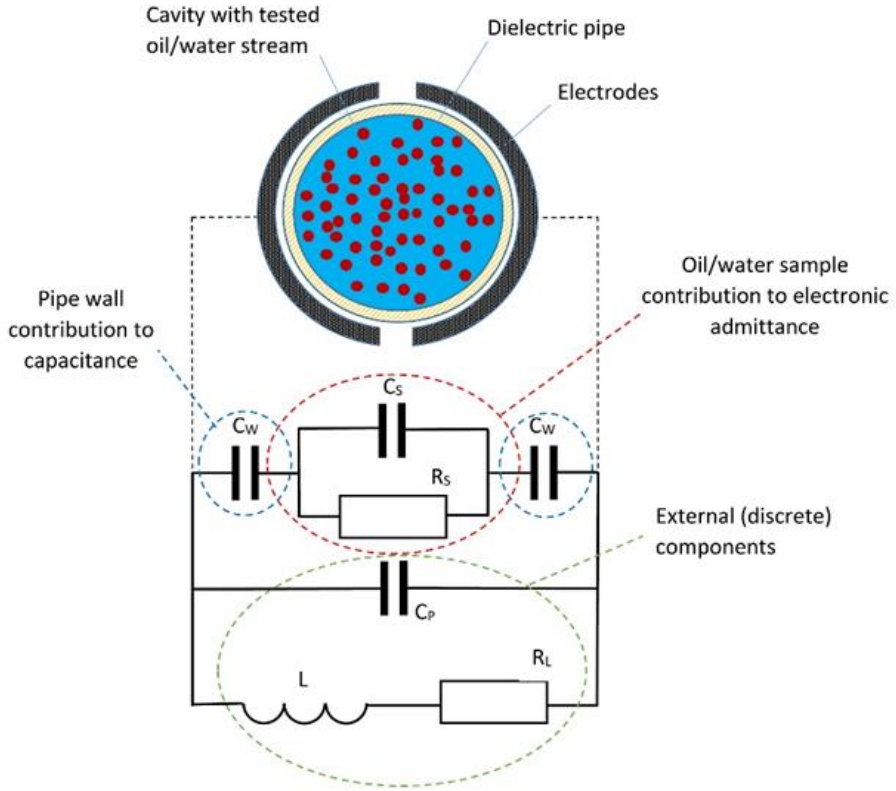

Figure 18. The equivalent circuit of the dielectric sensor modeled by the complex impedance approach.

One important result of the complex impedance model is the effect of water conductivity on a dielectric sensor response shown in Figure 19. The transition point between the two mixture types was chosen arbitrarily at 70% oil since this was the behavior observed for the Hydrocal 300 oil. The model confirmed that the two-region response observed experimentally (Figures 6

and 7) is caused by water conductivity. Specifically, the typical seawater conductivity range between 1-5 siemens per meter (S/m) produces this undesirable effect. This theoretical confirmation of the experimental results motivated the move towards the two-sensor approach.

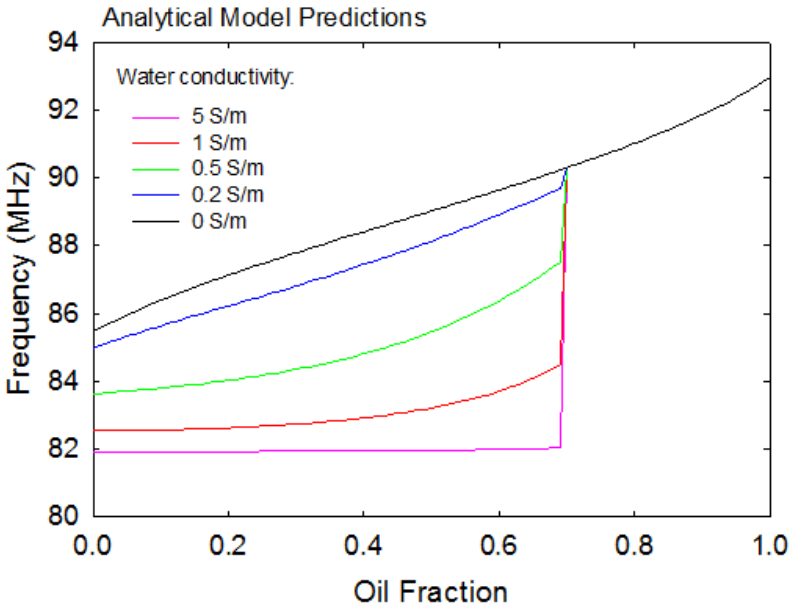

Figure 19. The frequency versus oil fraction curves for different waster salinity levels as predicted by the complex impedance model.

6.2 COMSOL Multiphysics Modeling

COMSOL Multiphysics software applies the finite element approach to numerically model different physics phenomena for real geometries. The AC/DC module provides the capability to solve the electromagnetic Maxwell equations that describe classical electric and magnetic phenomena. COMSOL modeling is especially appropriate for the engineering aspects of the project that require an accurate description of the sensor geometry including items like the effects of a sensor's electrodes and enclosure, finite dimensions, uniformity of dielectric, and eddy current measurements.

The COMSOL model requires a realistic geometry definition, which includes all system components, accurate material properties representation, and all external system boundaries together with appropriate boundary conditions. The dielectric sensor geometry used in the model included the acrylic pipe with two metallic electrodes attached from outside. The system boundary was assumed to be a much larger cylindrical cavity made of conductive material. Figure 20 shows one of the dielectric sensor geometries implemented in COMSOL.

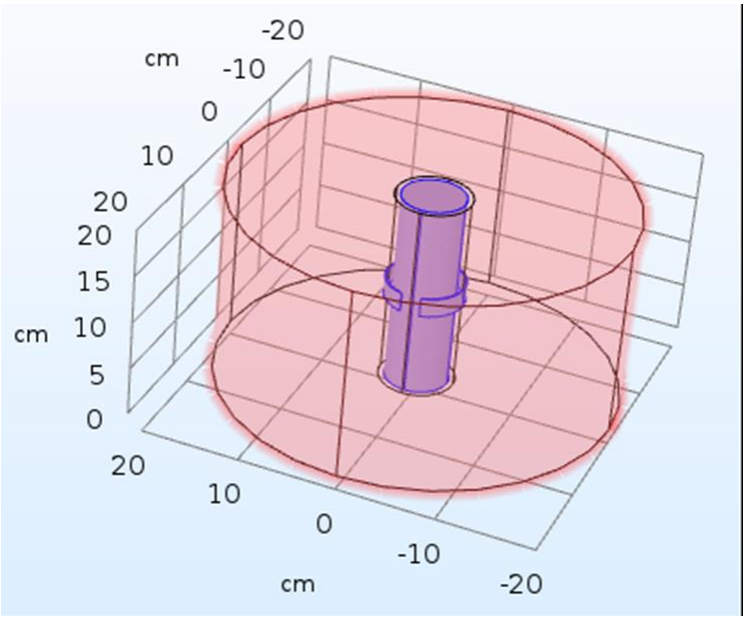

Figure 20. The dielectric sensor geometry defined in the COMSOL Multiphysics model.

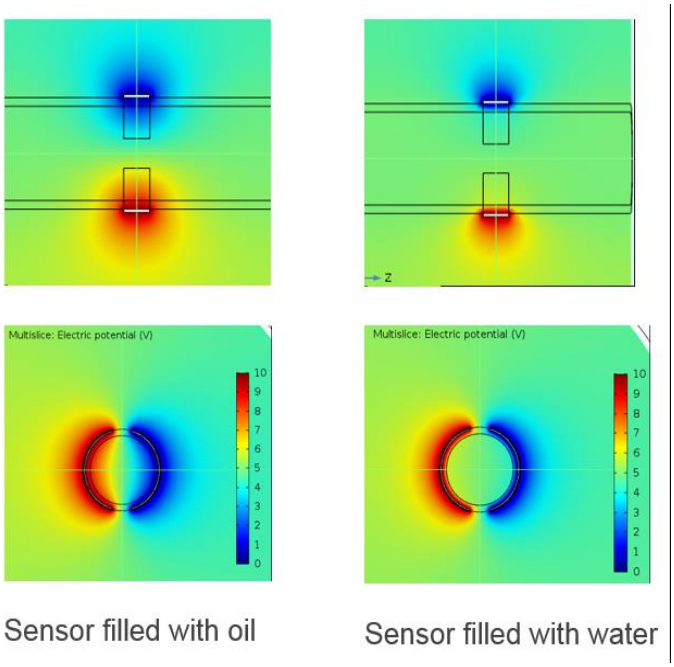

Figure 21. Typical electrostatic potential distributions predicted by COMSOL Multiphysics model applied in the electrostatic mode.

The COMSOL AC/DC module provides several models for different types of electromagnetic effects. The simple static model assumes no flowing currents and no magnetic fields, which is appropriate for electrostatic phenomena. This version of the model is appropriate for evaluation of complex capacitor geometries that include multiple components and different materials. A typical output of the static COMSOL model is a prediction of electric potential, or electric field,

distribution within the system. Figure 21 shows a typical potential distribution around the dielectric sensor electrodes for the sensor cavity filled with oil and with saline water.

7. Construction of Sensor Prototype

The prototype sensor was designed to be installed in an oil skimmer recovery hose. It uses a 4" diameter pipe with standard 4" camlock fittings as shown in Figure 22. The prototype overall length is approximately 22 inches.

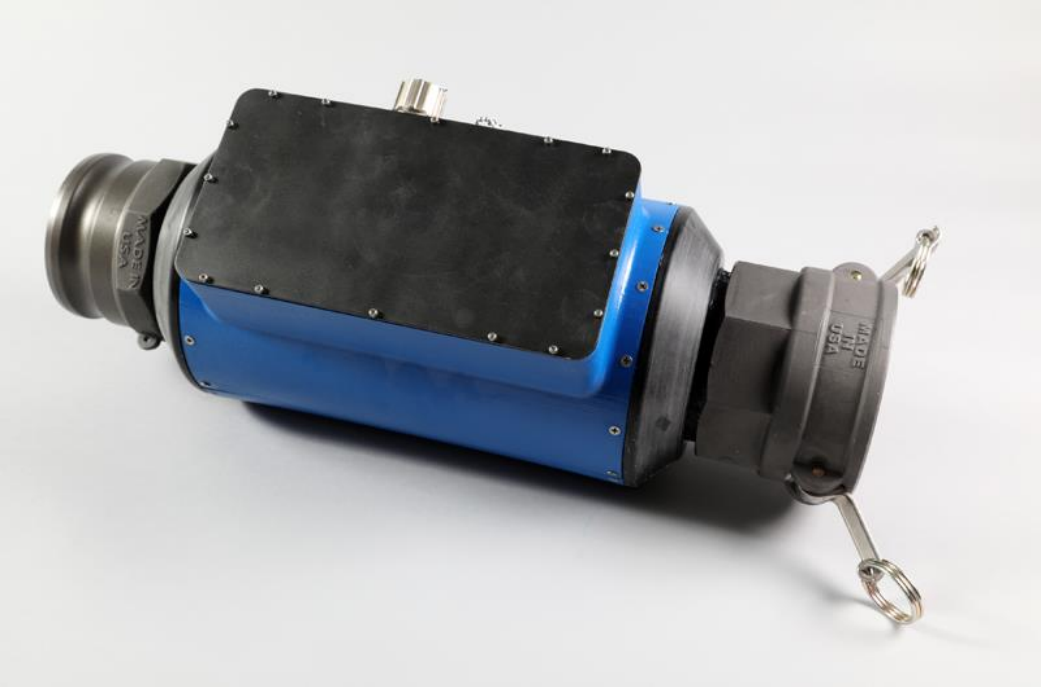

Figure 22. The prototype sensor tested at Ohmsett.

The sensor's electronic controller was built into the unit's enclosure. To operate, the controller needed to be connected into an external power supply (5 VDC, 1A) and a laptop computer with an internet browser. Figure 23 presents the graphic user interface (GUI), which allows for sensor control and a reading of measured oil fraction. The sensor was capable of recording measured oil fraction, in a tabular form, over extended periods of time. This feature was used to record data during tests at Ohmsett.

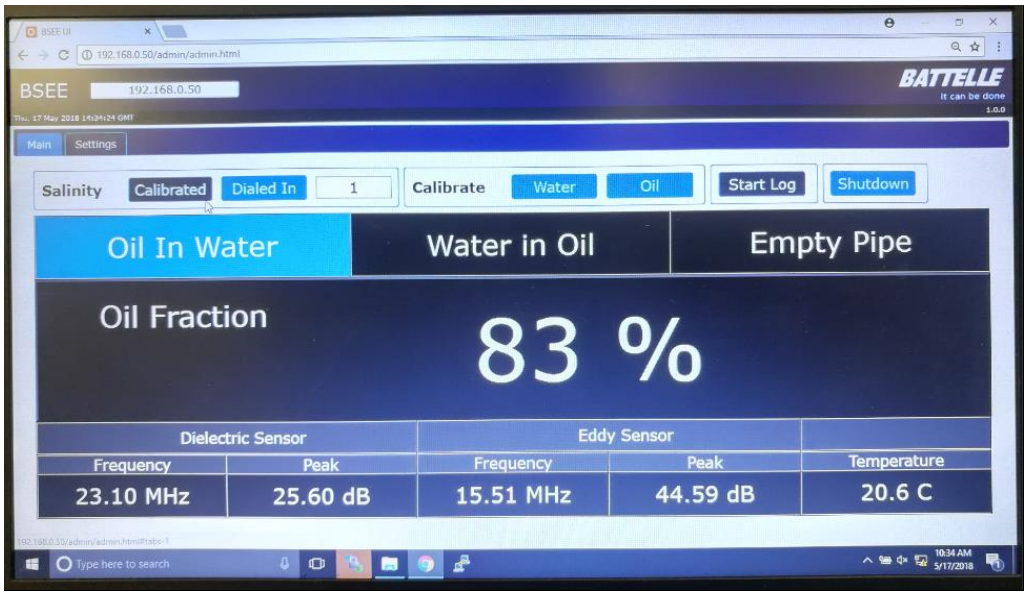

Figure 23. The GUI of the sensor's software.

8. Demonstration of Sensor Performance at Ohmsett

8.1 Tests and Calibration Carried out Prior to Ohmsett Tests

Prior to testing at Ohmsett, the sensor prototype was calibrated to enable proper interpretation of different water salinity levels and oil concentrations. The calibration was necessary because the prototype sensor was larger than the sensor used in laboratory tests described in section 4, and because the sensor was surrounded by a partially conductive enclosure. The calibration tests and their results are presented in the appendix section 10.3.

8.2 Tests at Ohmsett

Between 6/4/2018 and 6/8/2018, the prototype sensor was tested at the BSEE's Ohmsett facility in Leonardo, New Jersey. The sections below describe these tests in detail.

8.2.1 Test Setup

The testing setup was assembled on the Ohmsett west deck as shown in Figure 24. The circulation loop was designed to minimize the fluid volume and provide a continuous flow at a controllable flow rate for an indefinite time, allowing for flexibility and long-term data collection. For this evaluation a homogeneous mix of fluid was desired; this was accomplished by incorporating a static mixer into the loop. The loop flow was initiated from the main bridge storage tank driven by the Moyno progressive cavity pump. The loop included two 3-inch diameter by fifty-foot petroleum hoses, an injection port, a static mixer, a sample port, isolation valves and the prototype recovery efficiency sensor.

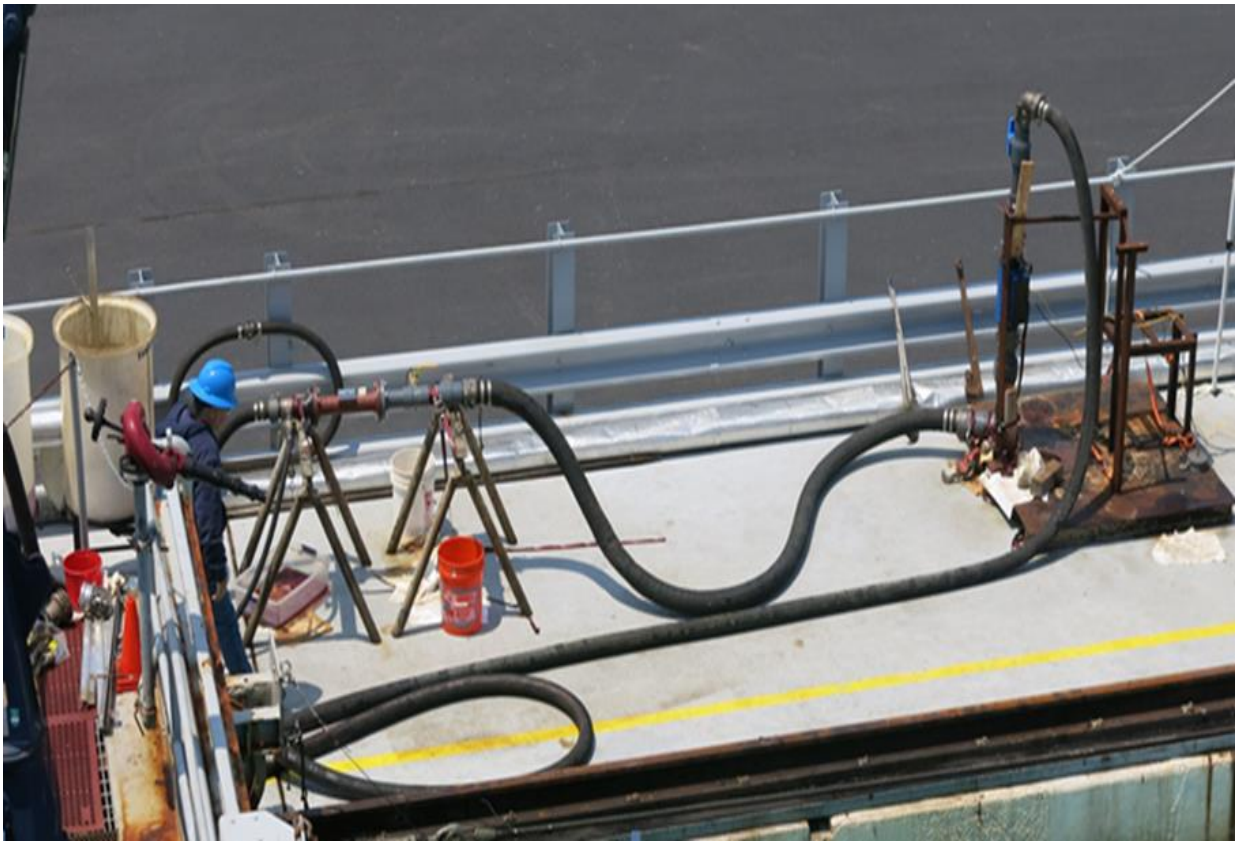

Figure 24. The testing setup at Ohmsett.

The test fluids were measured and pumped into the loop from portable storage tanks using a double diaphragm pump through the injection port-valve. Quantities were measured manually using level measurement and converting to gallons.

Fluids used in the tests included saltwater at two salinities; 15.5 and 36 ppt (1.55 wt% and 3.60 wt%) and two test oils, Hydrocal 300 and diesel. The saltwater was made by adding solar salt to fresh water and mixing within totes. One batch at each salinity was mixed and was a sufficient volume for all testing. Basic oil properties were measured at the Ohmsett laboratory and are provided in Table 3.

Table 3: Properties of the two oils used during Ohmsett testing.

Oil	Sample #	Density (g/ml @20°C)	Viscosity (cP @20°C)	S.T. (dynes/cm @20°C)	I.F.T. (dynes/cm @20°C)	% Water
Hydrocal 300	671-01	0.907	178	33.4	27.8	1.2
Diesel	671-02	0.845	4	31.6	14.8	0.0

The sensor was secured with straps to a rigid base allowing for changes in the orientation from vertical to horizontal, as shown in Figure 25. Isolation valves were provided at the sensor ends allowing for removal with the loop circuit full of fluid.

Figure 25. The sensor secured to a rigid base.

8.2.2 Test Method

As per the test matrix, a series of oil/water ratios ranging from 100% to 0% oil were created. The test matrix required conditions ranging from 100% oil to 100% water. The ratios were created by starting with 100% oil in the loop and then adding a known volume of water through the injection port to achieve the desired ratio. When changing the oil/water ratio, the fluid in the loop was circulating at a nominal rate to evenly distribute the water being added into the loop. Similarly, when the initial conditions required 100% water, subsequent test parameters with oil/water ratios were created by injecting a known volume of oil into the loop while circulating.

Whenever it was necessary to change test parameters within the circulation loop, the loop was evacuated by disconnecting the petroleum hoses and fittings and draining them into the test basin. When changing oil types and/or salinity the system was purged by pumping test basin water into the main bridge tank. As water was added to the tank, the Moyno pump evacuated the water through the open loop until clean water was visually observed at the discharge.

The sensor data was recorded as an electronic file during each test. The data was recorded for a period of 3 to 10 minutes. The shorter recording times were used if the sensor's oil fraction reading appeared stable. In cases where the oil fraction was fluctuating, longer data collection times, typically 5 to 10 minutes, were used.

8.2.3 Discussion of Observations

A matrix defining all desired test parameters to be evaluated was composed prior to the actual testing. The order of testing was altered to the most efficient order to save time; numbering was sequential by day and time. For test in which there were changes in flow rates only, the test numbers remained the same and the different flow rates were denoted as A, B, etc. Oil percentage values were obtained from grab samples from the sample port. Measurements were made at Ohmsett laboratory, using a separatory funnel for the initial separation of oil and water followed by a centrifuge analysis.

The circulation loop design provided for a convenient means of creating the required oil/water ratios and the wide range of controllable flow rates through the sensor. Not anticipated was the holdup of fluid that could not be evacuated within the pump used for circulation (main bridge Moyno). This effect was notable when preparing for tests requiring 100% oil. The sampling results indicated approximately 10% water within the loop when establishing this condition. As a result, this offset was carried into subsequent tests when starting with 100% oil and then adding water to create defined oil/water ratios. Tests series starting with 100% water and then adding oil to create the required ratios should not have been affected since the circulation loop purge process used saltwater.

Another unexpected condition was observed during collection of grab samples in mason jars, which revealed that air was entrained in the fluid. This condition was more predominant during tests performed at high flow rates. This condition may have caused an error in the sensor ratio measurements.

A preliminary estimate for volume in the loop was 70 gallons; after the setup was assembled, water was injected to fill the loop and the volume to fill the circuit with approximately 8 inches of fluid above the pump inlet was 60 gallons. Due to the identification of air in the fluid it was decided to increase the nominal circuit volume to 65 gallons in an effort to minimize ingestion of air into the loop at the pump inlet. The actual cause of air entering the fluid stream is not definitively known but the two most likely sources are the pump inlet not being completely flooded and/or air being entrained into the fluid when exiting from the return line into the tank.

8.2.4 Experimental Results

Table 4 summarizes all results obtained during testing. The grab sample oil fractions were determined by the Ohmsett testing method. The oil fractions indicated by sensor were calculated as time averages using the electronic data files collected by the sensor. Appendix section 10.4 shows the oil fraction recorded as a function of time for all tests performed. In several cases data are not available because the grab sample was not collected or because the sensor's electronic data file was not recorded. The tests with part of the data not available were excluded from the sensor accuracy analysis.

Table 4: Summary of results.

Test #	Oil Type	Salinity (wt%)	Flow (gpm)	Target Oil Fraction (vol%)	Grab Sample Oil Fraction (vol%)	Oil Fraction Indicated by Sensor (vol%)
1	Hydrocal	1.55	60	0	NA	0.1
2	Hydrocal	1.55	120	0	NA	-0.1

Test #	Oil Type	Salinity (wt%)	Flow (gpm)	Target Oil Fraction (vol%)	Grab Sample Oil Fraction (vol%)	Oil Fraction Indicated by Sensor (vol%)
3	Hydrocal	1.55	60	25	16.6	0.2
3A	Hydrocal	1.55	120	25	18.7	15.7
3B	Hydrocal	1.55	225	25	17.6	15.9
3C	Hydrocal	1.55	225	25	17.6	16.0
4	Hydrocal	1.55	120	50	41.0	36.7
4A	Hydrocal	1.55	225	50	41.0	38.3
5	Hydrocal	1.55	120	70	64.1	65.7
6	Hydrocal	1.55	120	60	54.8	62.5
7	Hydrocal	1.55	120	57	53.0	61.6
7A	Hydrocal	1.55	120	53	53.0	NA
8	Hydrocal	1.55	60	100	91.8	97.2
9	Hydrocal	1,55	120	100	90.9	99.4
10	Hydrocal	1.55	60	86	79.6	90.2
10A	Hydrocal	1.55	120	86	79.6	89.7
11	Hydrocal	1.55	120	71	66.8	NA
11A	Hydrocal	1.55	60	71	66.8	74.3
12	Diesel	1.55	60	100	89.0	95.5
12A	Diesel	1,55	120	100	89.0	95.6
13	Diesel	1.55	60	85	77.4	85.6
13A	Diesel	1.55	120	85	77.4	85.5
14	Diesel	1.55	60	71	68.4	68.5
14A	Diesel	1.55	120	71	68.4	68.5
15	Diesel	1.55	120	50	52.8	44.2
15A	Diesel	1.55	60	50	52.8	40.6
16	Diesel	1.55	120	0	2.8	0.9
16A	Diesel	1.55	60	0	2.8	-0.6
17	Diesel	1.55	225	25	22.0	19.6
17A	Diesel	1.55	120	25	22.0	18.4
18	Diesel	1.55	225	50	41.7	36.5
18A	Diesel	1.55	120	50	41.7	36.0

Test #	Oil Type	Salinity (wt%)	Flow (gpm)	Target Oil Fraction (vol%)	Grab Sample Oil Fraction (vol%)	Oil Fraction Indicated by Sensor (vol%)
19	Hydrocal	3.6	0	0	NA	0.3
20	Hydrocal	3.6	225	25	23.4	24.2
20A	Hydrocal	3.6	120	25	23.4	23.0
21	Hydrocal	3.6	225	50	47.4	38.9
21A	Hydrocal	3.6	120	50	47.4	39.0
22	Hydrocal	3.6	225	70	71.8	51.0
22A	Hydrocal	3.6	120	70	71.8	51.8
23	Hydrocal	3.6	225	100	94.2	98.1
23A	Hydrocal	3.6	120	100	94.2	NA
24	Hydrocal	3.6	30	86	80.1	88.5
24A	Hydrocal	3.6	60	86	80.1	87.9
25	Hydrocal	3.6	30	70	64.9	74.8
25A	Hydrocal	3.6	120	70	64.9	74.6
26	Hydrocal	3.6	30	61	63.9	64.4
26A	Hydrocal	3.6	120	61	63.9	63.6
27	Hydrocal	3.6	120	61-41	47.1	43.5
28	Hydrocal	3.6	30	41	38.8	29.4
29	Diesel	3.6	60	0	0.3	2.1
30	Diesel	3.6	120	15	9.7	16.0
30A	Diesel	3.6	225	15	12.3	19.5
31	Diesel	3.6	30	15	14.5	29.8
31A	Diesel	3.6	120	15	14.5	NA
31B	Diesel	3.6	60	15	14.5	17.0
32	Diesel	3.6	60	50	39.5	40.9
32A	Diesel	3.6	120	50	39.5	41.7
32B	Diesel	3.6	225	50	39.5	41.5
33	Diesel	3.6	60	50	50.0	39.3
33A	Diesel	3.6	120	50	50.0	39.6
33B	Diesel	3.6	225	50	50.0	40.4
34	Diesel	na	60	100	93.6	97.7

Test #	Oil Type	Salinity (wt%)	Flow (gpm)	Target Oil Fraction (vol%)	Grab Sample Oil Fraction (vol%)	Oil Fraction Indicated by Sensor (vol%)
35	Diesel	3.6	60	71	71.4	77.3
35A	Diesel	3.6	120	71	71.4	77.9
36	Diesel	3.6	30	71	76.8	66.7
36A	Diesel	3.6	60	71	69.4	79.0
36B	Diesel	3.6	120	71	71.4	77.4

8.2.5 Estimation of Sensor's Accuracy

Figure 26 shows the comparison between true oil fraction obtained from analysis of grab samples, and oil fraction obtained from the sensor. The bottom part of this figure shows a correlation plot for both variables. The correlation is very significant across the entire range of oil-water mixtures. The top part of the figure shows the error of measurement defined as a difference between measured and true oil fractions.

Two of the data points included on Figure 26 should possibly be eliminated from data analysis since they represent tests with likely explainable abnormalities. Test 3 was carried out with significant amount of Hydrocal 300 oil introduced into the loop (25% target, 16.6% determined by sample analysis) while the sensor indicated near 0% oil content. This was likely caused by the small flow of 60 gpm which was not sufficient to disperse oil within the loop. Increased flows of 120 and 225 gpm used during tests 3A and 3B dispersed the oil and resulted in measured oil fractions of 15.7% and 15.9% respectively. Test 31 was carried out with diesel water mixture containing very large amount of entrained air which was noticed during mixture sampling. Table 5 presents the correlation coefficients between the true and measured oil fractions as well as the average and maximum errors of measurements. The analysis is carried out for two cases, with all data presented in Figure 26, and with tests 3 and 31 eliminated. Both cases produce excellent correlation coefficients above 0.96. The average errors in both cases is below 7% while the maximum error, detected in test 22, is below 21%. These values represent the estimation of sensor accuracy during the Ohmsett tests.

Table 5: Correlation coefficient between the measures and true oil fraction and error of measurement.

Data	Correlation coefficient between measured and true oil fraction	Average error	Maximum error
All data presented in Figure 26	0.9647	6.43%	+15.3% (Test 31) -20.8% (Test 22)
All data presented in Figure 26 minus Tests 3 & 31	0.9678	6.11%	+10.6% (Test 10) -20.8% (Test 22)

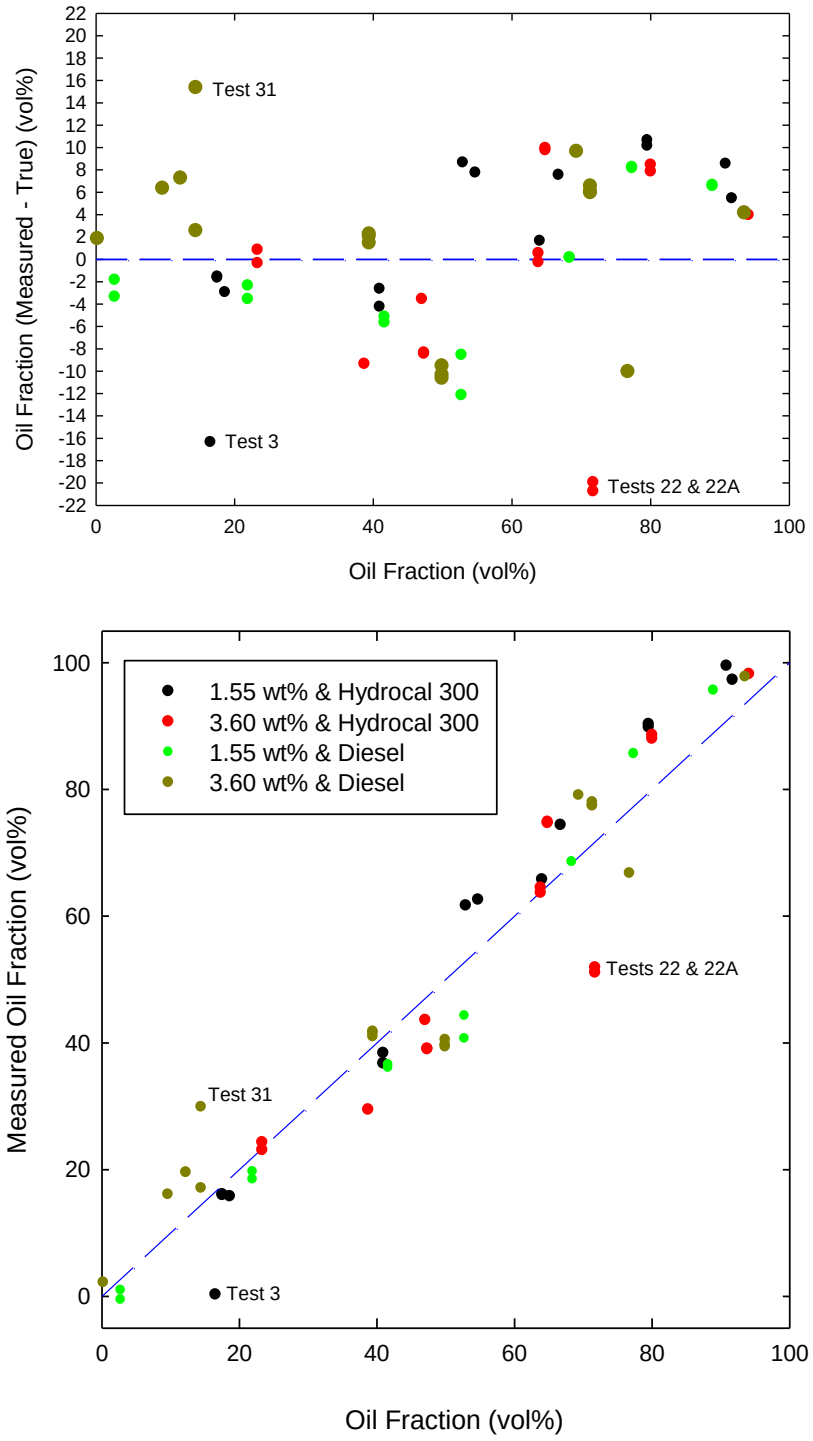

Figure 26. The distribution of errors for the oil content measurement (top) and the correlation between measured and true oil fractions (bottom).

8.2.6 Effects of Sensor Orientation and Flow Direction

Several tests were carried out with the same oil-water mixture and different sensor orientation. In the case of vertical orientation, both flow directions, up and down flows, were tested. Table 6 presents results obtained during these tests.

Table 6: Tests designed to probe effects of different sensor orientations.

Test #	Oil Type, Salinity	Sensor orientation, flow direction	Flow (gpm)	Target Oil Fraction (vol%)	Grab Sample Oil Fraction (vol%)	Oil Fraction Indicated by Sensor (vol%)
3B	Hydrocal 1.55wt%	Vertical, flow up	225	25	17.6	15.9
3C		Vertical, flow down	225	25	17.6	16.0
30A	Diesel 3.60 wt%	Vertical, flow down	225	15	12.3	19.5
31		Horizontal	30	15	14.5	29.8
31B		Horizontal	60	15	14.5	17.0
32	Diesel 3.60 wt%	Horizontal	60	50	39.5	40.9
32A		Horizontal	120	50	39.5	41.7
32B		Horizontal	225	50	39.5	41.5
33		Vertical, flow down	60	50	50.0	39.3
33A		Vertical, flow down	120	50	50.0	39.6
33B		Vertical, flow down	225	50	50.0	40.4

Tests 3B and 3C were carried out with 17.6% of Hydrocal 300 oil mixed with 1.55 wt% salinity water and with the sensor mounted vertically. Both tests produced essentially identical measured oil fractions indicating that the flow direction does not affect the sensor performance.

Tests 30A, 31, and 31B were carried out with 12-15% of diesel mixed with 3.60 wt% salinity water with the sensor mounted vertically and horizontally. The test 31 produced significantly different measured oil fraction, however, this was possibly due to low mixture flow of 30 gpm. Once flow was increased to 60 gmp in test 31B, the measured oil fraction reached 17.0% which is reasonably close to the 19.5% observed in test 30A.

Tests 32 to 33B were carried out with 40-50% of diesel mixed with 3.60% salinity water. Tests 32-32B were carried out with the sensor mounted horizontally, while test 33-33B had the sensor mounted vertically with the flow going downward. All six tests produced essentially identical

measured oil fractions in the 39.6 to 41.9% range. However, these tests are partially inconclusive since true oil fraction determined based on sample analysis experienced increased from 39.5 to 50.0%. This increase suggests that the change of sensor orientation from horizontal to vertical caused additional diesel dispersion which was not detected by the sensor.

The overall conclusion from the orientation and flow direction tests is that there is no significant evidence that these factors influence sensor performance. Clearly the air entrapment effects have much more significant effect on the sensor's measurement.

9. Conclusions and Next Steps

9.1 Conclusions

The novel enhanced oil recovery sensor developed in this project was demonstrated to work with a broad range of oils and water salinities and provide reliable oil fraction measurements for all oil concentrations including pure oil and pure water cases. The sensor's accuracy observed in both laboratory and Ohmsett tests is sufficient for oil recovery operations. This includes measurements in coarse oil-water mixtures and in emulsions. The sensor's construction as a flow through, internally open pipe, without any flow obstructions, the minimal power requirements, as well as relatively small sensor size and weight make this sensor practical and convenient to handle. The preferred sensor orientation is horizontal since it fits readily into typical oil recovery operations that usually involve horizontal petroleum hoses laying on a collection boat's deck.

The drawbacks of the current sensor implementation include: (1) its inability to distinguish air from oil, (2) the need to calibrate for different water salinities, and (3) the sensitivity of its algorithm in the transition region at the interface between oil- and water-rich mixtures. The issue of air present in the oil-water stream is the major one since "pumping empty" conditions are typical in oil recovery operations. The commercial sensor implementation must be able to work with air present in the pumped stream. The need for recalibration every time the water salinity changes is a nuisance for operators which, if possible, should be eliminated. The sensor algorithm's sensitivity to work in the transition region should be eliminated to further improve sensor's accuracy.

9.2 Next Steps in Sensor Development

Battelle will propose a second phase of the project which will address the drawbacks of the sensor while maintaining its positive characteristics. Specifically, the following will be proposed:

- The sensor's measuring approach and algorithm will be modified to allow for testing of oil-water streams containing a significant fraction of air and still correctly measuring the oil fraction in the oil-water mixture. This will allow for the sensor to be used in realistic oil recovery situations where "pumping empty" conditions are common. Furthermore, the modified sensor will be able to correctly measure averaged oil fraction of streams that are changing over time due to slug or wavy flow patterns, changing flow rates, or changing influent stream compositions.
- The sensor's algorithm will be upgraded to make it more accurate, robust, and capable of handling oil-water-air streams with different degrees of mixing and dispersion. This will allow for accurate oil fraction measurement including the transition region where the mixture changes between the oil-in-water and the water-in-oil types.

- The sensor will be upgraded to reduce and possibly eliminate the need for salinity calibration. The dialed in salinity mode will be maintained but the calibrated salinity mode will be replaced with a mode where the sensor analyzes collected data and constantly adapts to water salinity conditions. This upgrade will both simplify the sensor's operations and allow its use under changing salinity conditions.

The desired sensor characteristics that will be maintained will include: (1) flow through design without any internal flow obstructions, (2) horizontal sensor orientation, and (3) approximately the current sensor size and weight.

10. Appendix - Complete Experimental Results

10.1 Laboratory Tests of Dielectric Sensor

Tests were performed using the setup shown in Figure 3 with only the dielectric sensor attached to the 3-inch cavity pipe. The sensor used a 10 pF external capacitor and 3-turn, 0.5-inch diameter inductors that provided resonance frequencies in the 85-96 MHz range. The lowest mixer speed was selected based on a visual observation of mixing conditions that provided uniform mixing in both parts of the setup. The Hydrocal 300 oil and Hoops crude required about 500 RPM speed for uniform mixing. The Calsol oil and Pacific Energy A-38 crude, perhaps due to their high viscosity, required about 700 RPM to be uniformly mixed. The higher mixing conditions were tested at mixer speeds increased by about 200 RPM. Testing at both mixing speeds were performed in succession, with 1-2 minute equilibration time allowed after each change of mixer speed. Oil content of mixtures was changed by draining and adding appropriate amounts of water or oil. In most cases, the entire sequence of measurements for the given oil type and salinity was completed within several hours. In a couple of cases, a group of tests were spread out over two days. All tests were carried out using fresh oils, as received from BSEE.

10.1.1 Results Obtained with Hydrocal 300 Oil

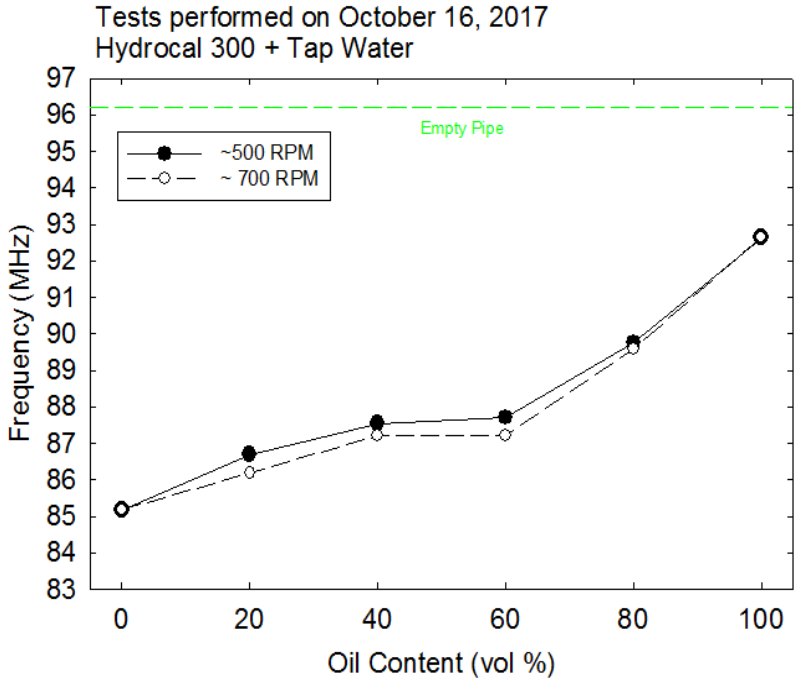

Figure 27. Dielectric sensor response Hydrocal 300 oil and tap water.

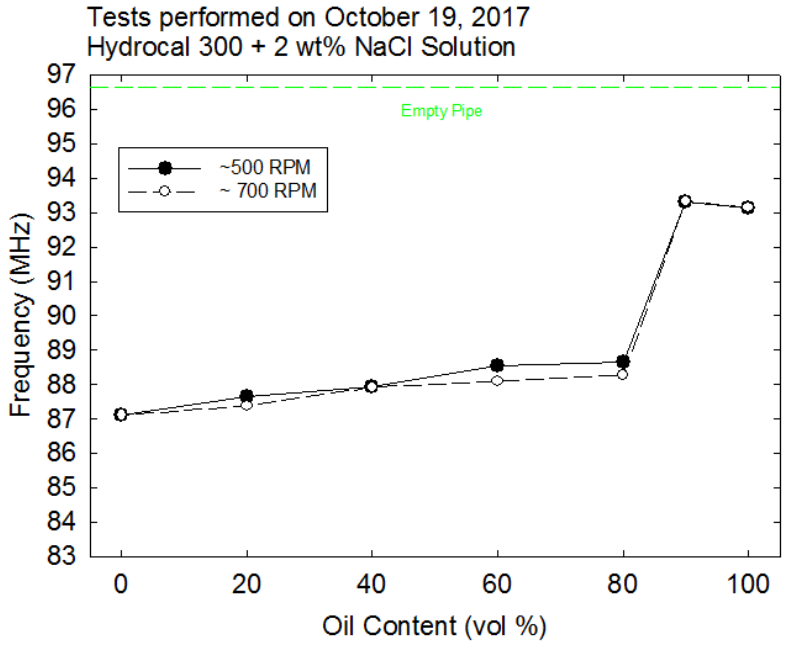

Figure 28. Dielectric sensor response for Hydrocal 300 oil and 2 wt% NaCl solution.

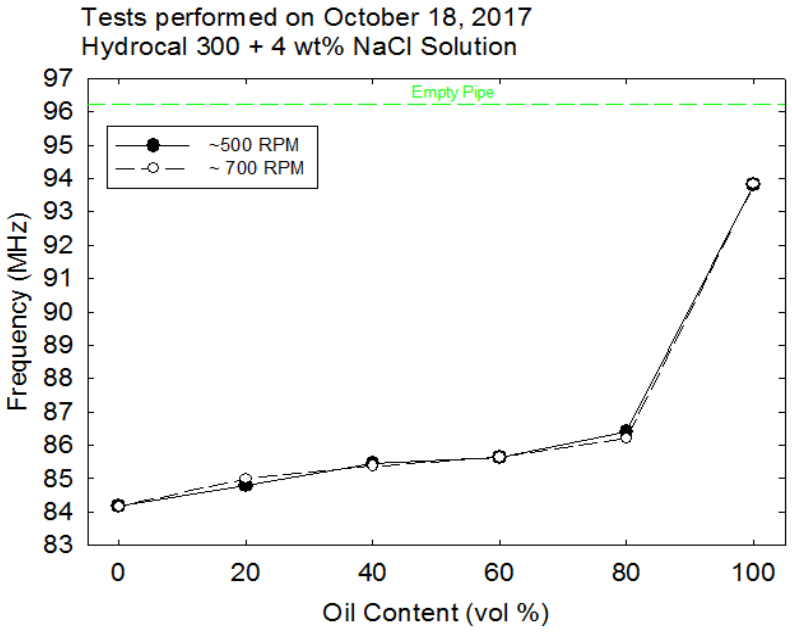

Figure 29. Dielectric sensor response Hydrocal 300 oil and 4 wt% NaCl solution.

10.1.2 Results Obtained with Calsol Oil

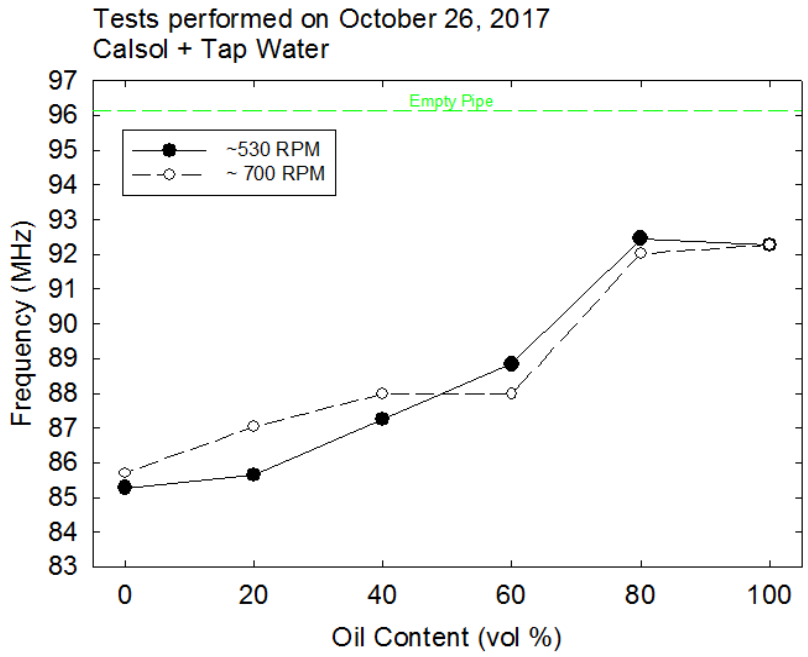

Figure 30. Dielectric sensor response Calsol oil and tap water.

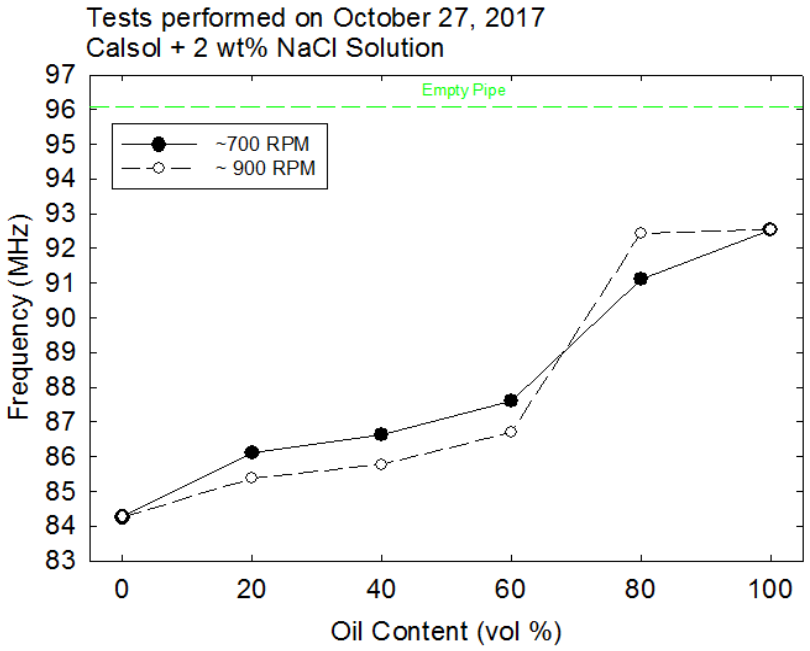

Figure 31. Dielectric sensor response Calsol oil and 2 wt% NaCl solution.

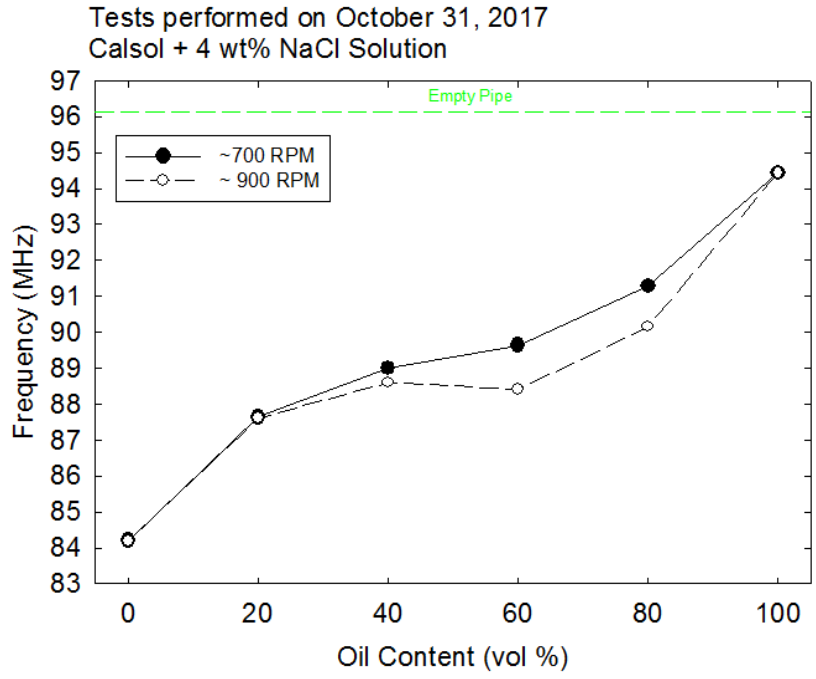

Figure 32. Dielectric sensor response Calsol oil and 4 wt% NaCl solution.

10.1.3 Results Obtained with Hoops Crude

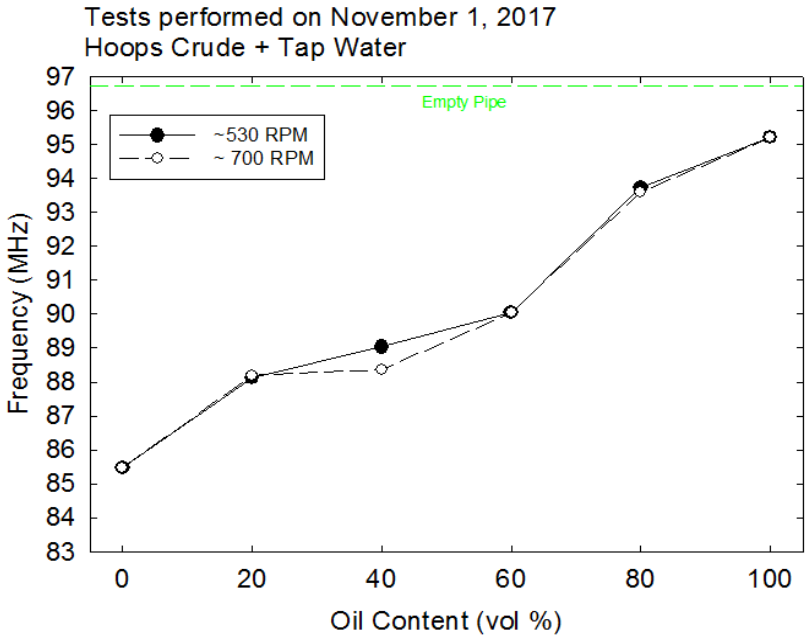

Figure 33. Dielectric sensor response Hoops crude oil and tap water.

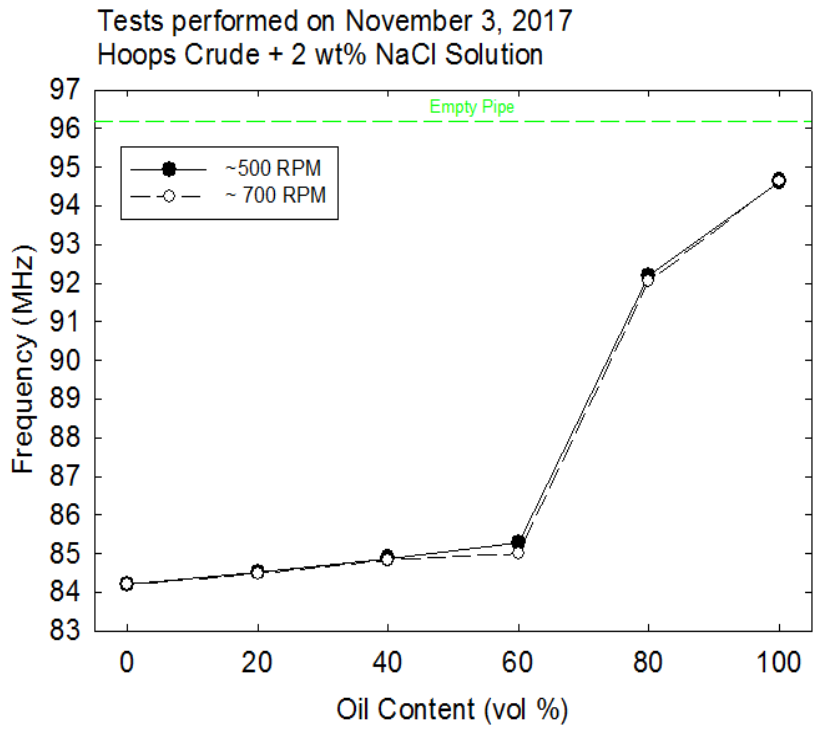

Figure 34. Dielectric sensor response Hoops crude oil and 2 wt% NaCl solution.

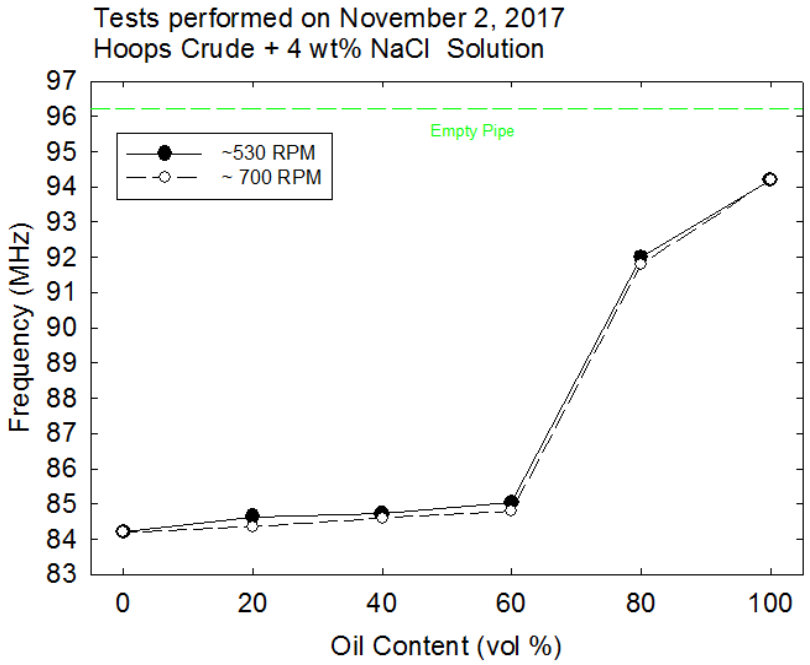

Figure 35. Dielectric sensor response Hoops crude oil and 4 wt% NaCl solution.

10.1.4 Results Obtained with Pacific Energy A-38 Crude

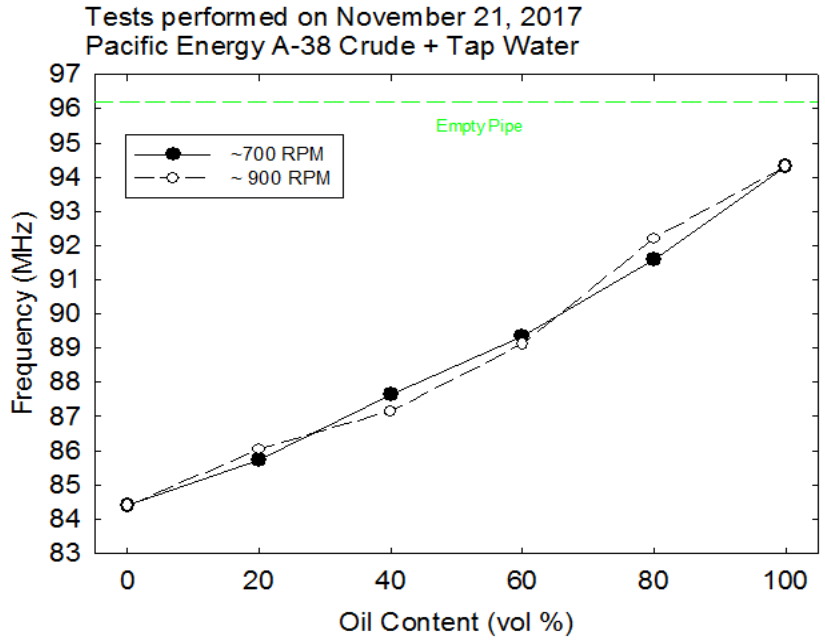

Figure 36. Dielectric sensor response Pacific Energy A-38 crude oil and tap water.

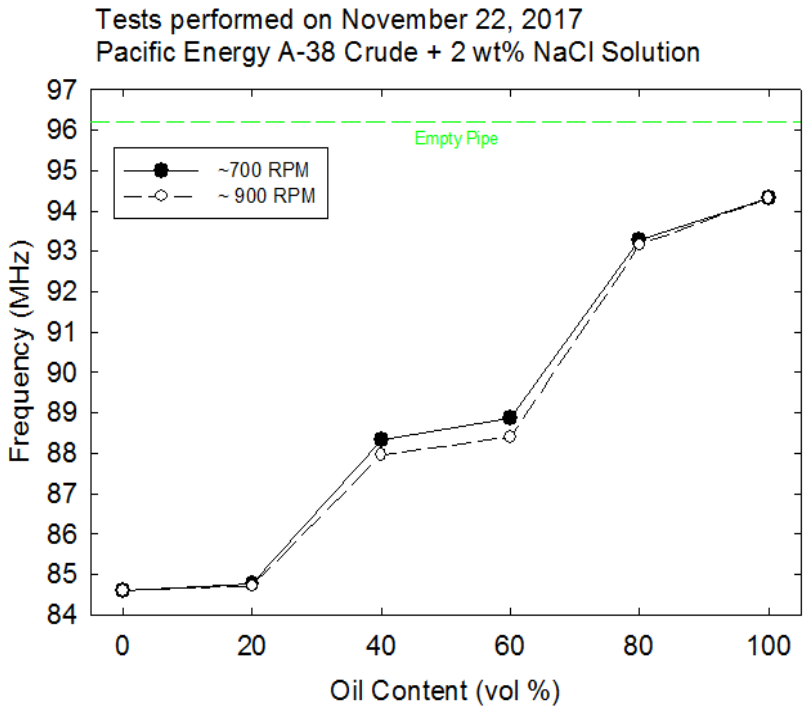

Figure 37. Dielectric sensor response Pacific Energy A-38 crude oil and 2 wt% NaCl solution.

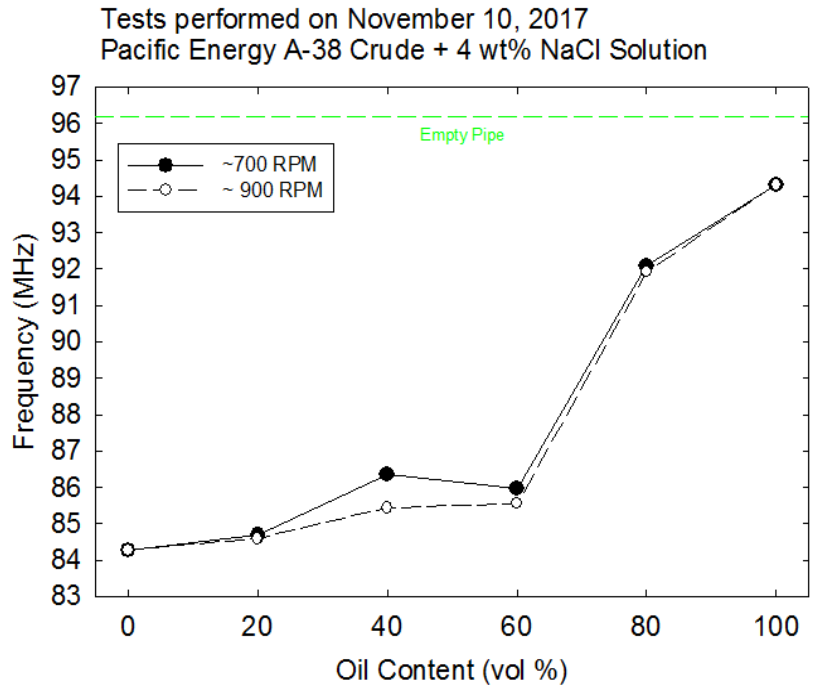

Figure 38. Dielectric sensor response Hoops crude oil and 4 wt% NaCl solution.

10.2 Laboratory Tests of Combined Dielectric and Eddy Currents Sensor

Tests were performed using the setup shown in Figure 3 with both types of sensors attached to the sensor pipe. The dielectric sensor used a 20-pF external capacitor and 5-turn, 0.5-inch diameter inductors that provided resonance frequencies in the 35-41 MHz range. The eddy current sensor's primary coil was constructed as a single loop of copper wire connected with a 200-pF ceramic capacitor. This configuration provided a resonance frequency of about 22 MHz. The secondary coil was constructed in the same way and placed 1 inch away from the primary coil.

The lowest mixer speed was selected based on a visual observation of mixing conditions that provided uniform mixing in both parts of the setup. Each oil concentration was tested at four mixer speeds - the minimum speed, and three higher speeds in 100 RPM increments. The dielectric and eddy current measurements were carried out sequentially using one SWR analyzer (AA-1400), which was connected via BNC quick connectors to the appropriate sensor. Most of the tests were carried out using fresh oils, as received from BSEE. One oil-salinity combination, Calsol and 2 wt% salinity, had to be performed partially with recycled oil due to insufficient supply of this type of fresh oil. The few data points collected with recycled Calsol oil closely followed the trends observed with fresh oils.

10.2.1 Results Obtained with Hydrocal 300 Oil

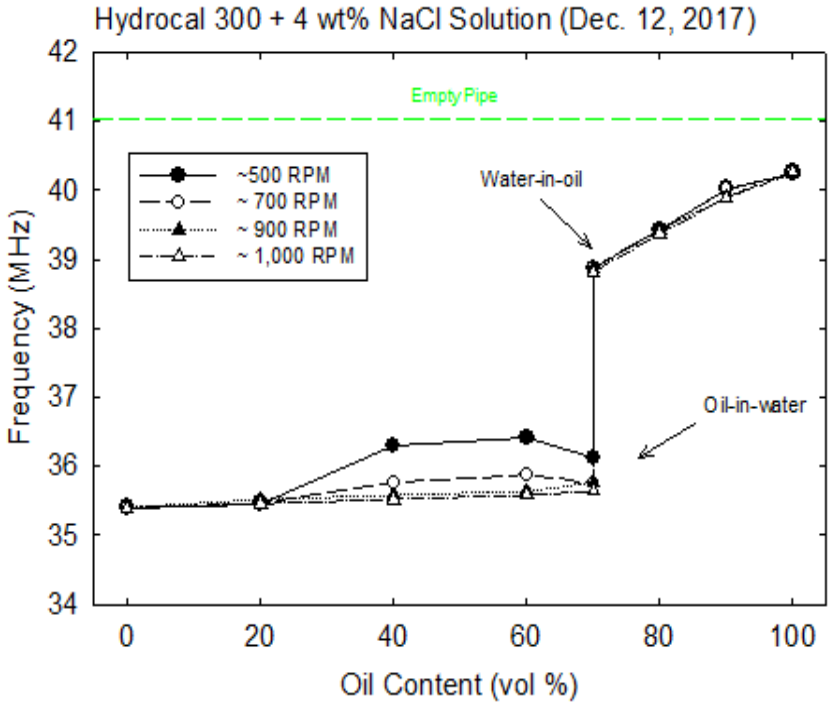

Figure 39. Dielectric sensor response for Hydrocal 300 oil and 4 wt% NaCl solution.

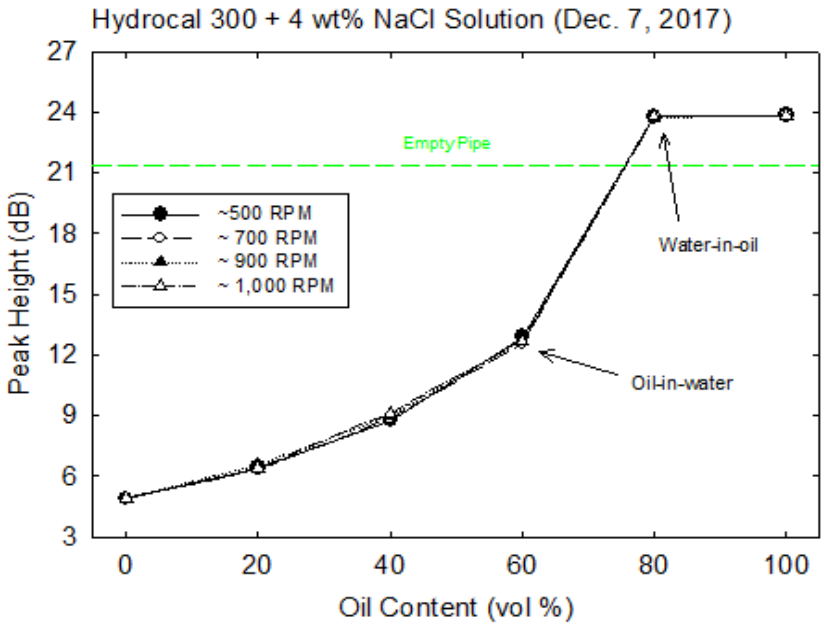

Figure 40. Eddy currents sensor response for Hydrocal 300 oil and 4 wt% NaCl solution.

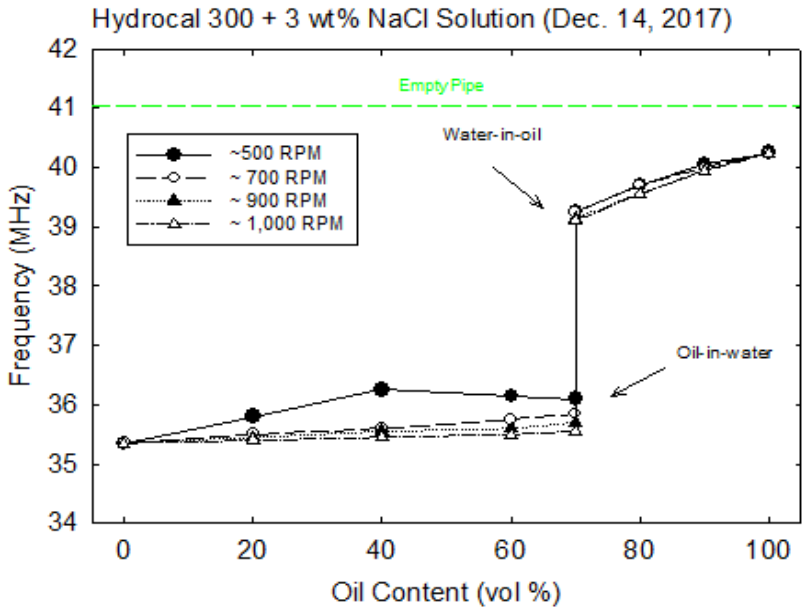

Figure 41. Dielectric sensor response for Hydrocal 300 oil and 3 wt% NaCl solution.

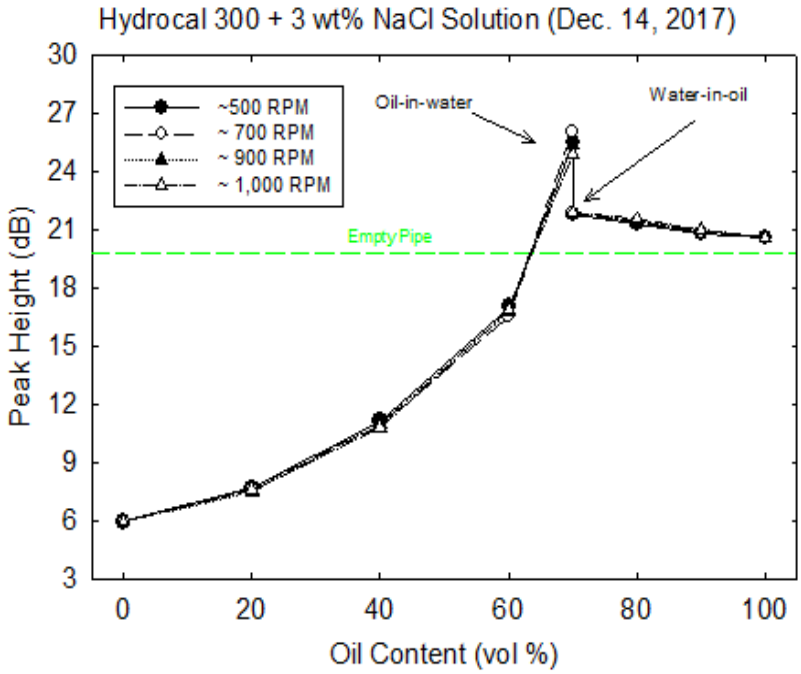

Figure 42. Eddy currents sensor response for Hydrocal 300 oil and 3 wt% NaCl solution.

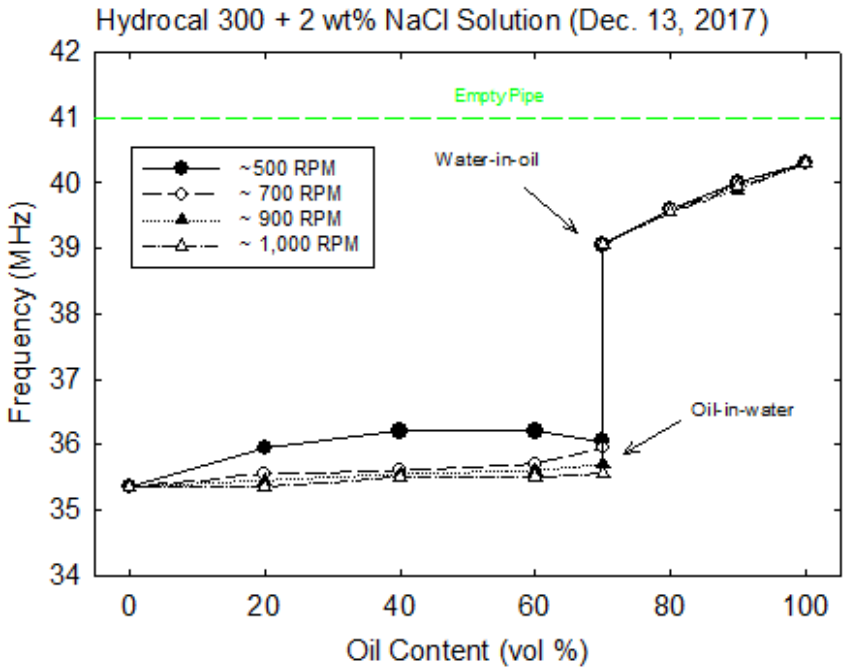

Figure 43. Dielectric sensor response for Hydrocal 300 oil and 2 wt% NaCl solution.

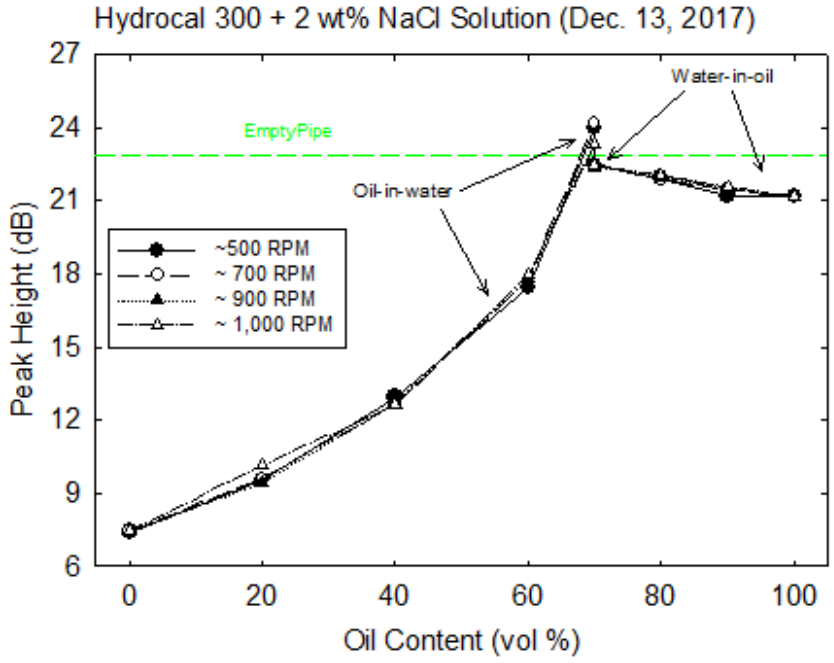

Figure 44. Eddy currents sensor response for Hydrocal 300 oil and 3 wt% NaCl solution.

10.2.2 Results Obtained with Calsol Oil

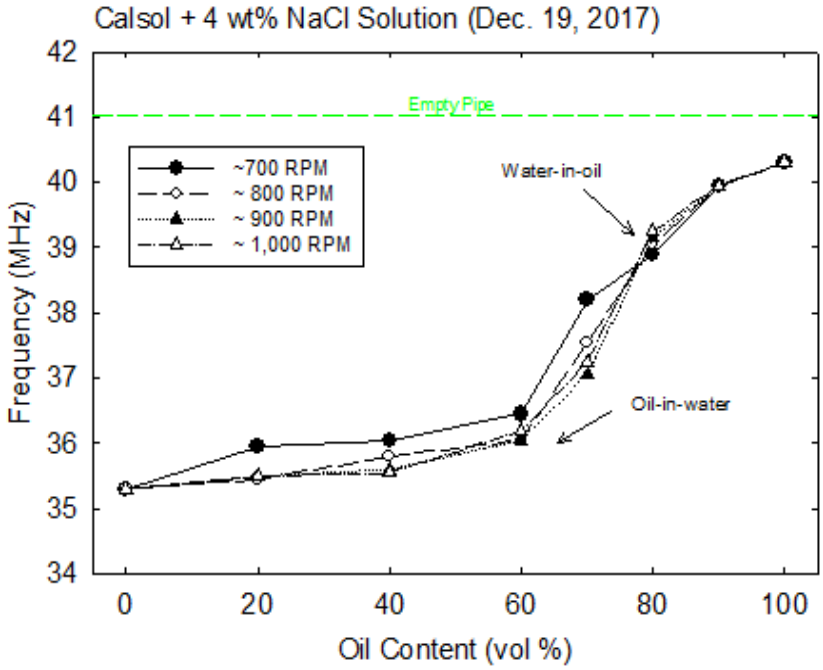

Figure 45. Dielectric sensor response for Calsol oil and 4 wt% NaCl solution.

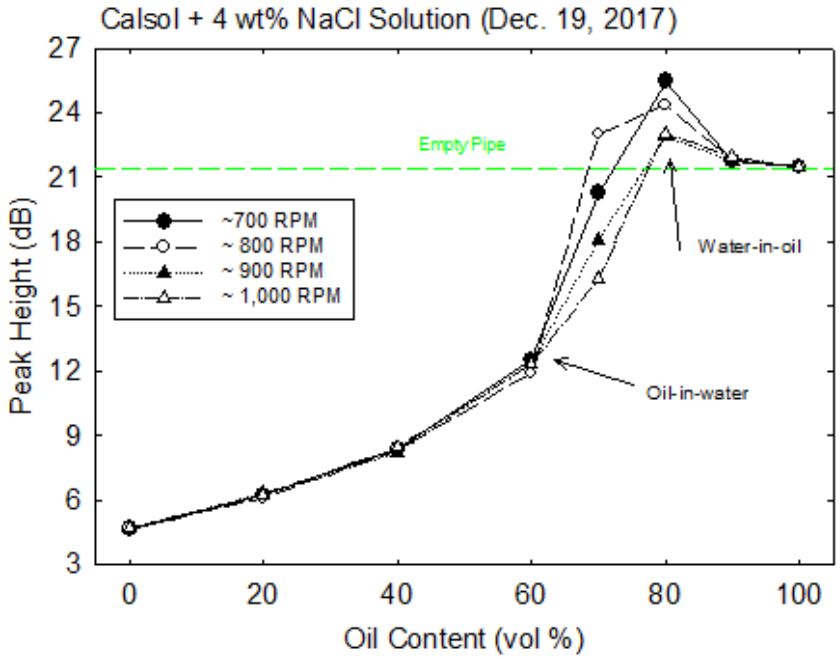

Figure 46. Eddy currents sensor response for Calsol oil and 4 wt% NaCl solution.

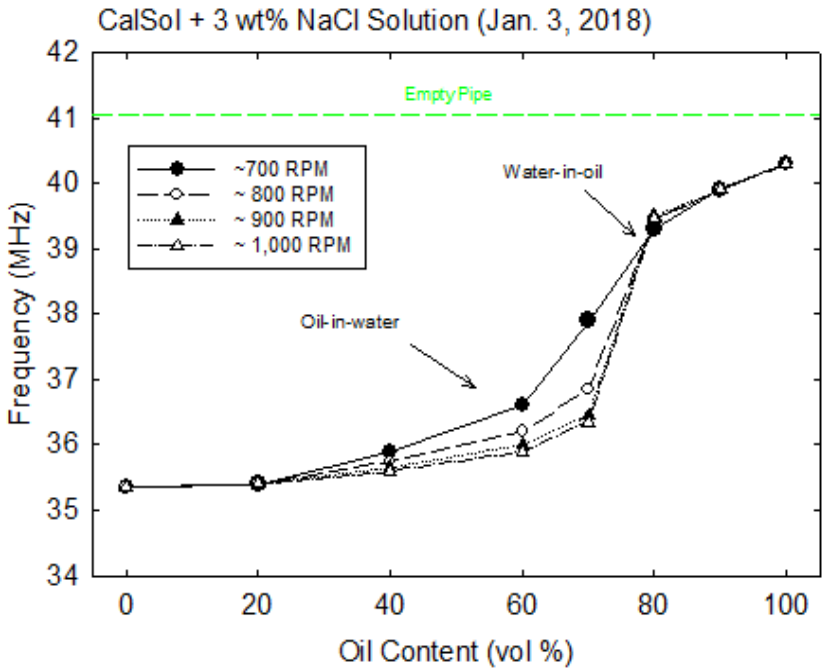

Figure 47. Dielectric sensor response for Calsol oil and 3 wt% NaCl solution.

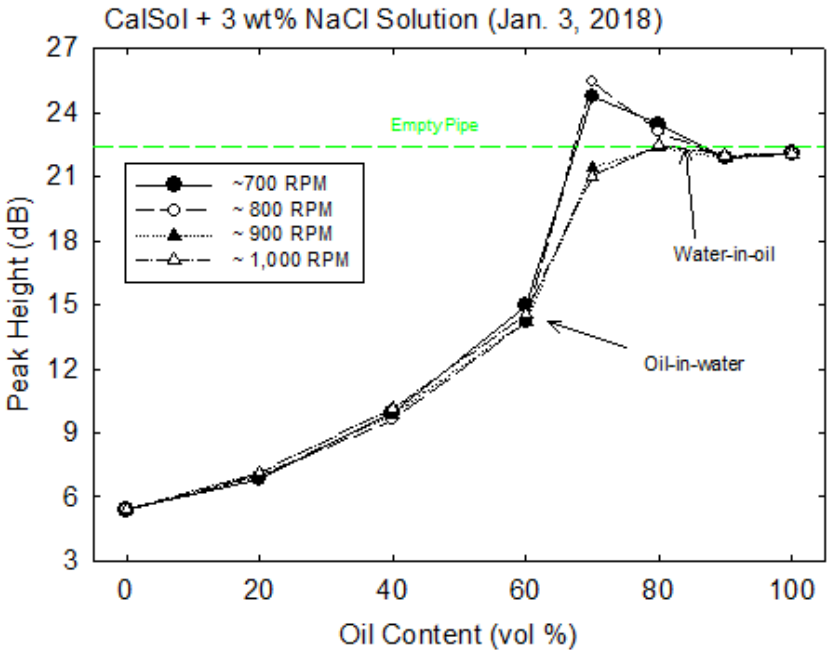

Figure 48. Eddy currents sensor response for Calsol oil and 3 wt% NaCl solution.

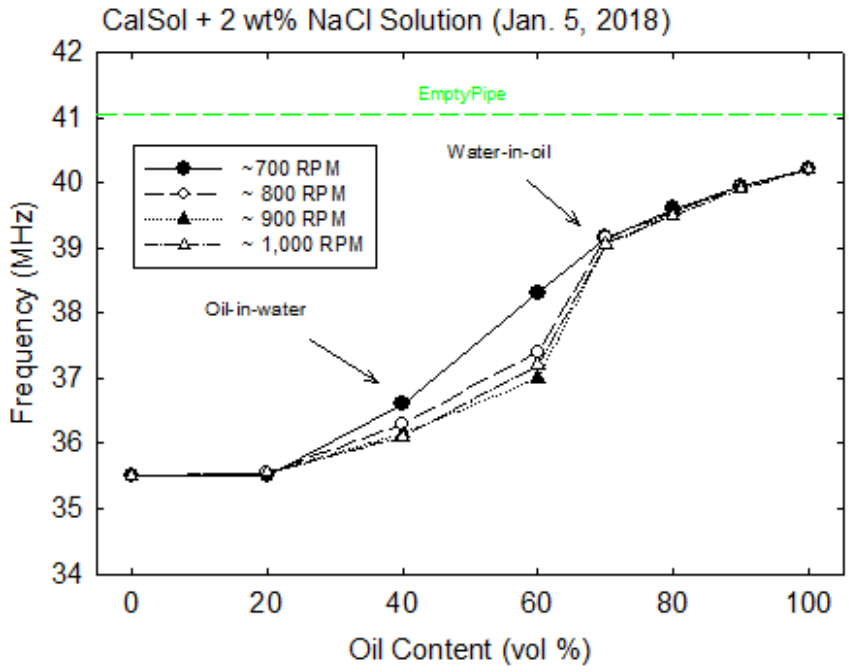

Figure 49. Dielectric sensor response for Calsol oil and 2 wt% NaCl solution.

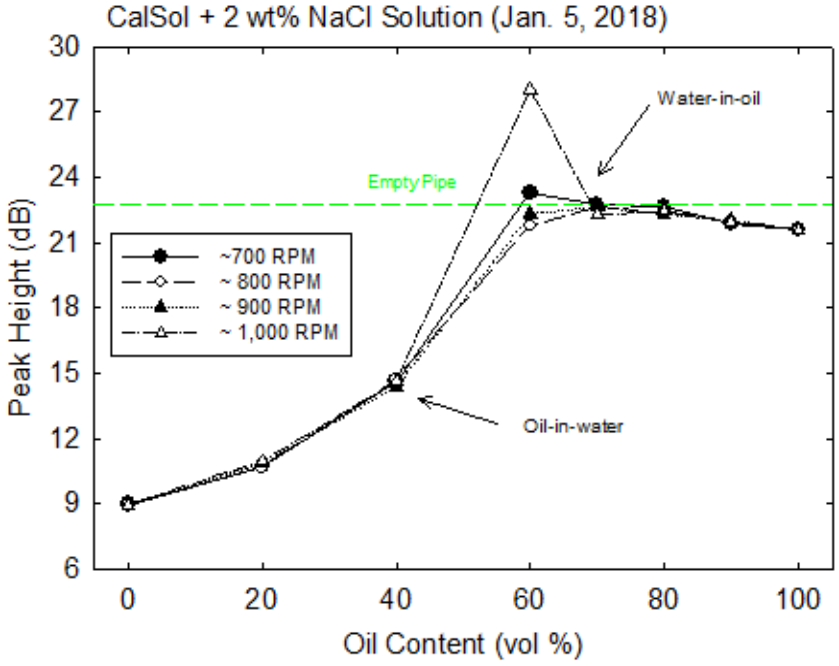

Figure 50. Eddy currents sensor response for Calsol oil and 3 wt% NaCl solution.

10.2.3 Results Obtained with Hoops Crude

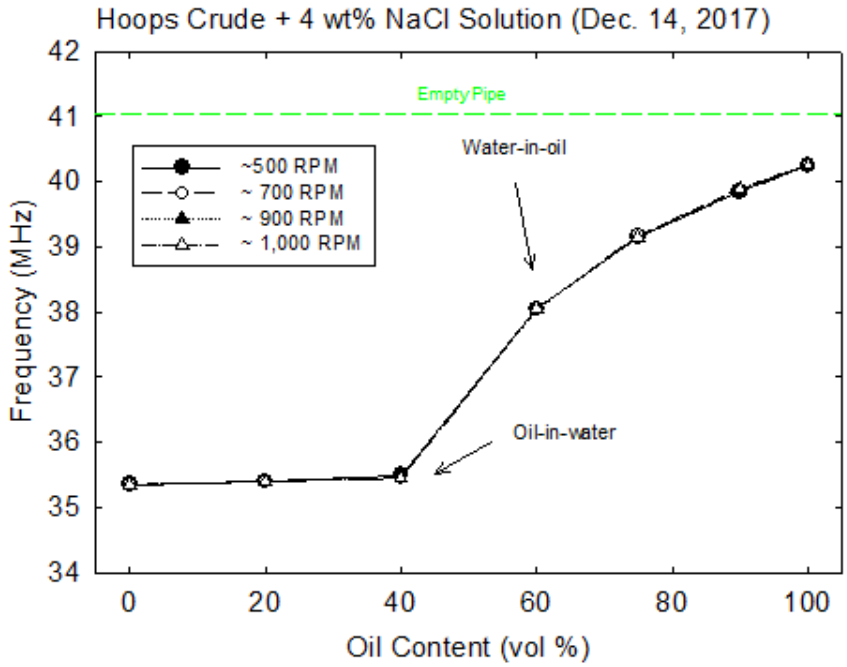

Figure 51. Dielectric sensor response for Hoops crude and 4 wt% NaCl solution.

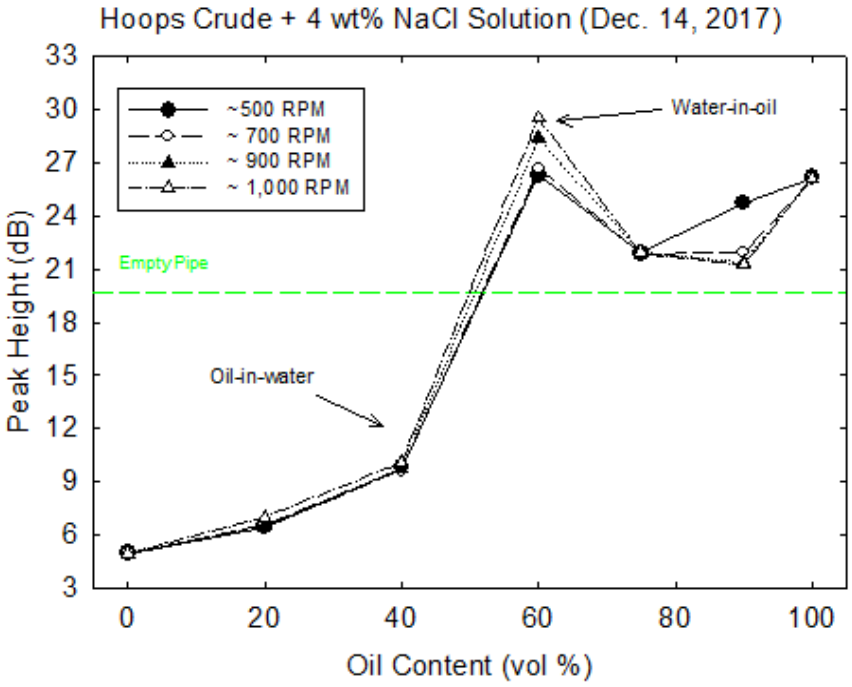

Figure 52. Eddy currents sensor response for Hoops crude and 4 wt% NaCl solution.

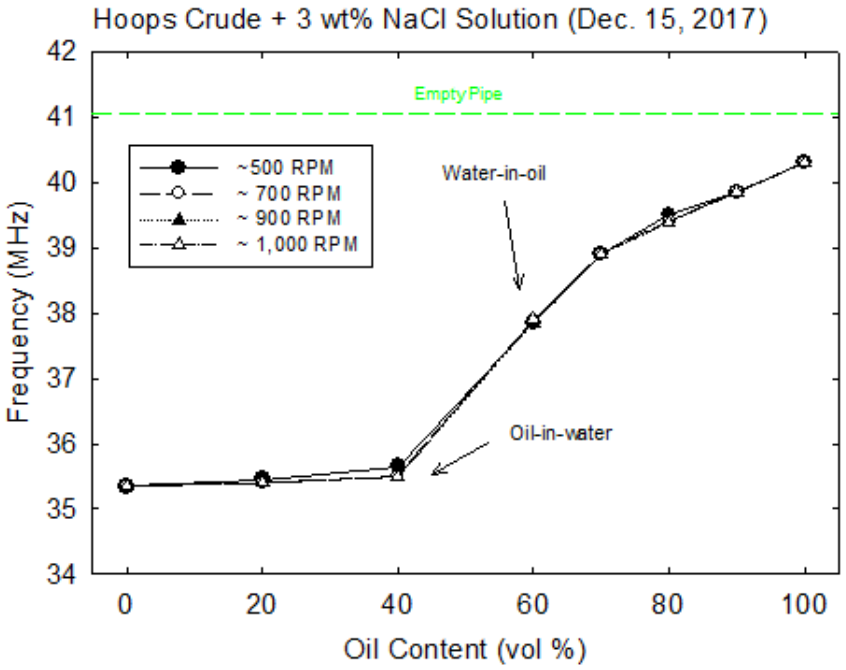

Figure 53. Dielectric sensor response for Hoops crude and 3 wt% NaCl solution.

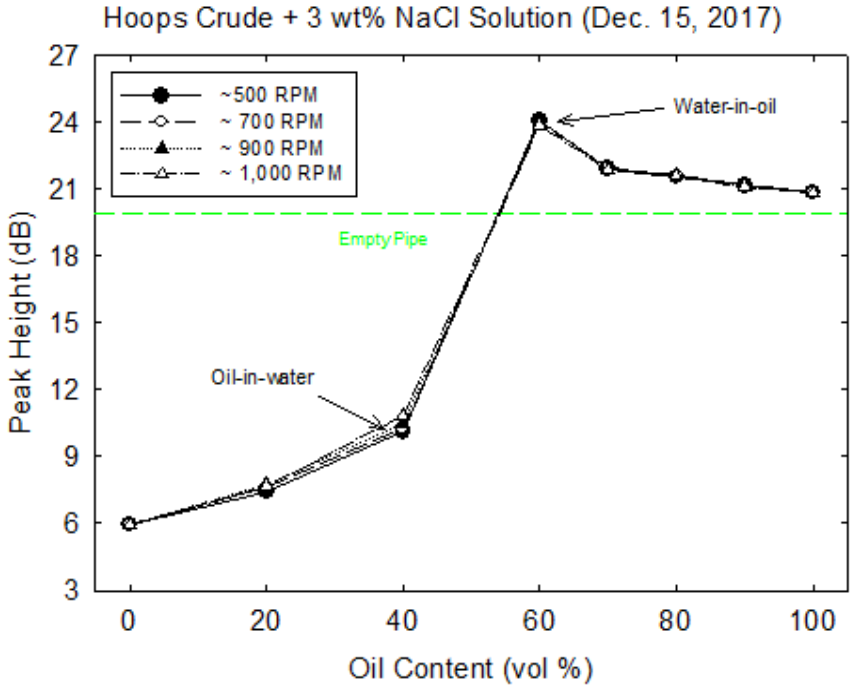

Figure 54. Eddy currents sensor response for Hoops crude and 3 wt% NaCl solution.

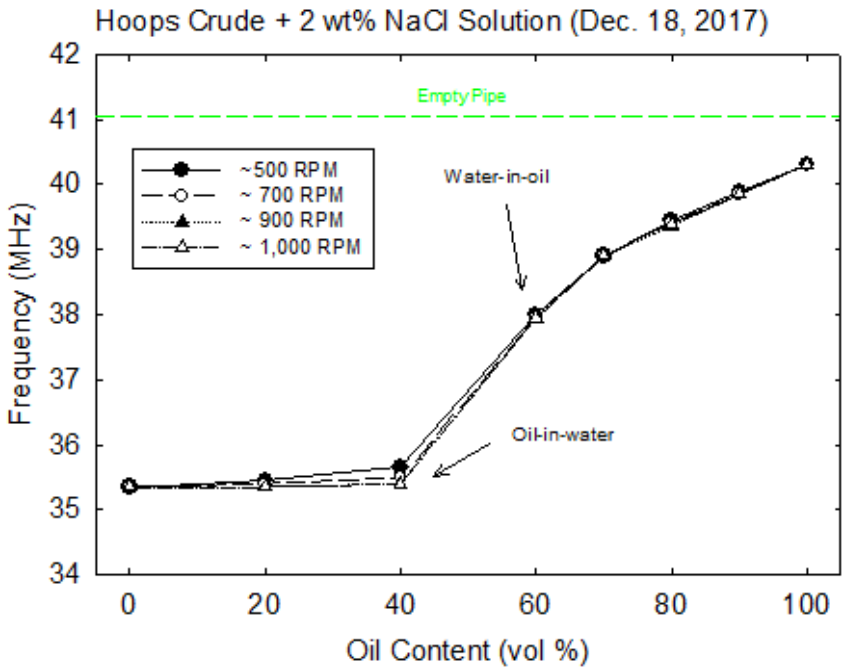

Figure 55. Dielectric sensor response for Hoops crude and 2 wt% NaCl solution.

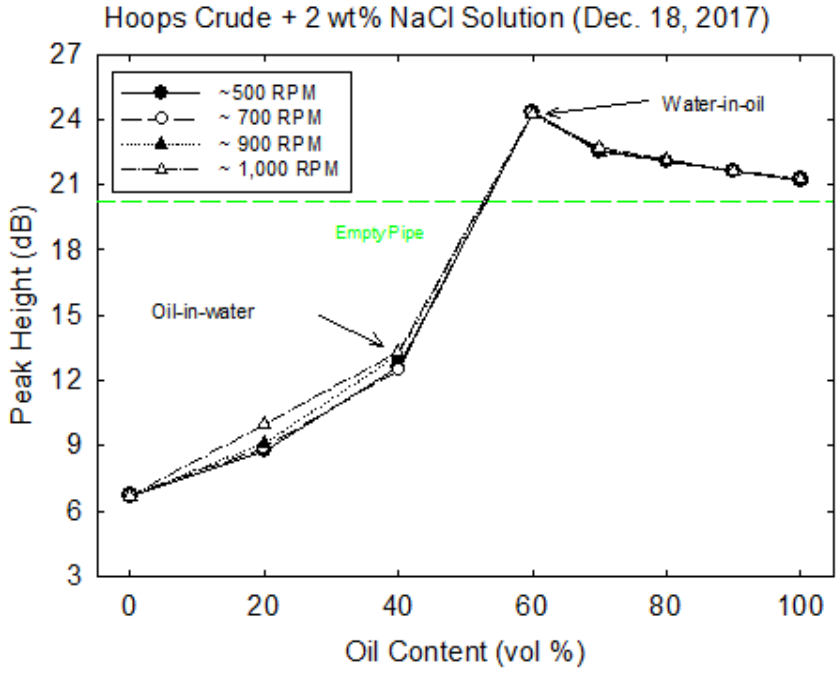

Figure 56. Eddy currents sensor response for Hoops crude oil and 3 wt% NaCl solution.

10.2.4 Results Obtained with Pacific Energy A-38 Crude

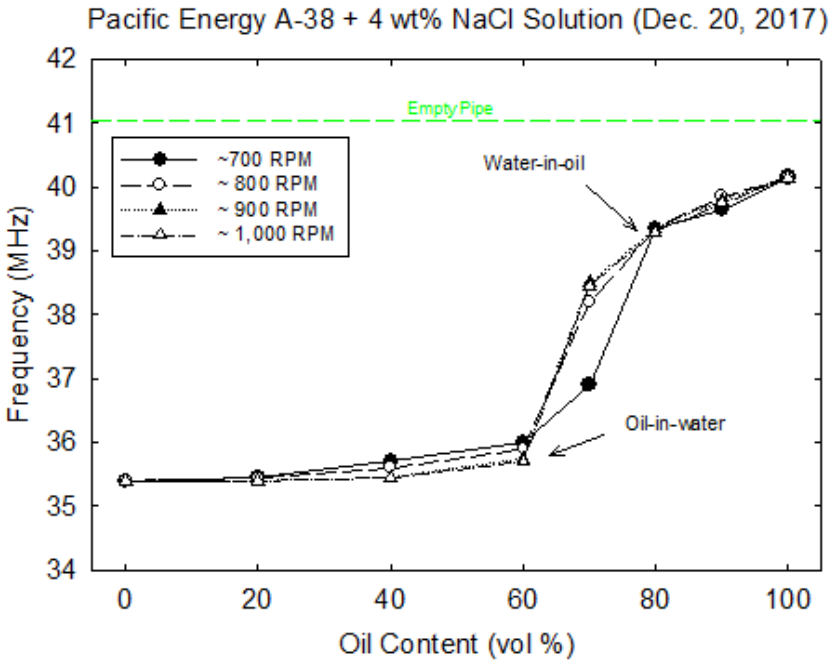

Figure 57. Dielectric sensor response for Pacific Energy A-38 crude and 4 wt% NaCl solution.

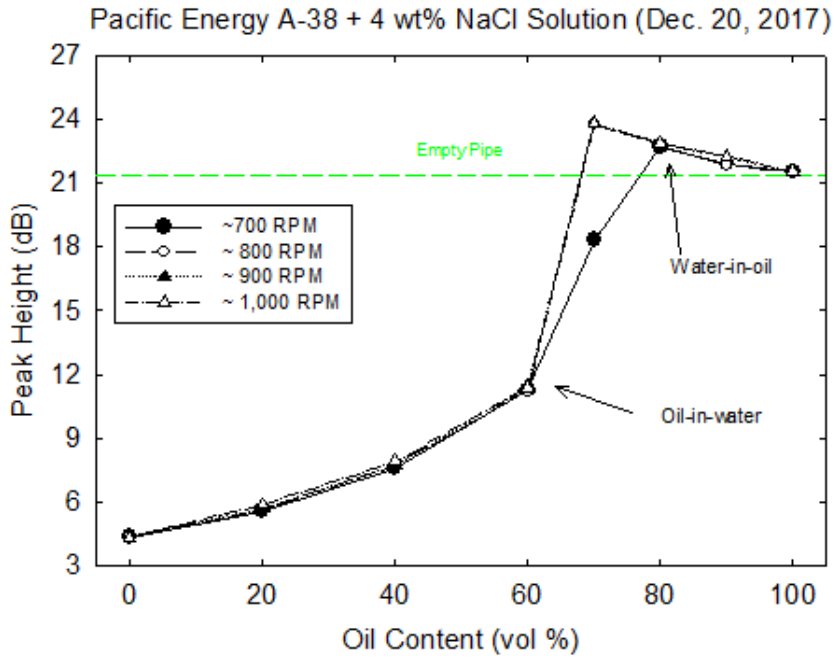

Figure 58. Eddy currents sensor response for Pacific Energy A-38 crude and 4 wt% NaCl solution.

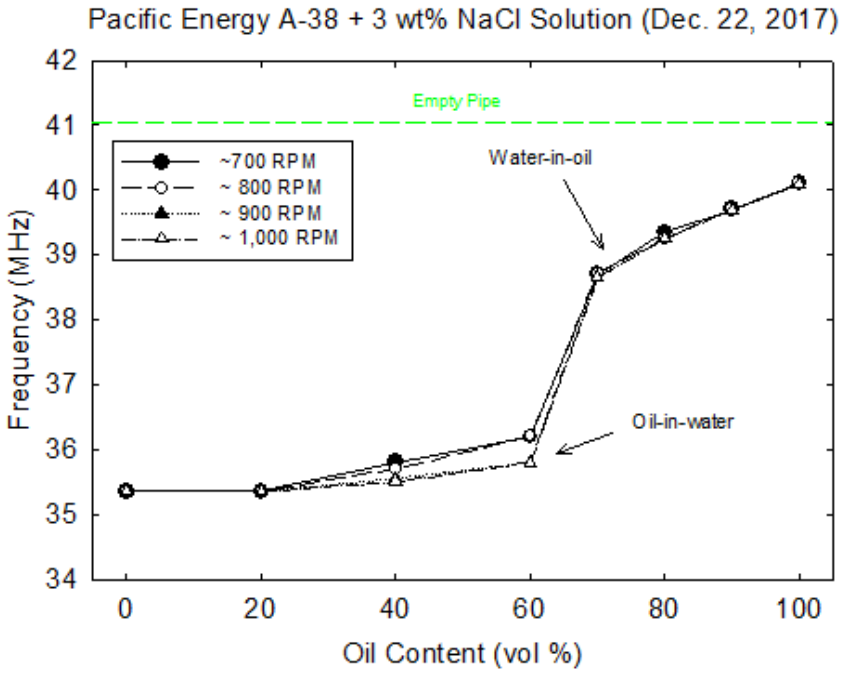

Figure 59. Dielectric sensor response for Pacific Energy A-38 crude and 3 wt% NaCl solution.

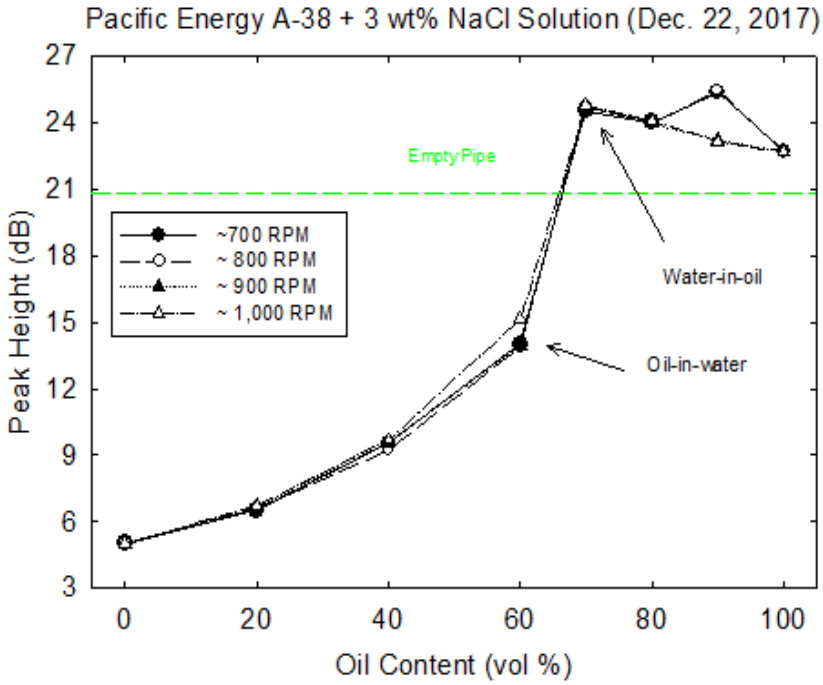

Figure 60. Eddy currents sensor response for Pacific Energy A-38 crude and 3 wt% NaCl solution.

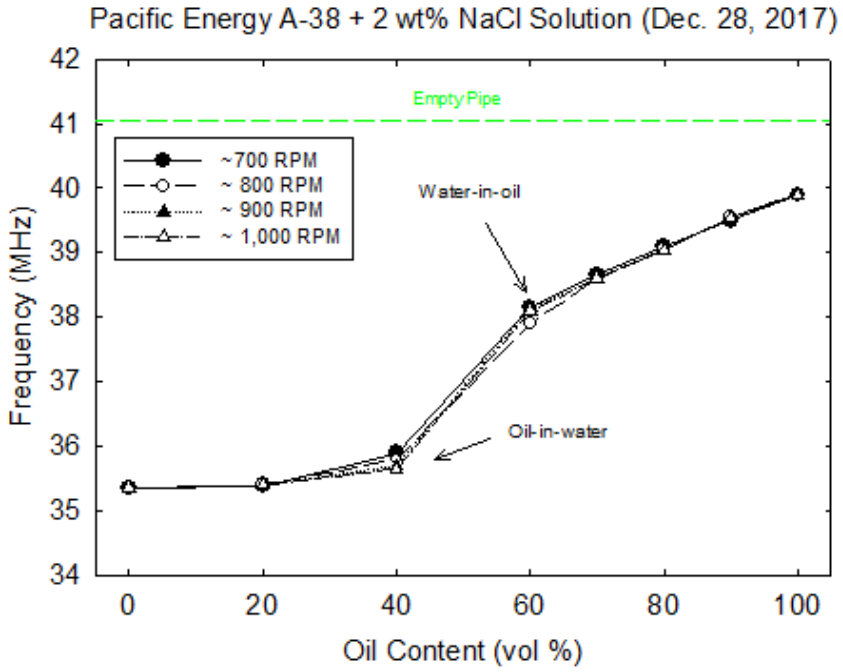

Figure 61. Dielectric sensor response for Pacific Energy A-38 crude and 2 wt% NaCl solution.

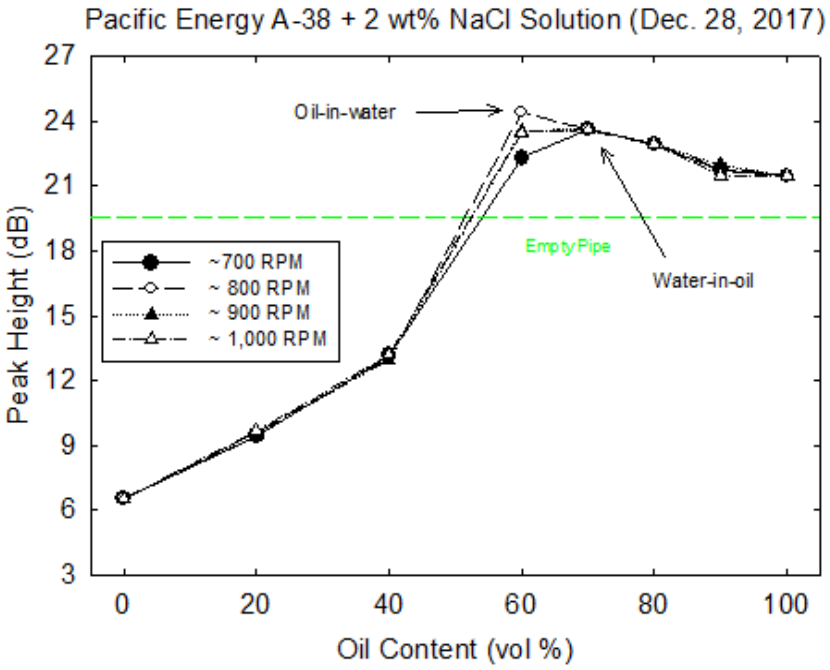

Figure 62. Eddy currents sensor response for Pacific Energy A-38 crude oil and 3 wt% NaCl solution.

10.3 Calibration and Tests of Prototype Sensor Prior to Ohmsett Testing

10.3.1 Tests with Saline Water (No Oil)

The eddy current sensor's peak size is a measure of electrical conductivity of tested oil-water mixtures and saline solutions. The sensor's algorithm needs to be calibrated to account for the peak size versus conductivity relation. The convenient method to perform this calibration is to test different salinities of water and different temperatures. Table 7 lists the tests performed for this purpose.

Table 7: Results obtained with 1-5 wt% Red Sea salt solutions (no oil).

Salinity (wt%)	Temperature (°C)	Electrical Conductivity (S/m)	Eddy Sensor	
			Frequency (MHz)	Peak Size (dB)
5.0	17.7	**6.168**	15.19	**5.07**
5.0	7	**4.791**	15.19	**6.33**
5.0	9.6	**5.114**	15.19	**6.04**
5.0	13.1	**5.560**	15.19	**5.59**
5.0	16.3	**5.981**	15.19	**5.34**
5.0	18.5	**6.276**	15.19	**5.16**
5.0	25.6	**7.266**	15.19	**4.61**
5.0	31	**8.057**	15.20	**4.29**
5.0	33.1	**8.374**	15.19	**4.20**
5.0	33.8	**8.480**	15.19	**4.13**
5.0	22.0	**6.757**	15.19	**5.27**
4.0	21.9	**5.518**	15.19	**5.99**
3.0	22.0	**4.270**	15.18	**7.16**
2.0	21.9	**3.033**	15.18	**9.10**
1.0	20.8	**1.754**	15.18	**12.32**
1.0	5.7	**1.124**	15.18	**15.52**
1.0	7.8	**1.218**	15.18	**14.83**
1.0	10.5	**1.335**	15.18	**14.20**
1.0	15	**1.524**	15.18	**13.25**
1.0	18.6	**1.668**	15.18	**12.55**
1.0	20.7	**1.750**	15.18	**12.16**
1.0	25.3	**1.922**	15.18	**11.43**
1.0	28.6	**2.040**	15.18	**11.02**

Salinity (wt%)	Temperature (°C)	Electrical Conductivity (S/m)	Eddy Sensor	
			Frequency (MHz)	Peak Size (dB)
1.0	31.6	**2.143**	15.18	**10.57**
1.0	34.4	**2.235**	15.18	**10.30**

Figure 63 shows the relation between eddy current peak size and electrical conductivity obtained from the data presented in Table 7 [11]. The values of conductivity were calculated based on water salinity and temperature. The relation is monotonic, close to inverse, and can be approximated by an inverse quadratic polynomial.

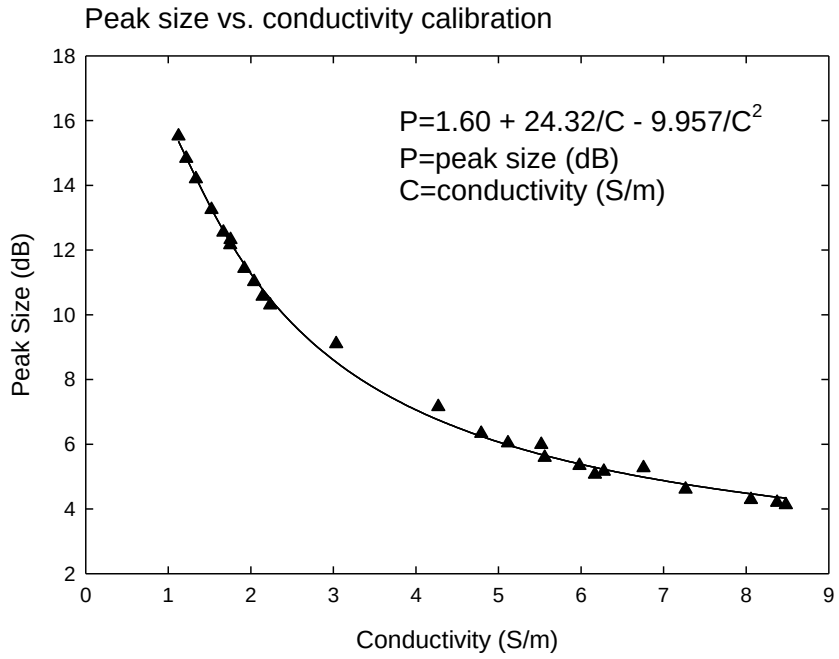

Figure 63. Eddy current sensor signal peak size as a function of water conductivity.

10.3.2 Tests with Oil-Water Mixtures

The bulk of the experiments carried out with the prototype sensor were tests with oil-water mixtures with different oil concentrations and various mixing conditions. Tables 8-11 presents data collected with four combinations of oil type and salinity used.

Table 8: Results obtained with Hydrocal 300 oil and 1 wt% Red Sea salt solution.

True Oil Fraction (%)	Stirrer Speed (rpm)	Eddy Sensor		Dielectric Sensor		Temperature (°C)
		Frequency (MHz)	Peak Size (dB)	Frequency (MHz)	Peak Size (dB)	
0	0	15.18	12.83	20.50	3.71	20.3
20	1700	15.18	15.79	20.50	5.52	20.3
20	1500	15.18	15.80	20.50	9.10	20.4
20	1000	15.18	15.57	20.50	5.05	20.4
20	700	15.18	15.43	20.50	6.11	20.4
40	1700	15.18	19.71	20.50	5.87	20.4
40	1500	15.18	19.73	20.50	5.29	20.4
40	1000	15.18	19.24	20.50	5.27	20.4
40	700	15.18	19.16	20.50	5.39	20.4
60	1700	15.18	26.47	20.50	7.61	20.5
60	1500	15.18	26.51	20.50	9.94	20.5
60	1000	15.18	26.72	20.89	12.13	20.5
60	700	15.18	28.97	21.61	14.70	20.5
73	1500	15.19	31.88	23.45	28.11	21.1
77	1500	15.19	31.34	23.57	25.74	21.0
77	1000	15.19	31.35	23.55	27.02	21.0
77	700	15.19	31.43	23.55	28.77	21.1
81	1700	15.19	31.55	23.70	28.89	20.9
81	700	15.19	31.33	23.70	29.76	20.9
90	1700	15.19	31.44	23.90	29.27	20.6
90	700	15.19	32.00	23.90	28.94	20.8
100	0	15.19	32.28	24.10	23.15	20.7

Table 9: Results obtained with Hydrocal 300 oil and 5 wt% Red Sea salt solution.

True Oil Fraction (%)	Stirrer Speed (rpm)	Eddy Sensor		Dielectric Sensor		Temperature (°C)
		Frequency (MHz)	Peak Size (dB)	Frequency (MHz)	Peak Size (dB)	
0	0	15.19	4.89	20.00	23.96	23.2
20	1700	15.18	6.37	20.36	24.10	22.8
20	1500	15.18	6.29	20.30	24.81	22.8
20	1000	15.19	6.23	20.16	24.59	22.8
20	700	15.18	6.16	20.34	25.63	22.8
40	1700	15.18	8.76	20.39	23.78	22.5
40	1500	15.18	8.64	20.20	22.21	22.4
40	1000	15.18	8.50	20.16	22.89	22.3
40	700	15.18	8.48	20.16	21.99	22.3
60	1700	15.18	12.75	20.30	19.78	22.2
60	1500	15.18	12.66	20.18	19.21	22.1
60	1000	15.18	12.50	20.16	19.54	22.1
60	700	15.18	12.53	20.16	19.11	22.1
72	1500	15.19	29.53	23.46	28.20	21.0
77	1500	15.19	29.26	23.58	29.86	21.1
77	1000	15.19	29.30	23.58	27.42	21.1
77	700	15.19	29.29	23.58	26.37	21.1
81	1500	15.19	29.17	23.75	24.16	21.1
81	1000	15.19	26.46	23.70	26.38	21.1
81	700	15.19	29.25	23.70	27.27	21.2
90	1700	15.19	29.34	23.88	29.74	21.1
90	1500	15.19	29.17	23.88	29.16	21.0
90	1000	15.19	29.20	23.88	29.20	21.0
100	0	15.19	29.62	24.06	30.70	21.2

Table 10: Results obtained with Hoops crude and 1 wt% Red Sea salt solution.

True Oil Fraction (%)	Stirrer Speed (rpm)	Eddy Sensor		Dielectric Sensor		Temperature (°C)
		Frequency (MHz)	Peak Size (dB)	Frequency (MHz)	Peak Size (dB)	
0	0	15.18	12.45	20.04	18.94	22.6
20	1500	15.18	15.14	20.05	16.68	22.4
20	1000	15.18	14.79	20.10	17.16	22.3
20	700	15.18	14.86	20.19	17.44	22.3
40	1500	15.18	18.75	20.10	14.31	22.1
40	1000	15.18	18.89	20.13	14.65	21.9
40	700	15.18	20.63	20.48	14.57	21.9
61	1500	15.18	29.69	22.20	15.18	21.8
61	1000	15.18	29.80	22.20	17.31	21.7
77	1700	15.19	29.22	23.40	25.85	20.8
77	1500	15.19	29.23	23.36	25.26	20.8
77	1000	15.19	29.06	23.34	26.91	20.8
81	1700	15.19	28.74	23.68	25.68	20.7
81	1500	15.19	28.85	23.64	26.17	20.7
81	1000	15.19	28.90	23.64	27.28	20.7
90	1700	15.19	28.94	23.88	37.55	20.6
90	1500	15.19	28.90	23.88	36.67	20.6
90	1000	15.19	28.93	23.88	35.89	20.6
100	0	15.19	29.35	24.06	34.00	20.6

Table 11: Results obtained with Hoops crude and 5 wt% Red Sea salt solution.

True Oil Fraction (%)	Stirrer Speed (rpm)	Eddy Sensor		Dielectric Sensor		Temperature (°C)
		Frequency (MHz)	Peak Size (dB)	Frequency (MHz)	Peak Size (dB)	
0	0	15.19	5.01	19.98	23.57	22.4
20	1500	15.18	6.80	19.98	22.29	22.3
20	1000	15.18	6.63	19.98	22.07	22.3
20	700	15.18	6.62	19.98	21.66	22.3
40	1700	15.18	11.98	19.98	18.75	22.0
40	1500	15.18	11.81	20.02	18.69	21.9
40	1000	15.18	11.60	20.04	19.21	21.9
40	700	15.18	11.49	20.04	19.42	21.9
60	1700	15.18	25.22	22.68	27.49	21.7
60	1500	15.18	25.24	22.68	34.45	21.6
60	1000	15.18	25.32	22.68	39.30	21.6
60	700	15.18	25.24	22.68	30.63	21.6
73	1500	15.19	25.13	23.34	39.21	20.7
73	1000	15.19	25.09	23.34	33.10	20.8
73	700	15.19	25.19	23.34	34.67	20.8
81	1500	15.19	25.17	23.64	30.72	20.6
81	1000	15.19	25.28	23.64	31.06	20.6
81	700	15.19	25.20	23.63	31.18	20.6
90	1700	15.19	24.96	23.88	34.44	20.4
90	1500	15.19	25.07	23.88	34.15	20.4
90	1000	15.19	25.10	23.88	33.22	20.4
90	700	15.19	25.07	23.88	33.14	20.4
100	0	15.19	25.02	24.06	27.27	20.7

10.3.3 Oil-Water Mixture Test with Changing Temperature

The eddy currents part of the oil fraction measurement is sensitive to electrical conductivity of water, which is a strong function of temperature. The sensor's algorithm is designed to use mixture temperature, measured by a temperature sensor, to determine the correct oil fraction regardless of temperature. To test this part of the algorithm, a mixture containing 40 % of Hydrocal 300 oil and 60 % of 3 wt% salt solution was tested at different temperatures. Table 12 presents this part of the data.

Table 12: Results obtained with 40 % Hydrocal 300 mixture with 3 wt% solution at different temperatures.

Temperature (°C)	Eddy Sensor		Oil Fraction Indicated by Sensor (vol%)
	Frequency (MHz)	Peak Size (dB)	
8.3	15.18	14.33	**37.9**
12.7	15.18	13.81	**39.9**
15.1	15.18	13.90	**40.8**
20.5	15.19	13.99	**44.0**
24.7	15.18	13.09	**42.9**
28.1	15.18	13.01	**44.0**
35.2	15.18	12.60	**45.6**

Figure 64 shows the oil fraction, indicated by the sensor, as a function of mixture temperature. As shown, the oil fraction remains relatively constant within the entire range of tested temperatures, indicating that the temperature correction part of the algorithm works correctly. The small increase of oil fraction with temperature needs to be investigated in the next phase of the project.

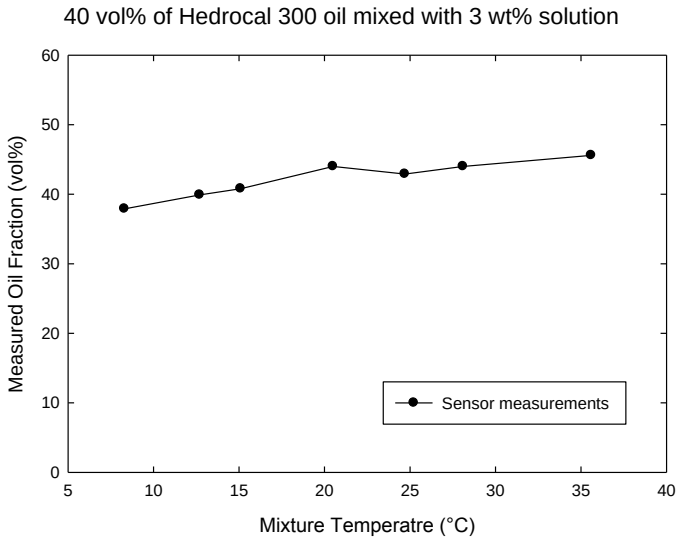

Figure 64. Measured oil fraction for a mixture containing 40% of oil as a function of temperature.

10.4 Tests Performed at Ohmsett

Figures 65-127 show a time dependence of measured oil fraction as recorded by the sensor. These plots have different appearance due the different nature of sensor algorithms. The dielectric sensor produces a step-like output since it compares a finite number of response frequencies and calculates the oil fraction based on the frequency which produce maximum response. The eddy current sensor produces a continuous peak size signal, which generates continuous range of oil fraction values that have noisy appearance. Outputs of both signals are affected by the time averaging function which was applied during some cases. For instance, test

4A (Figure 72) had the time averaging constant of 30 seconds applied in the middle of the data collection period. The time averaging function has no effect on the average oil fraction values shown in Tables 2 and 5 and in Figure 26. All data presented were collected using the calibrated sensor mode with the sensor being calibrated each time pure saline water was introduced.

Table 13 lists tests where abnormal test conditions were observed, with the description of problem given.

10.4.1 Results obtained with 1.5 wt% water and Hydrocal 300 Oil

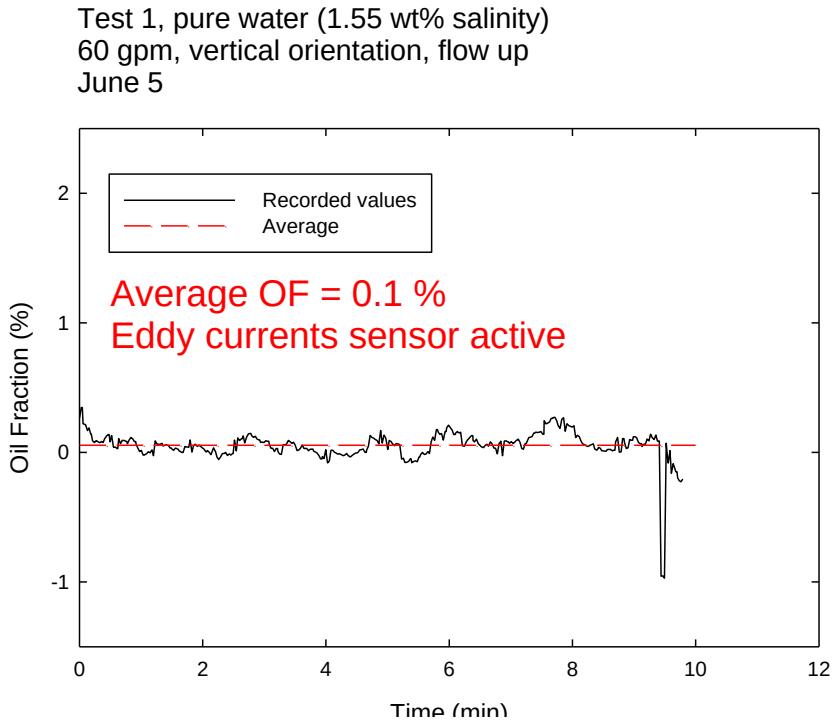

Figure 65. Test 1 - measured oil fraction as a function of time.

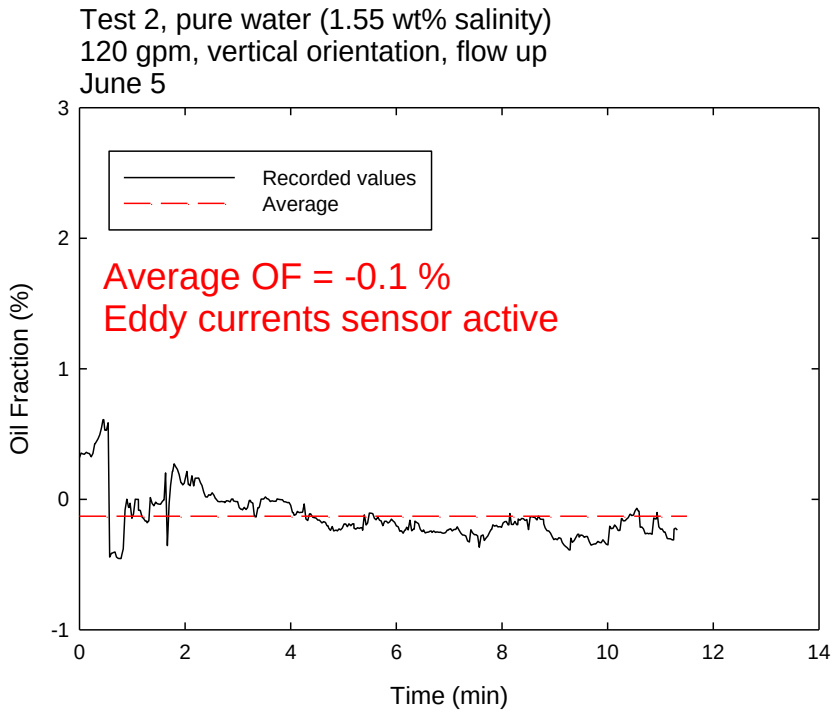

Figure 66. Test 2 - measured oil fraction as a function of time.

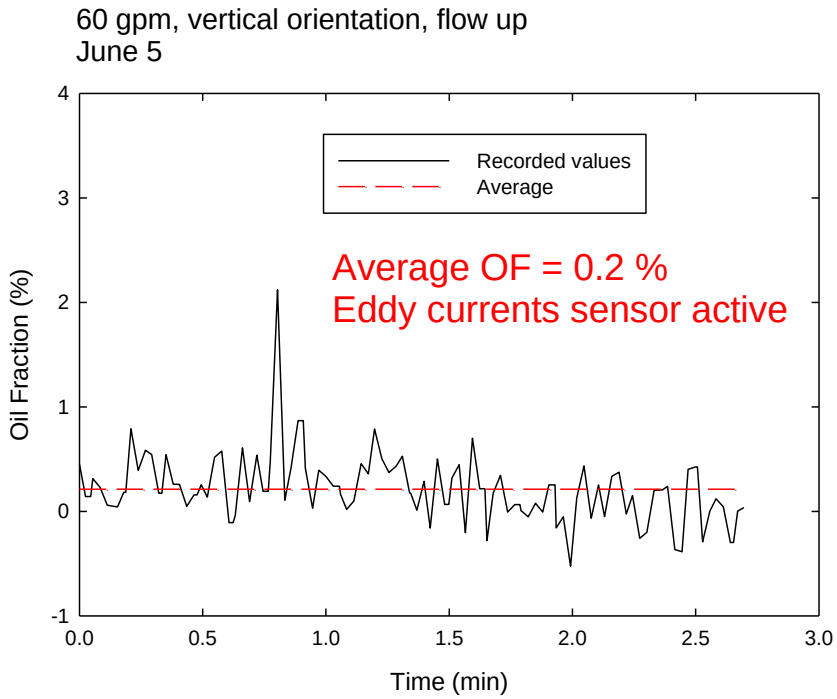

Figure 67. Test 3 - measured oil fraction as a function of time.

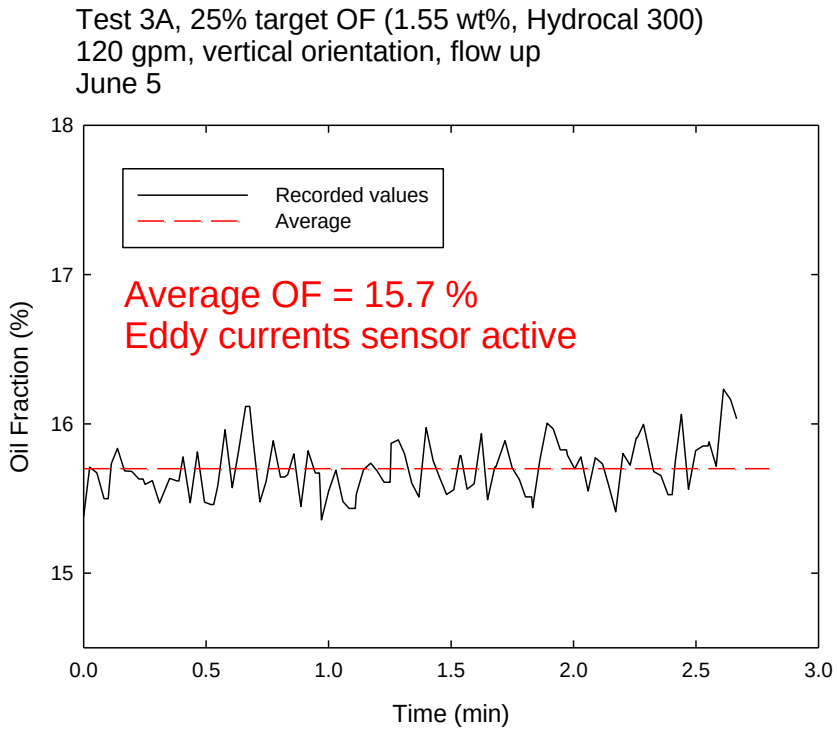

Figure 68. Test 3A - measured oil fraction as a function of time.

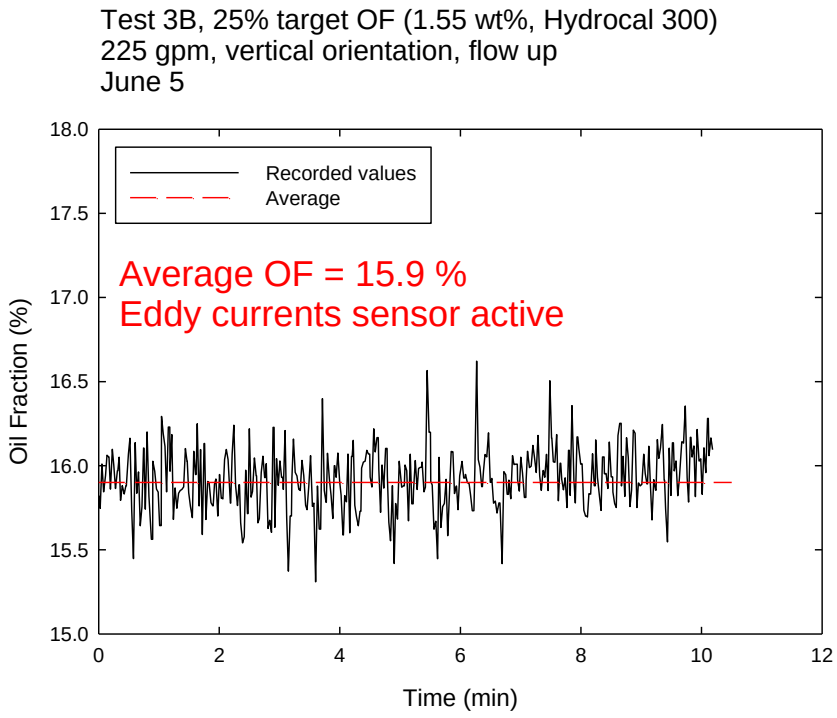

Figure 69. Test 3B - measured oil fraction as a function of time.

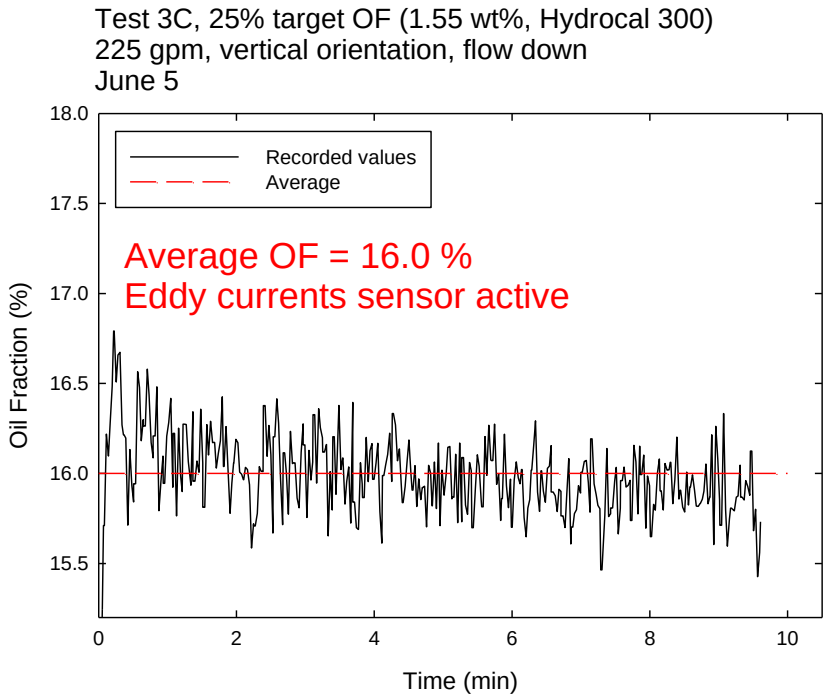

Figure 70. Test 3C - measured oil fraction as a function of time.

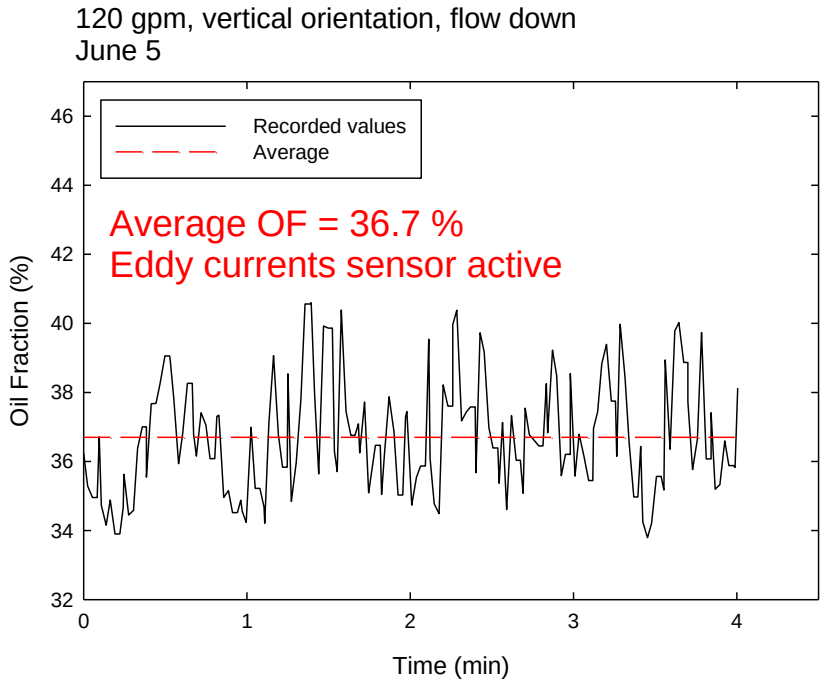

Figure 71. Test 4 - measured oil fraction as a function of time.

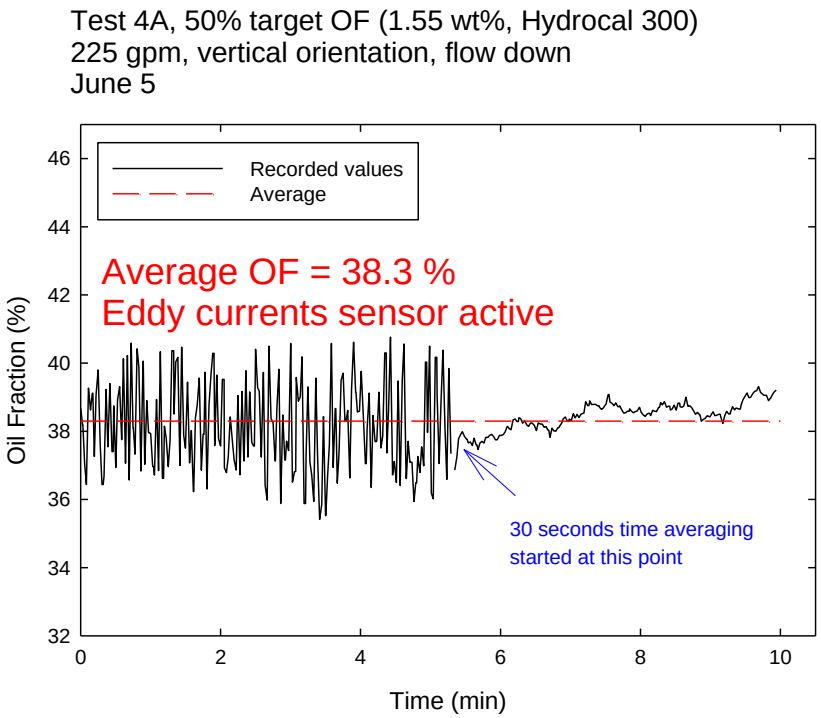

Figure 72. Test 4A - measured oil fraction as a function of time.

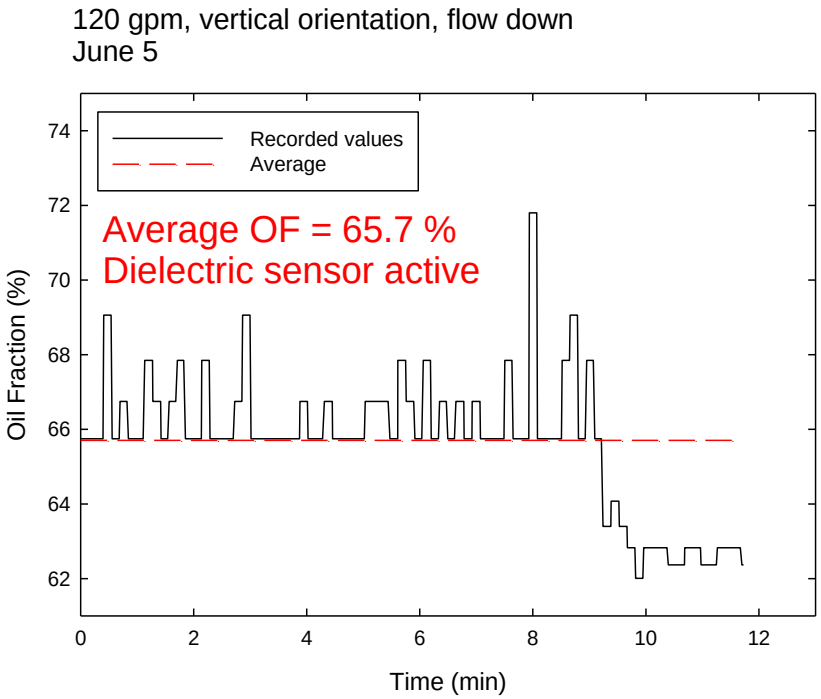

Figure 73. Test 5 - measured oil fraction as a function of time.

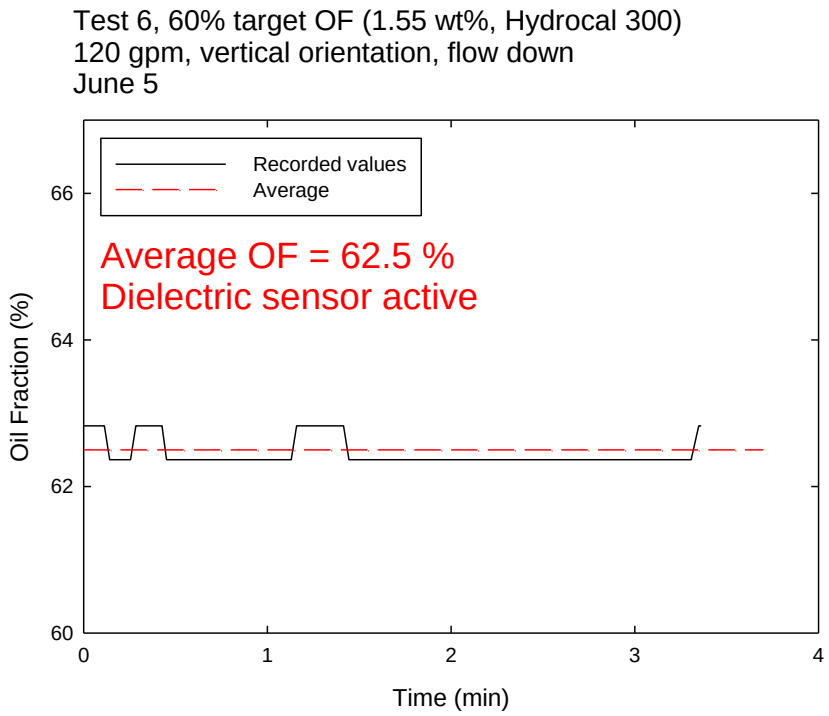

Figure 74. Test 6 - measured oil fraction as a function of time.

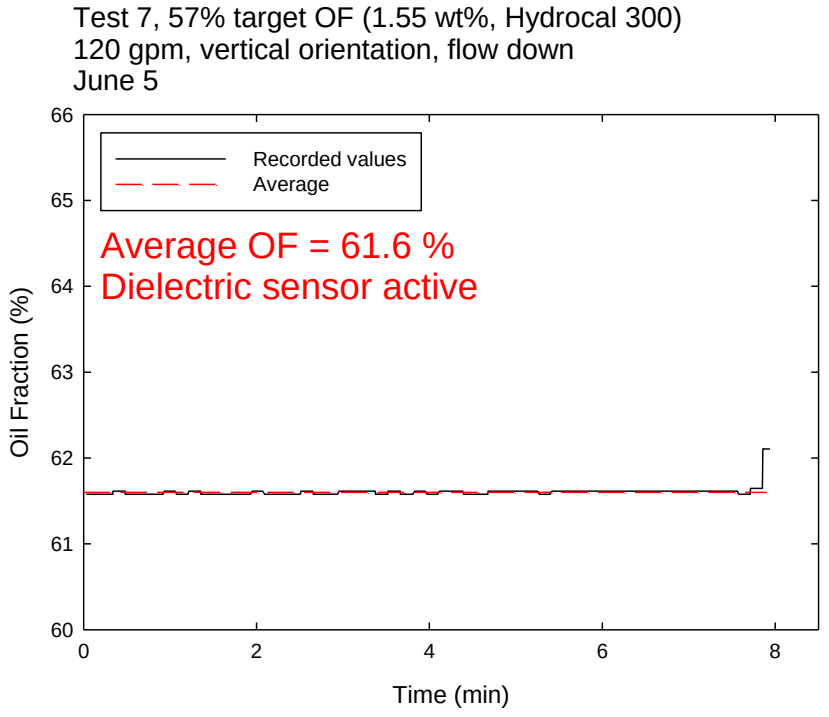

Figure 75. Test 7 - measured oil fraction as a function of time.

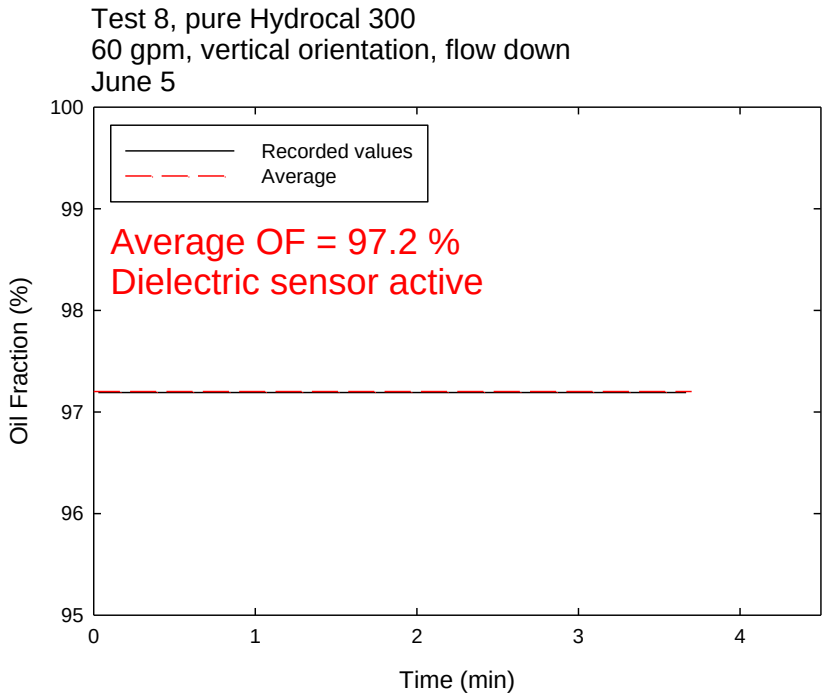

Figure 76. Test 8 - measured oil fraction as a function of time.

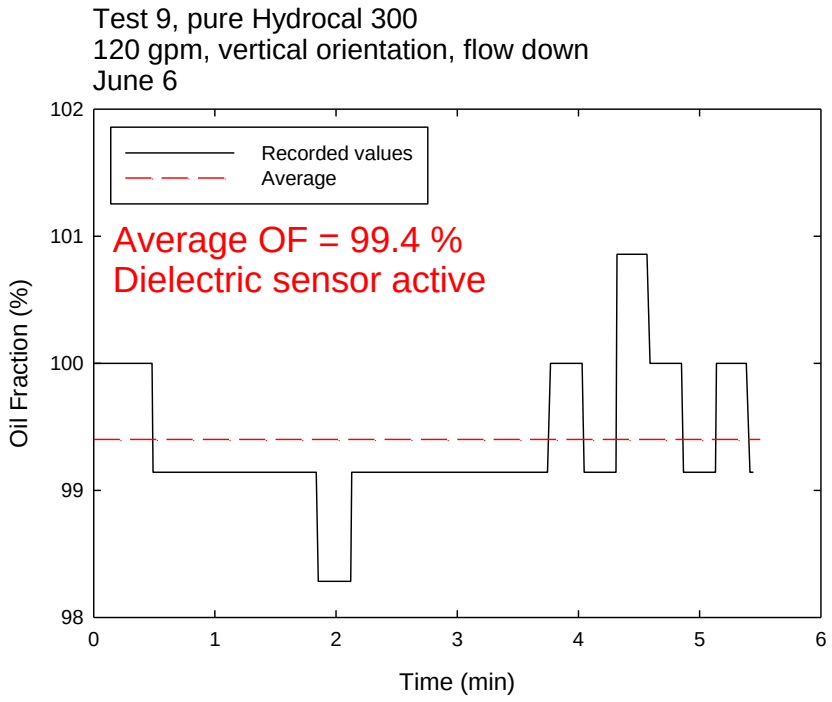

Figure 77. Test 9 - measured oil fraction as a function of time.

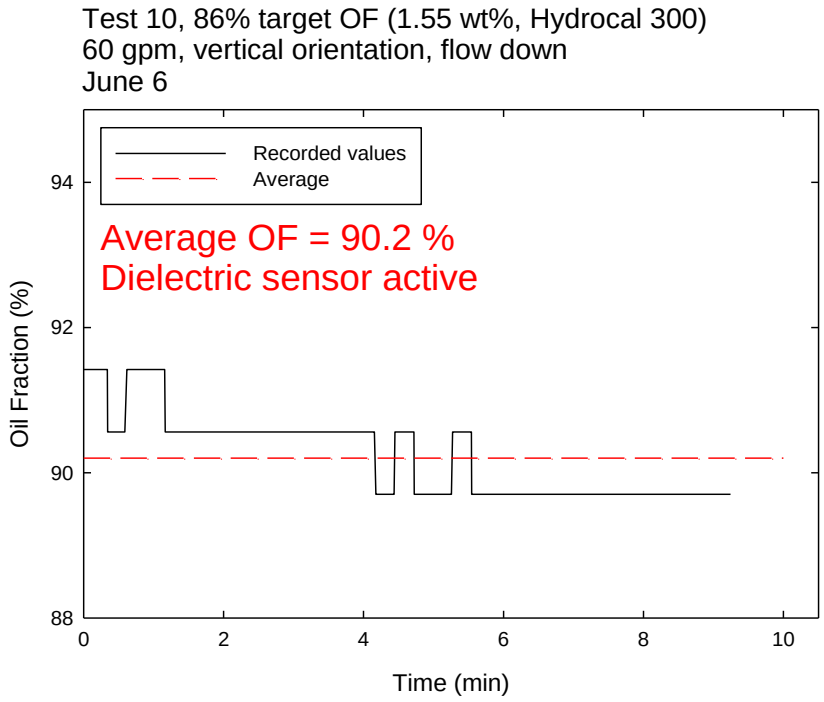

Figure 78. Test 10 - measured oil fraction as a function of time.

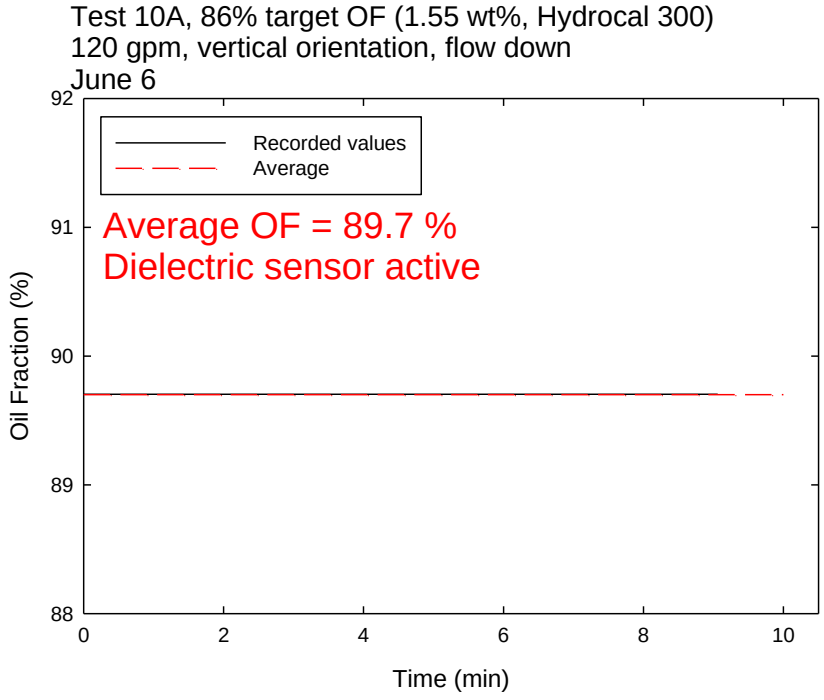

Figure 79. Test 10A - measured oil fraction as a function of time.

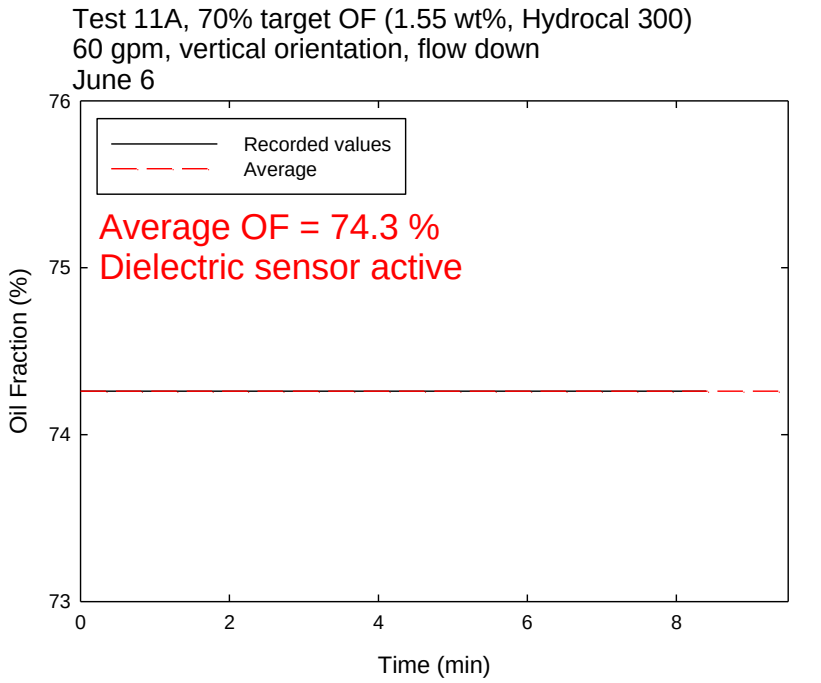

Figure 80. Test 11A - measured oil fraction as a function of time.

10.4.2 Results obtained with 1.5 wt% salinity water and diesel

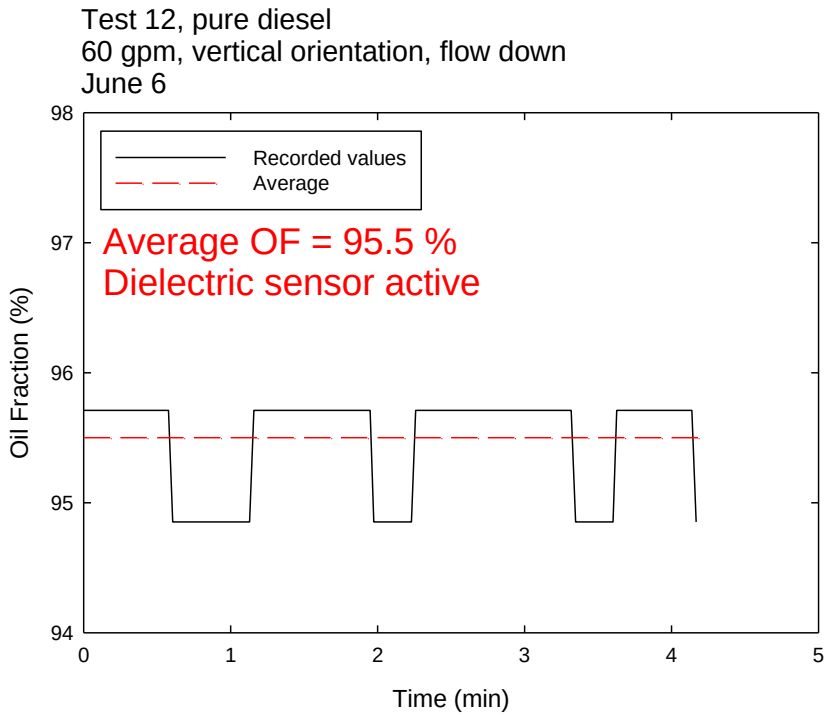

Figure 81. Test 12 - measured oil fraction as a function of time.

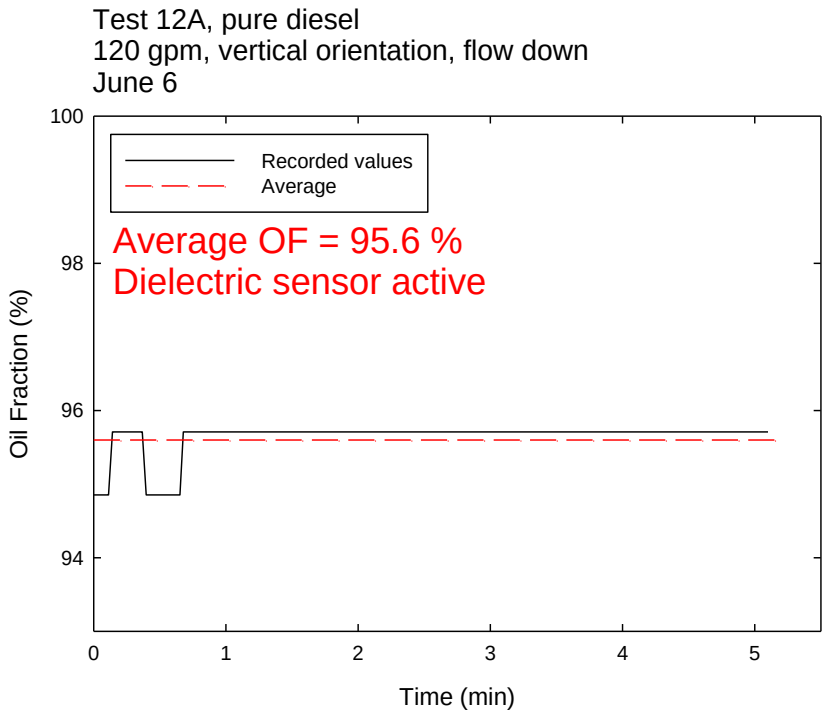

Figure 82. Test 12A - measured oil fraction as a function of time.

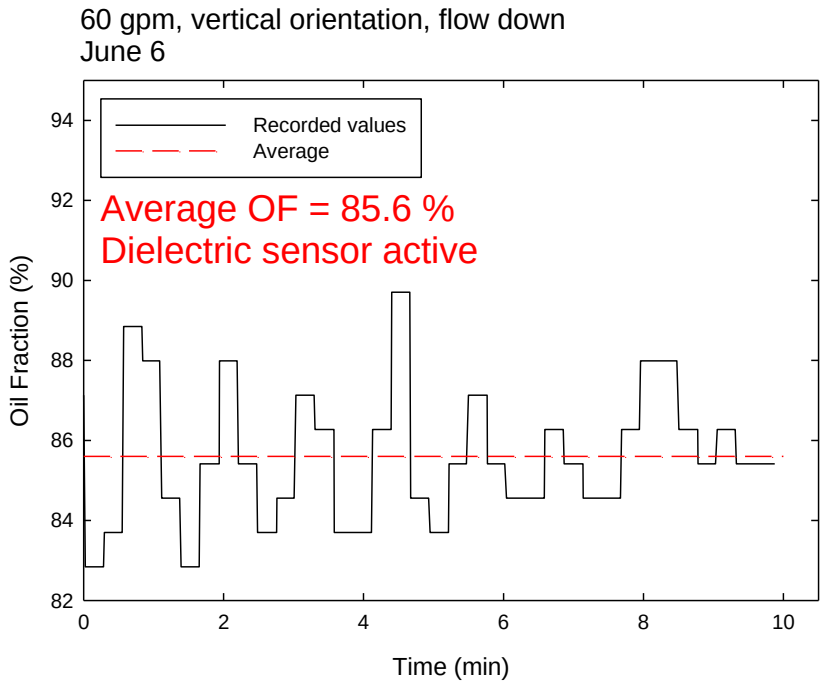

Figure 83. Test 13 - measured oil fraction as a function of time.

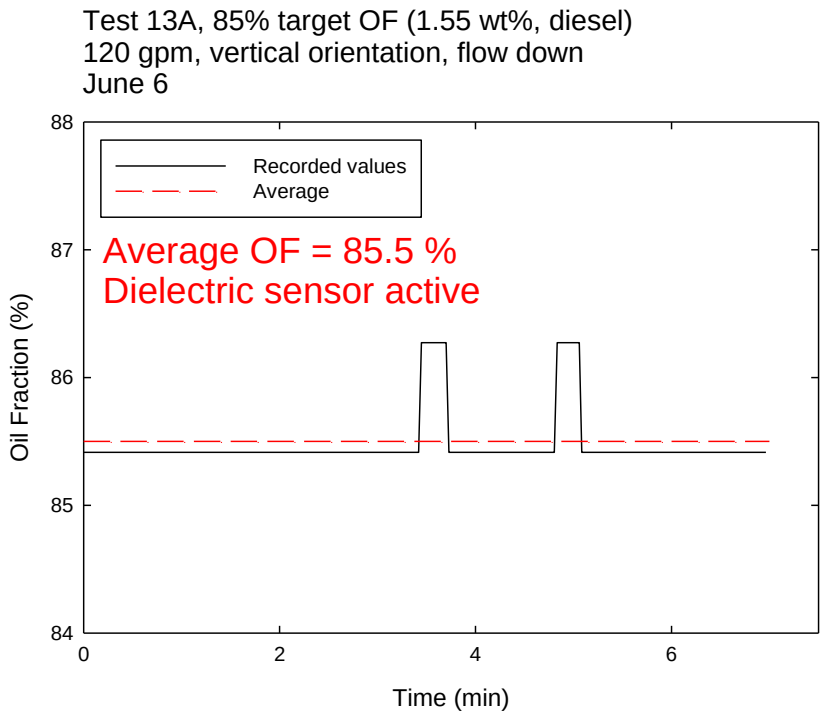

Figure 84. Test 13A - measured oil fraction as a function of time.

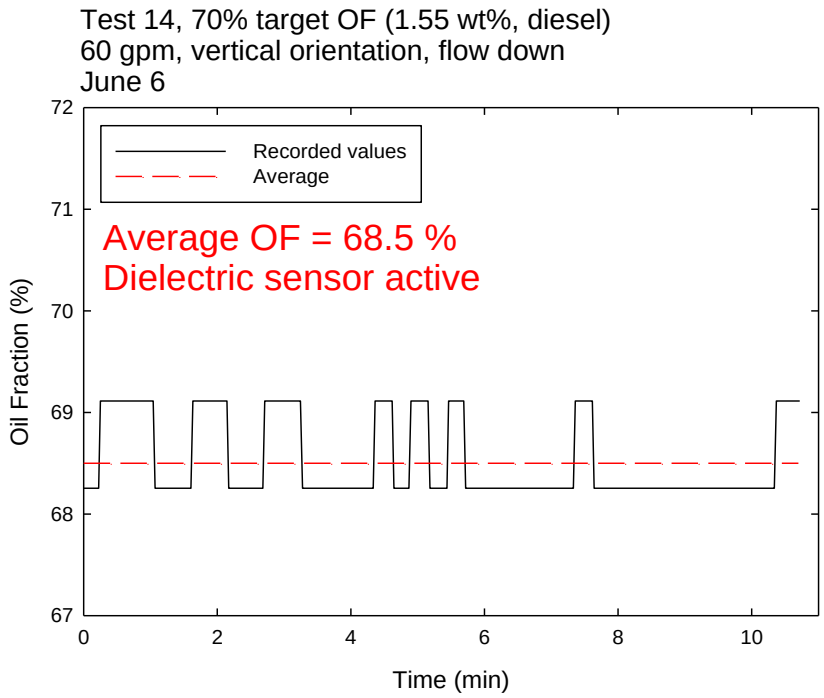

Figure 85. Test 14 - measured oil fraction as a function of time.

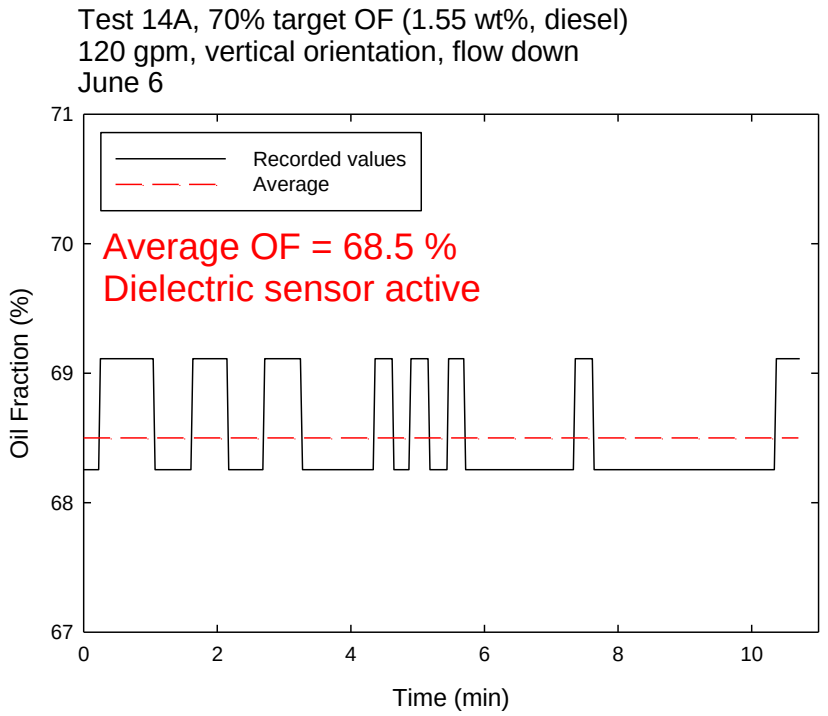

Figure 86. Test 14A - measured oil fraction as a function of time.

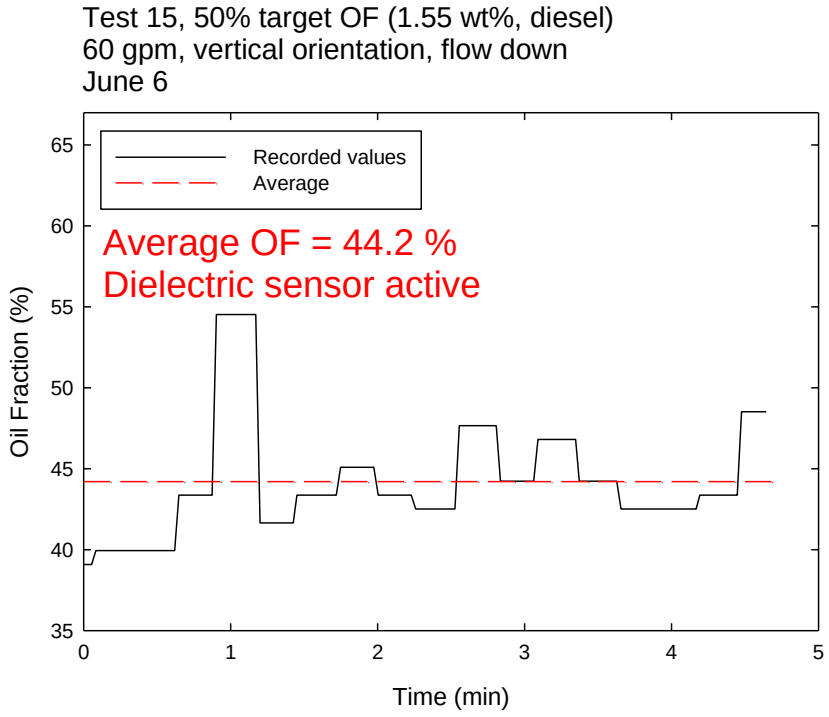

Figure 87. Test 15 - measured oil fraction as a function of time.

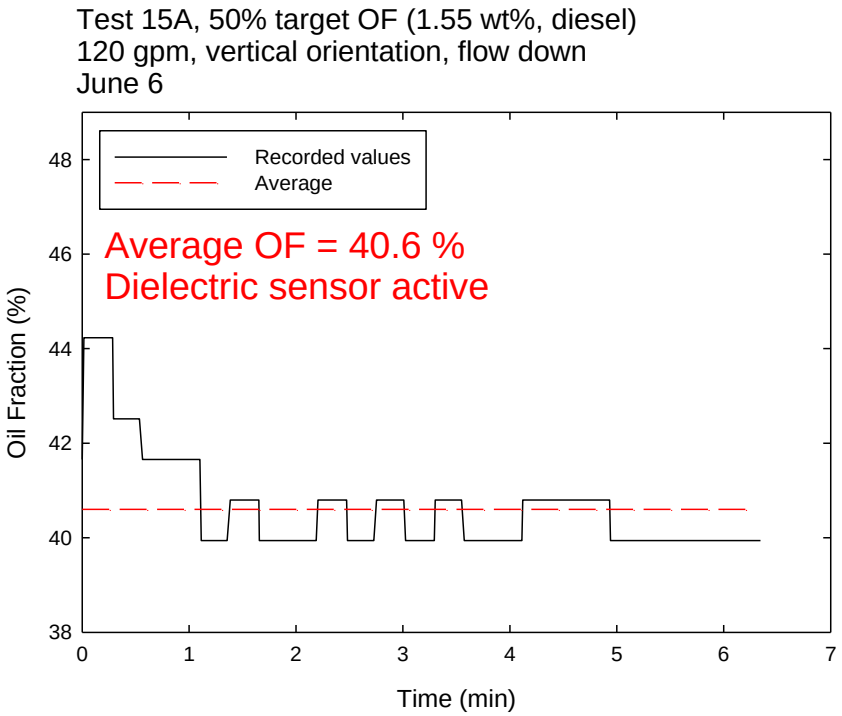

Figure 88. Test 15A - measured oil fraction as a function of time.

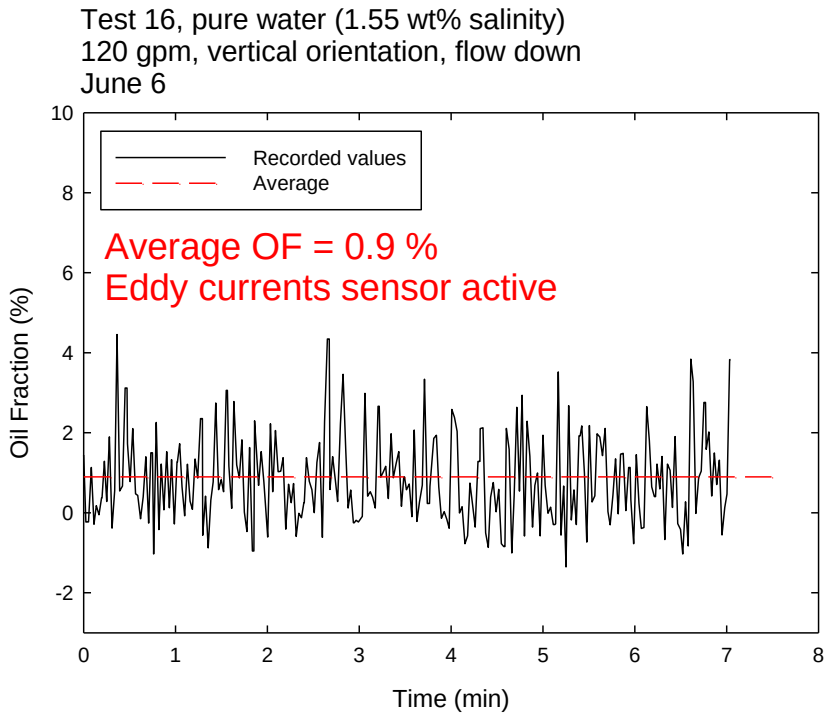

Figure 89. Test 16 - measured oil fraction as a function of time.

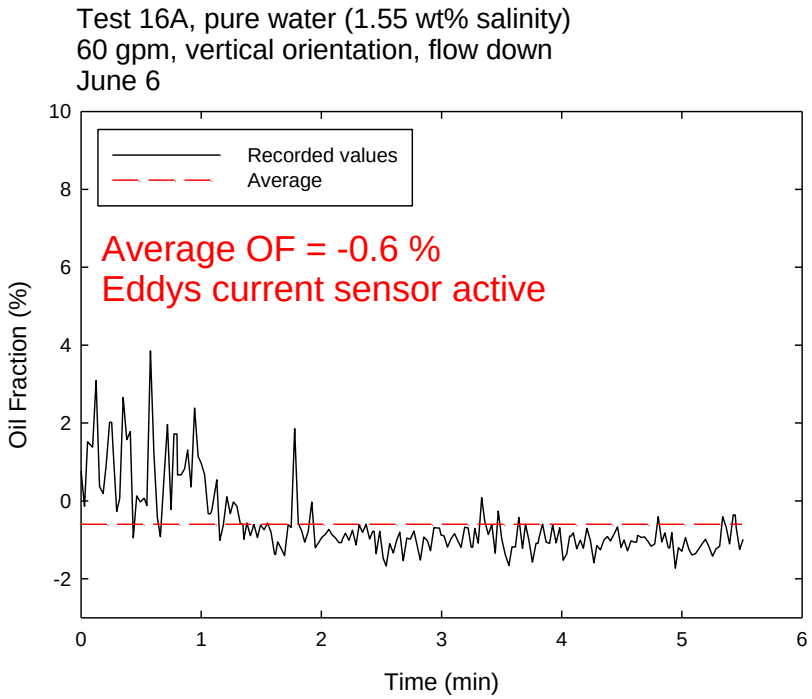

Figure 90. Test 16A - measured oil fraction as a function of time.

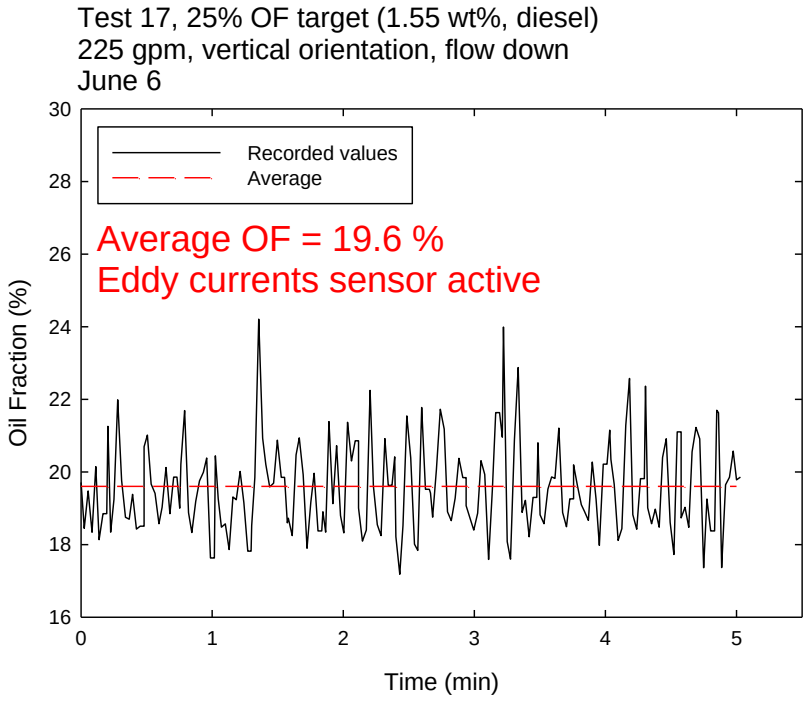

Figure 91. Test 17 - measured oil fraction as a function of time.

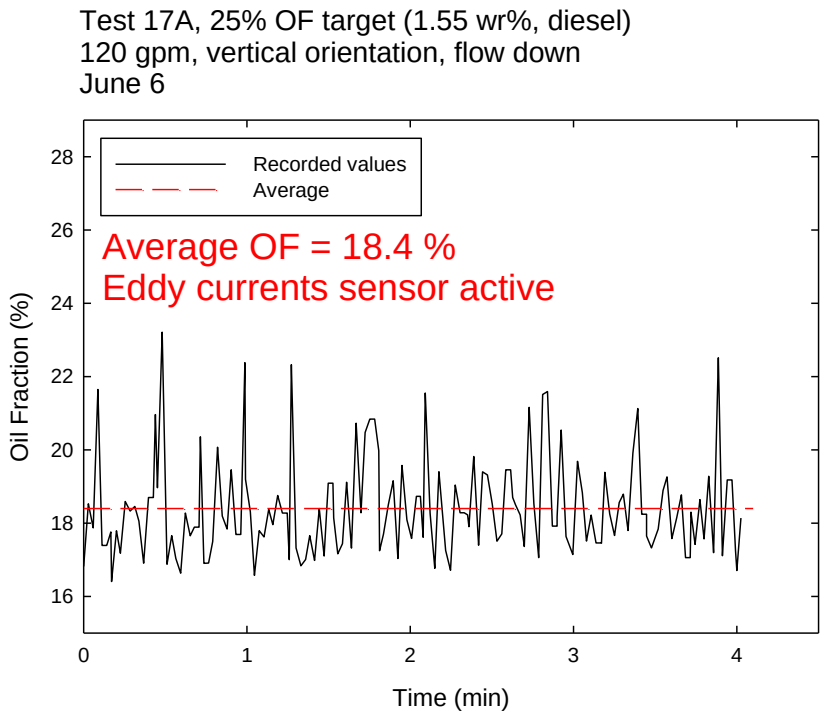

Figure 92. Test 17A - measured oil fraction as a function of time.

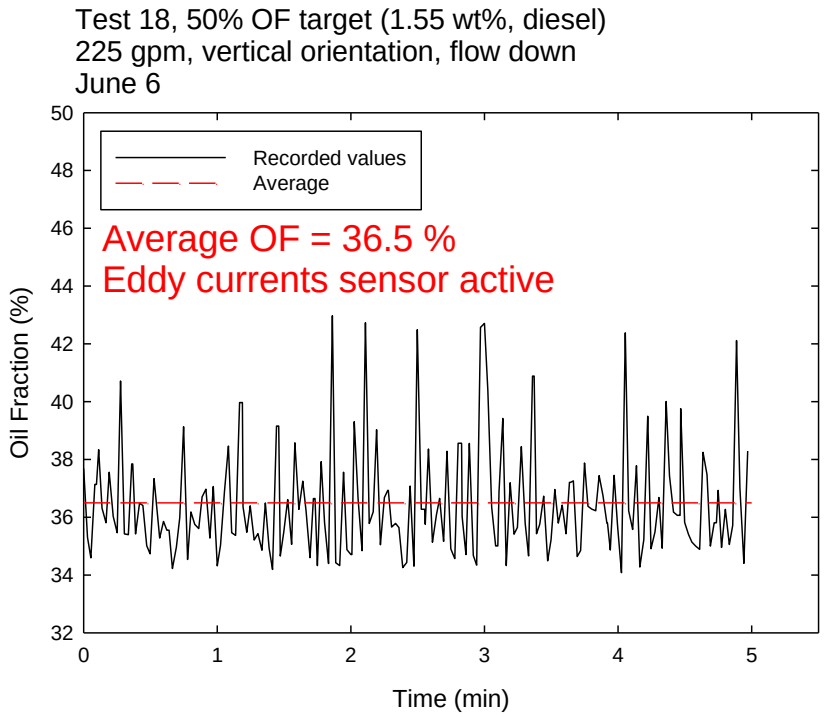

Figure 93. Test 18 - measured oil fraction as a function of time.

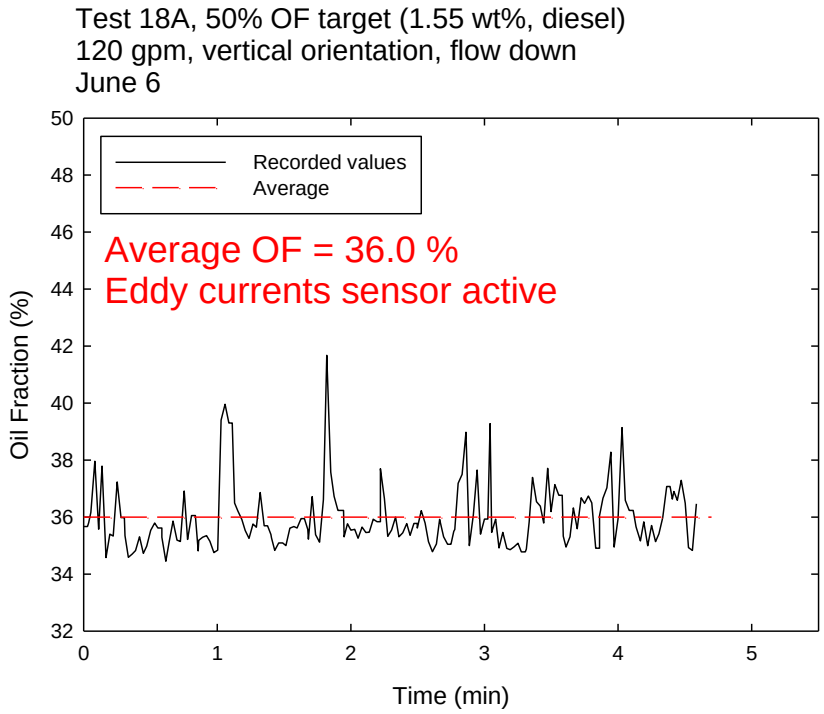

Figure 94. Test 18A - measured oil fraction as a function of time.

10.4.3 Results obtained with 3.60 wt% salinity water and Hydrocal 300 Oil

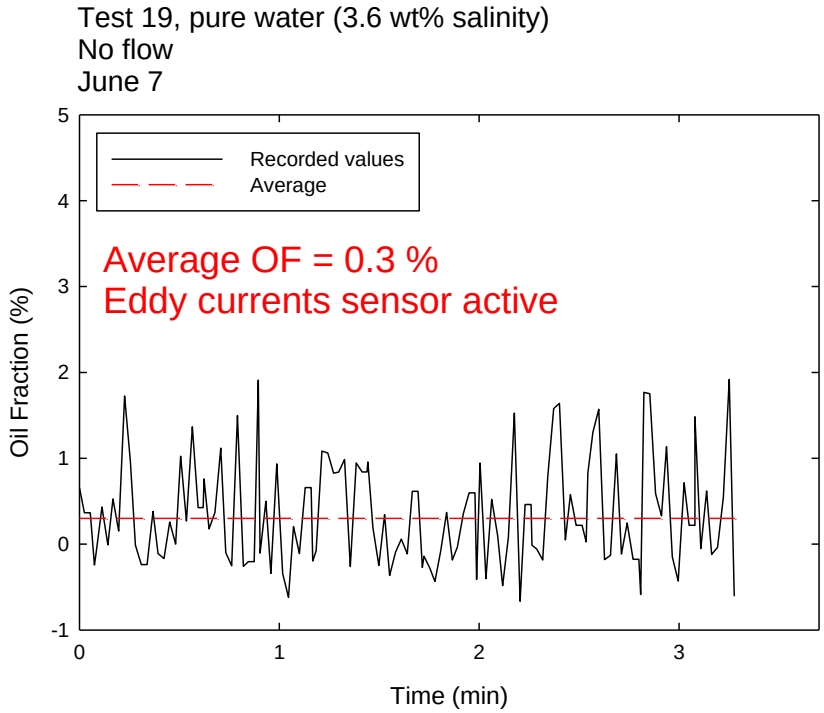

Figure 95. Test 19 - measured oil fraction as a function of time.

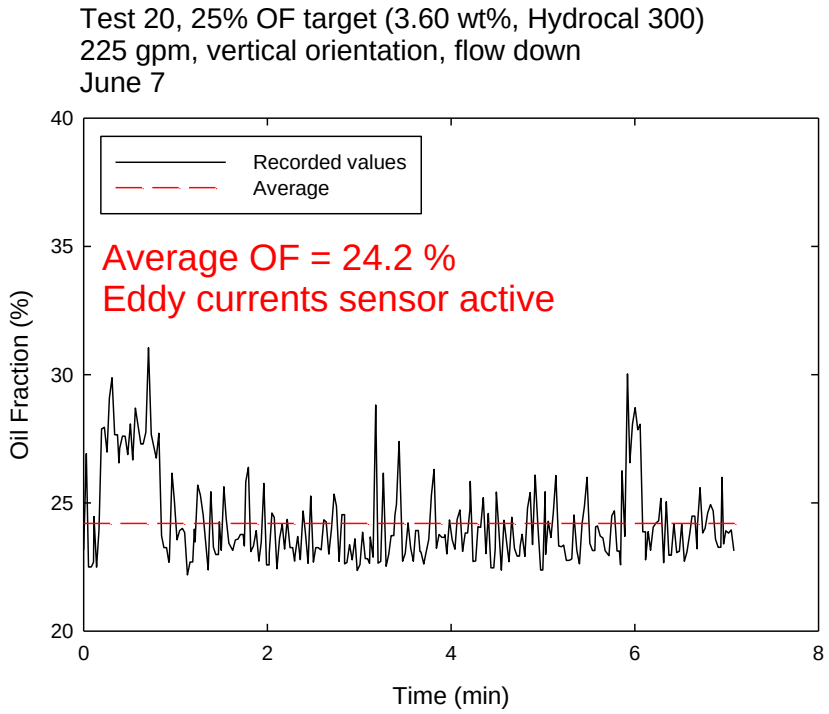

Figure 96. Test 20 - measured oil fraction as a function of time.

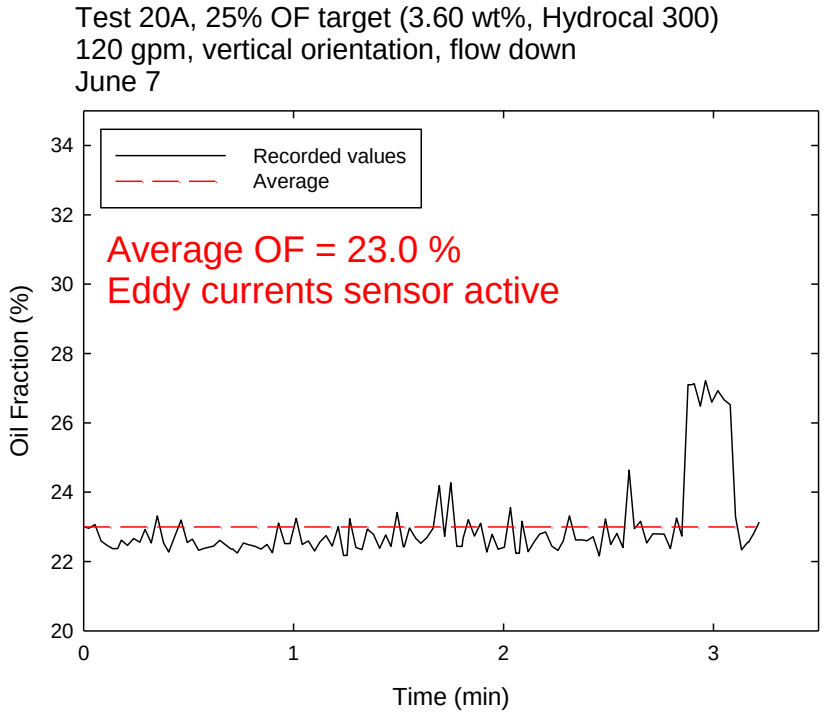

Figure 97. Test 20A - measured oil fraction as a function of time.

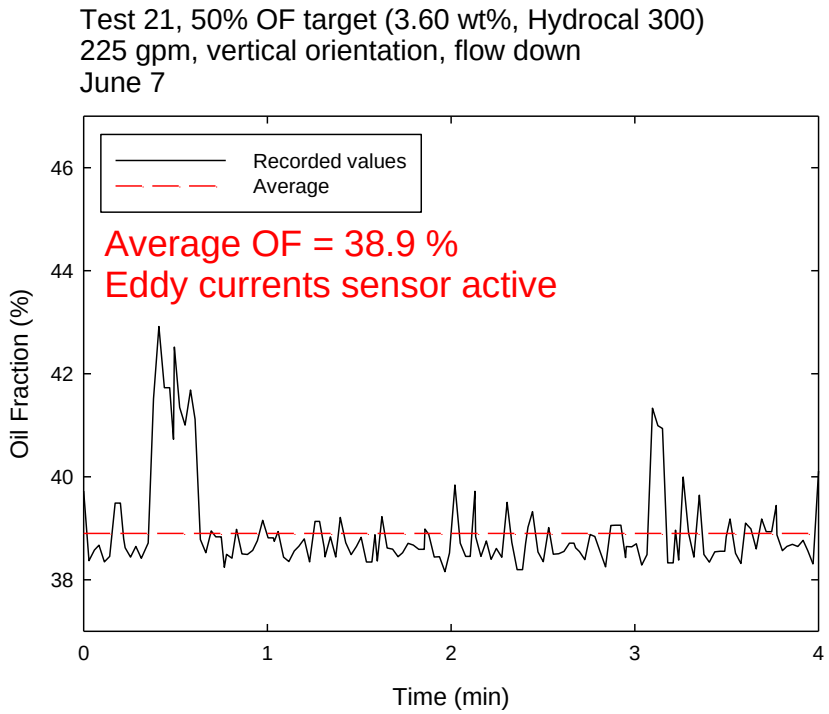

Figure 98. Test 21 - measured oil fraction as a function of time.

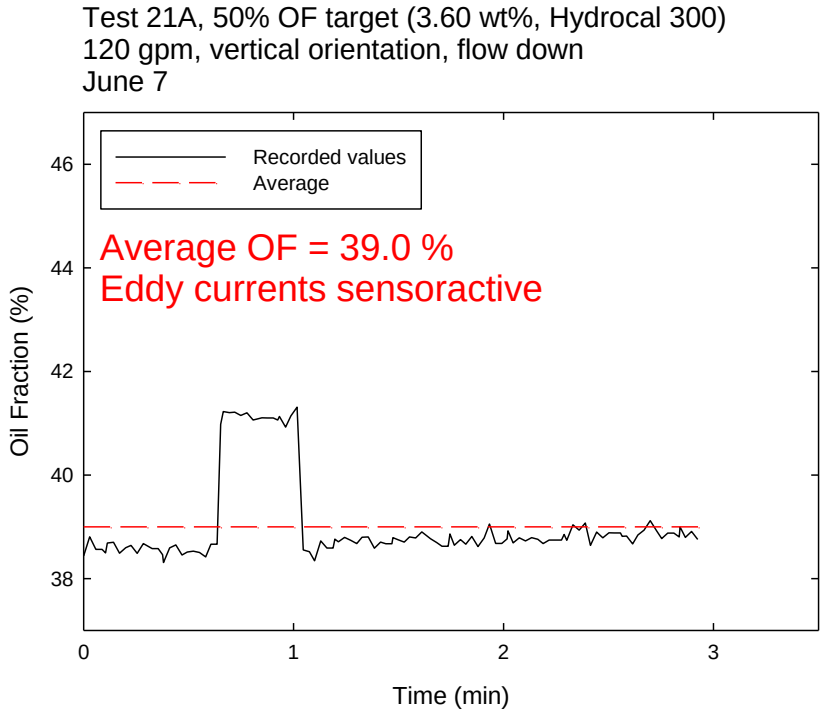

Figure 99. Test 21A - measured oil fraction as a function of time.

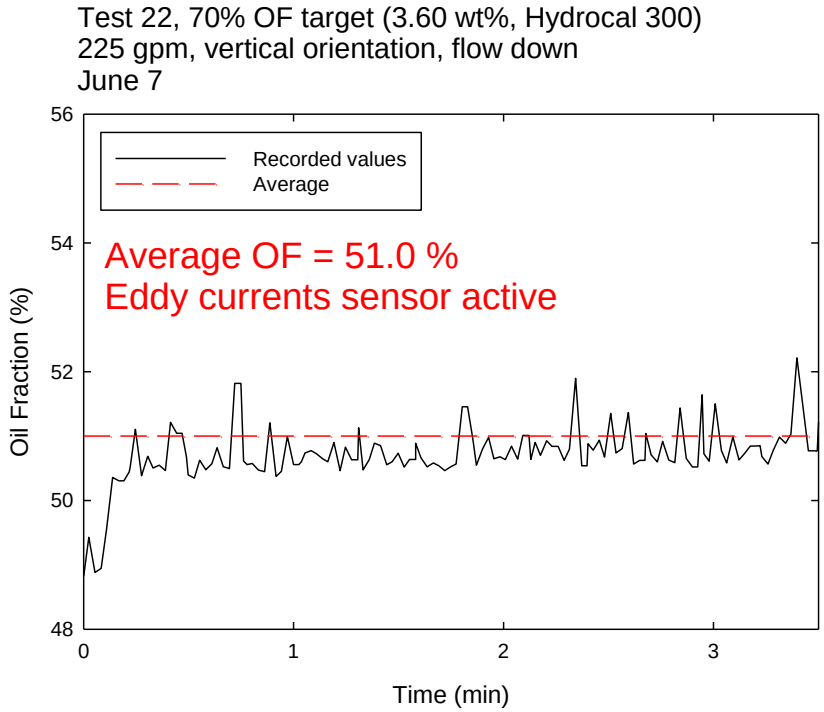

Figure 100. Test 22 - measured oil fraction as a function of time.

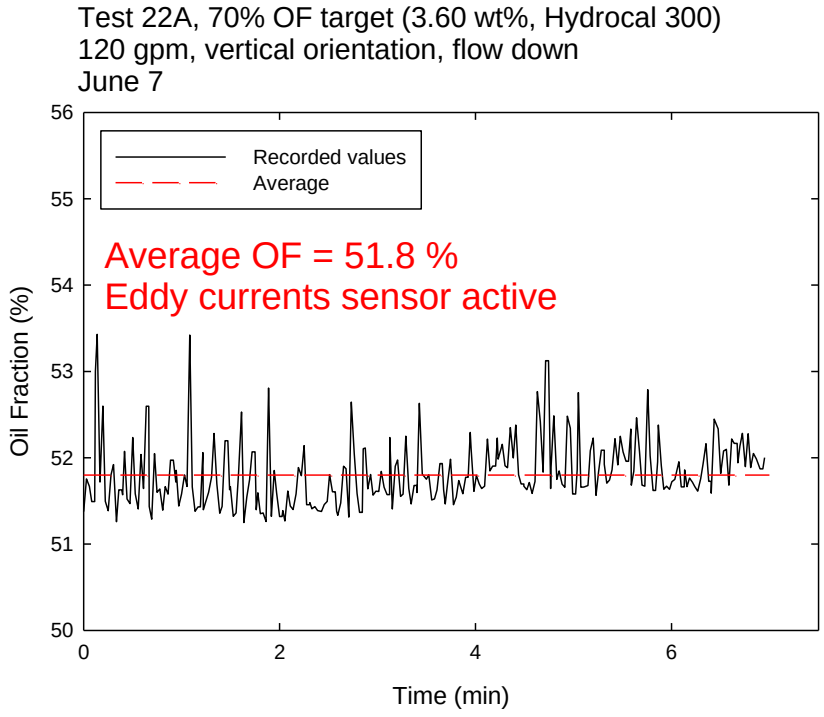

Figure 101. Test 22A - measured oil fraction as a function of time.

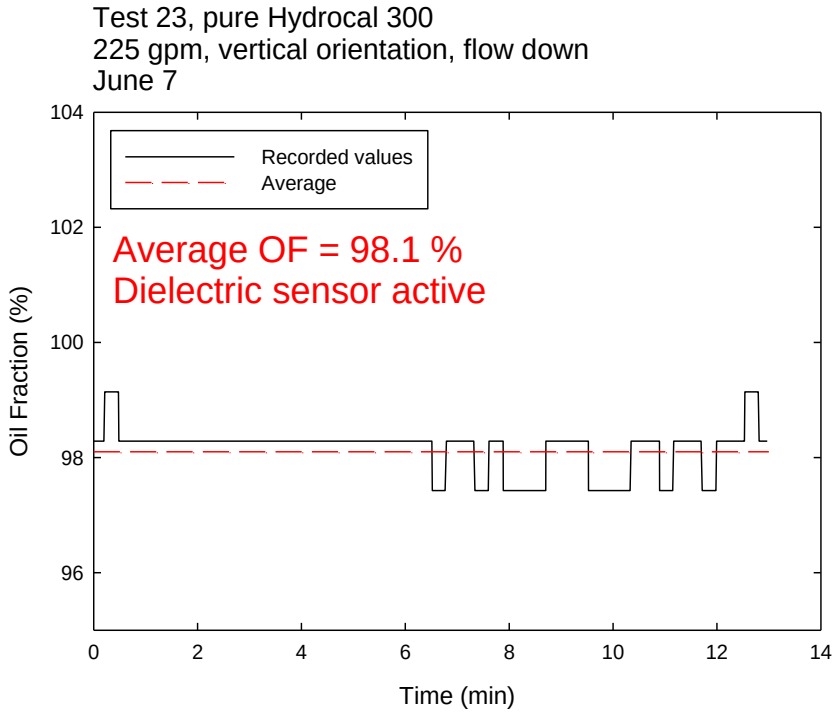

Figure 102. Test 23 - measured oil fraction as a function of time.

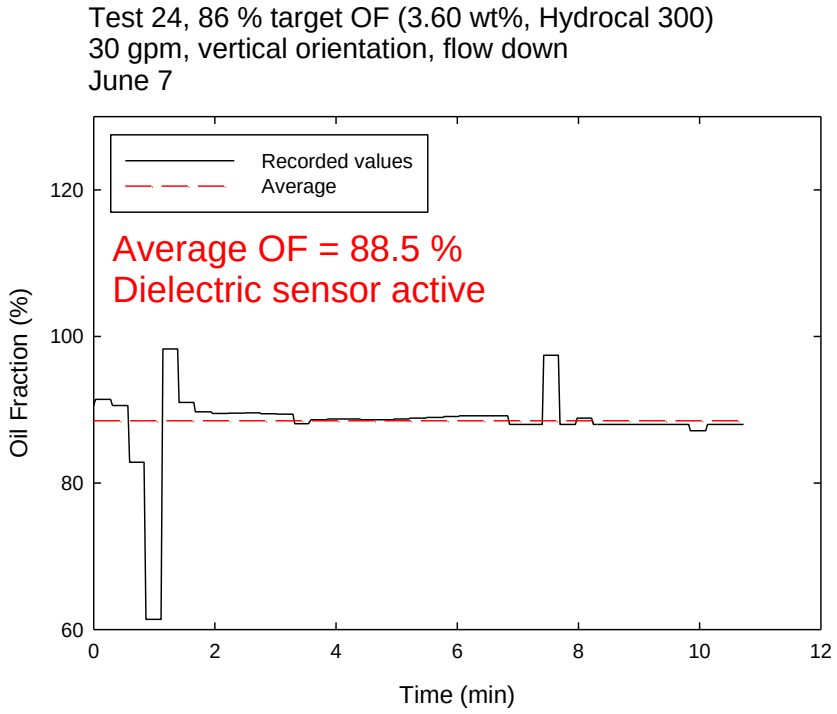

Figure 103. Test 24 - measured oil fraction as a function of time.

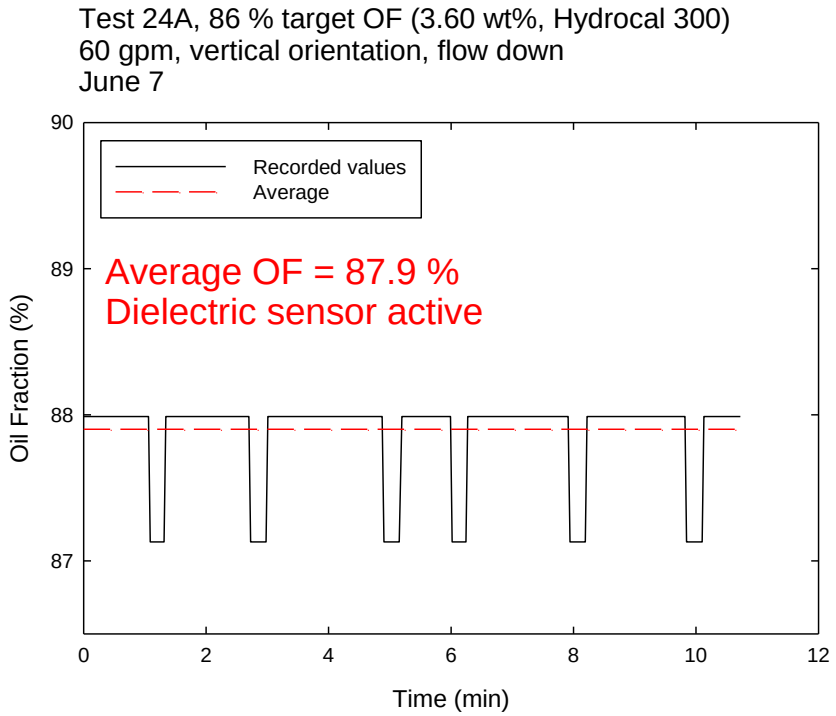

Figure 104. Test 24A - measured oil fraction as a function of time.

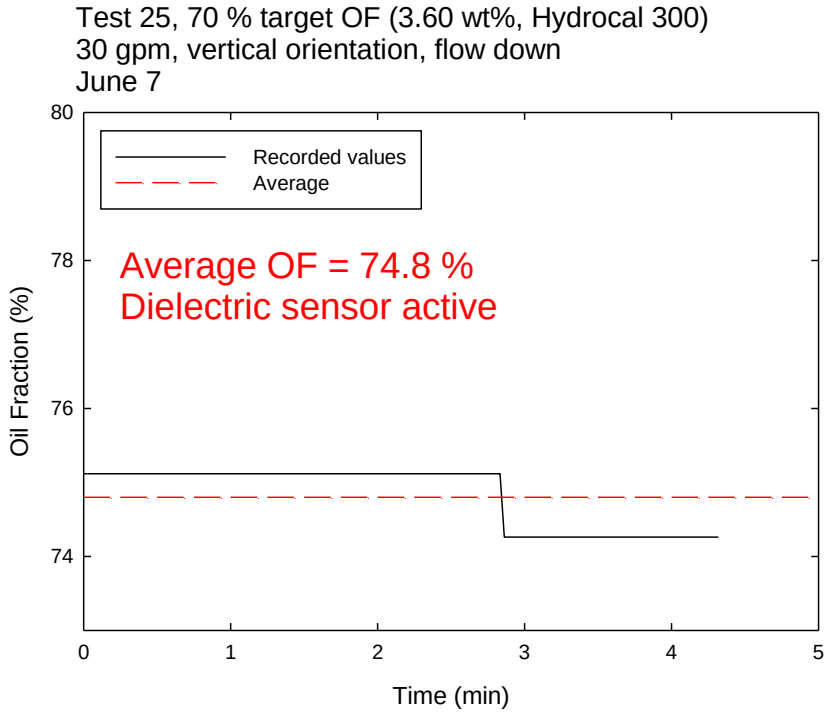

Figure 105. Test 25 - measured oil fraction as a function of time.

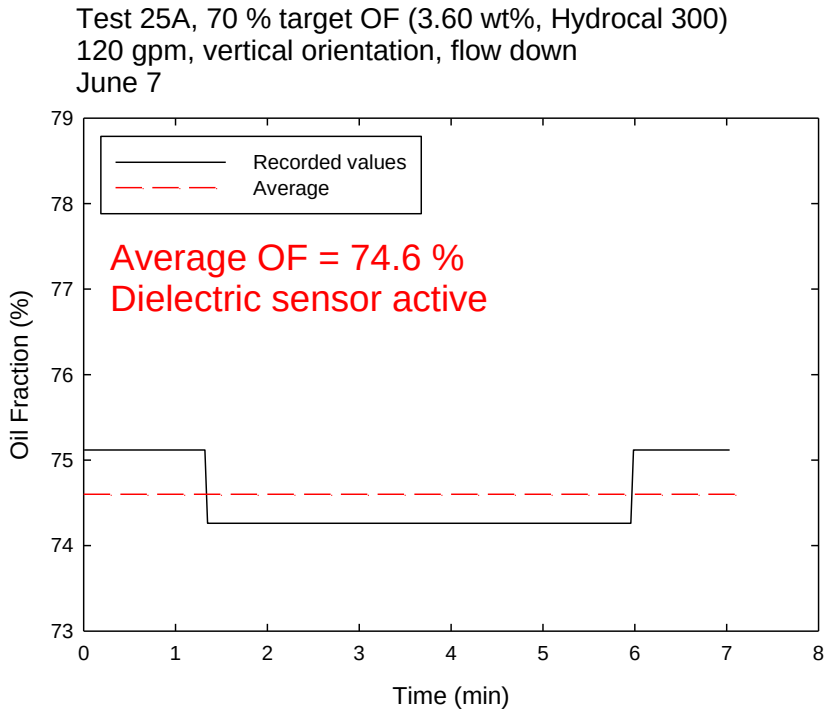

Figure 106. Test 25A - measured oil fraction as a function of time.

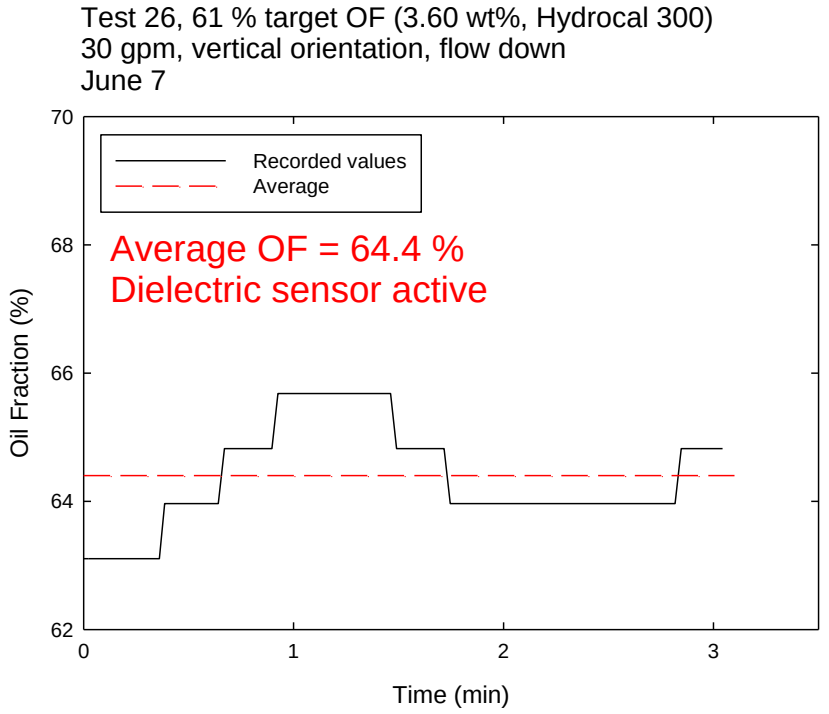

Figure 107. Test 26 - measured oil fraction as a function of time.

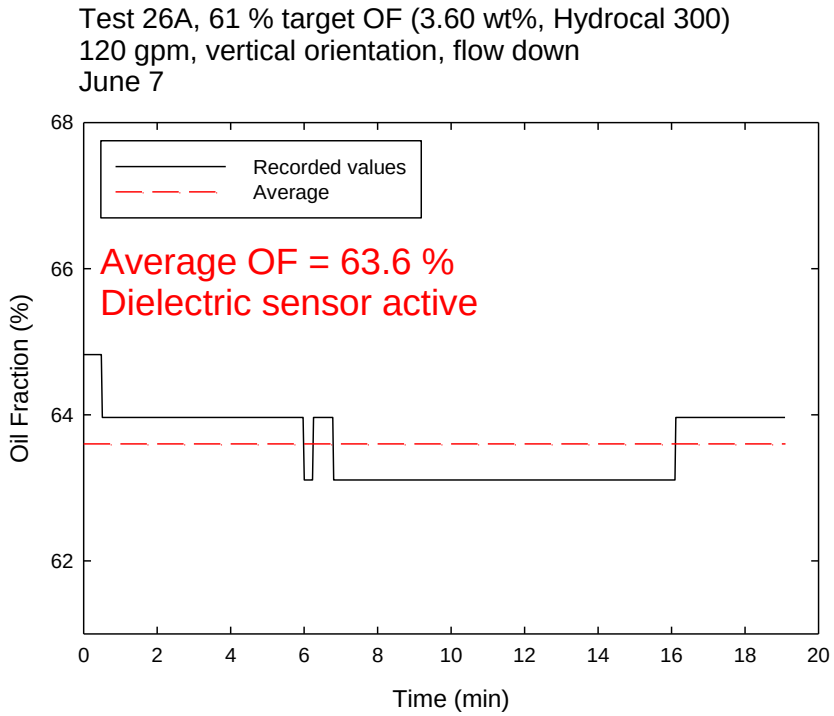

Figure 108. Test 26A - measured oil fraction as a function of time.

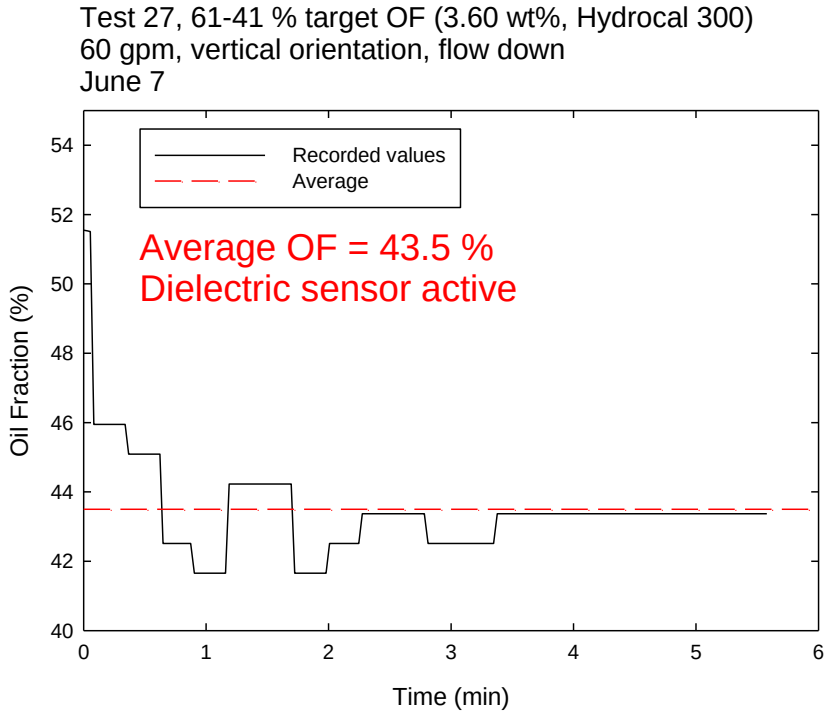

Figure 109. Test 27 - measured oil fraction as a function of time.

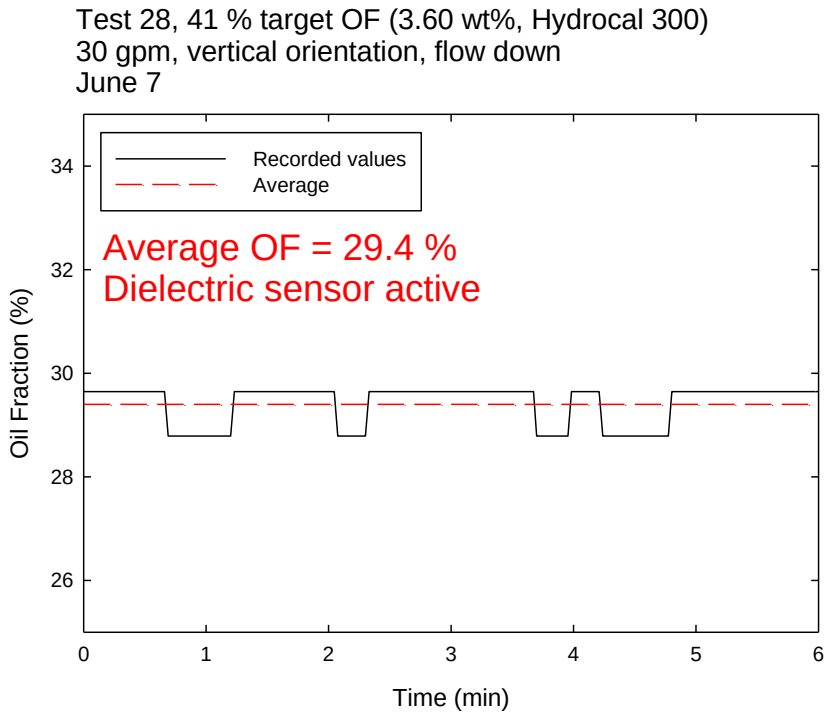

Figure 110. Test 28 - measured oil fraction as a function of time.

10.4.4 Results obtained with 3.60 wt% salinity water and diesel

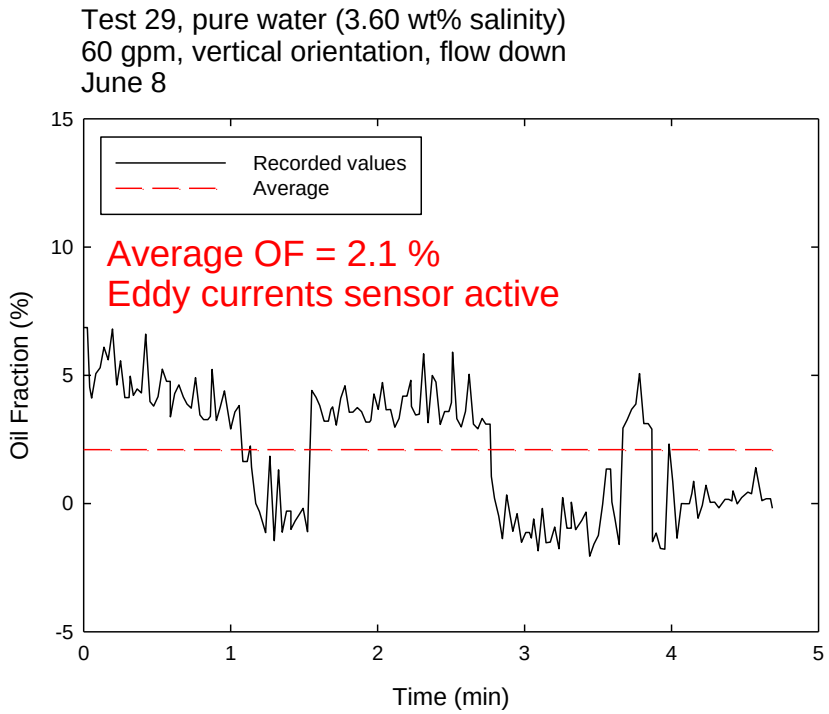

Figure 111. Test 29 - measured oil fraction as a function of time.

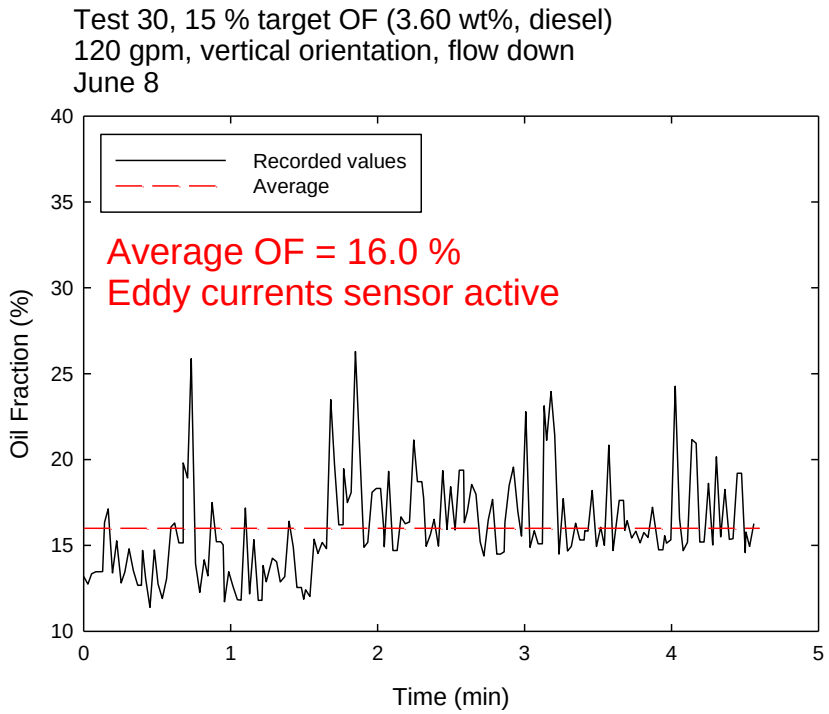

Figure 112. Test 30 - measured oil fraction as a function of time.

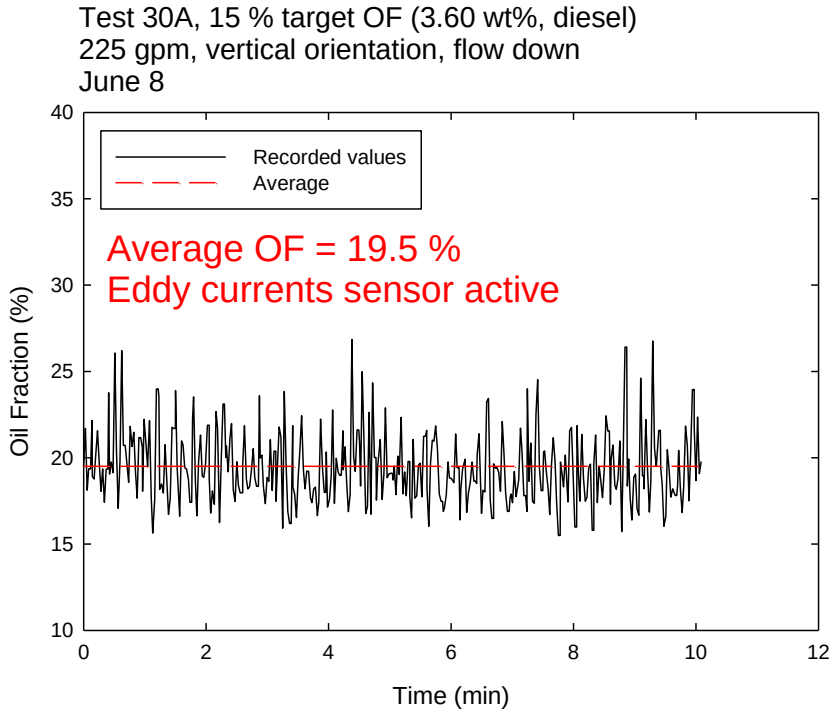

Figure 113. Test 30A - measured oil fraction as a function of time.

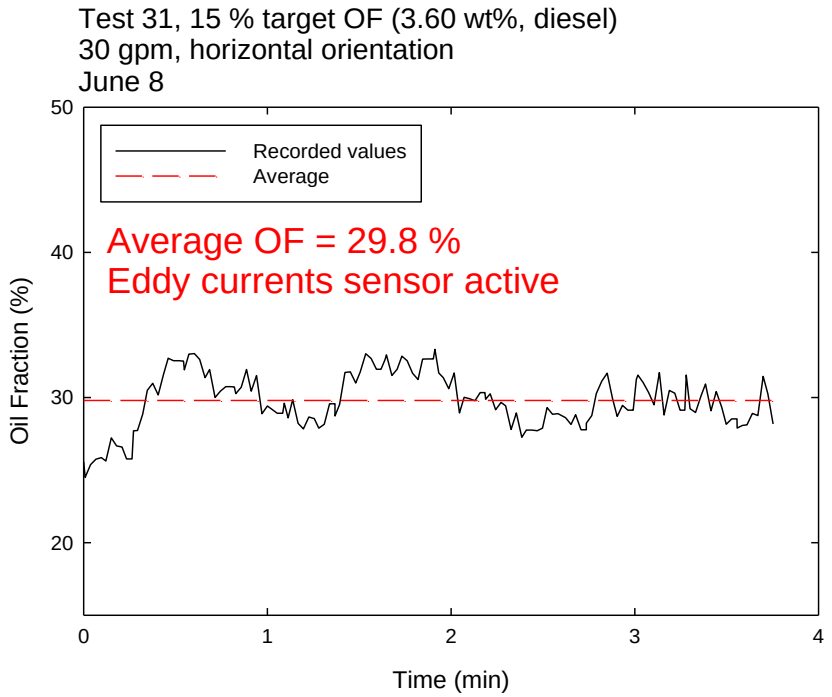

Figure 114. Test 31 - measured oil fraction as a function of time.

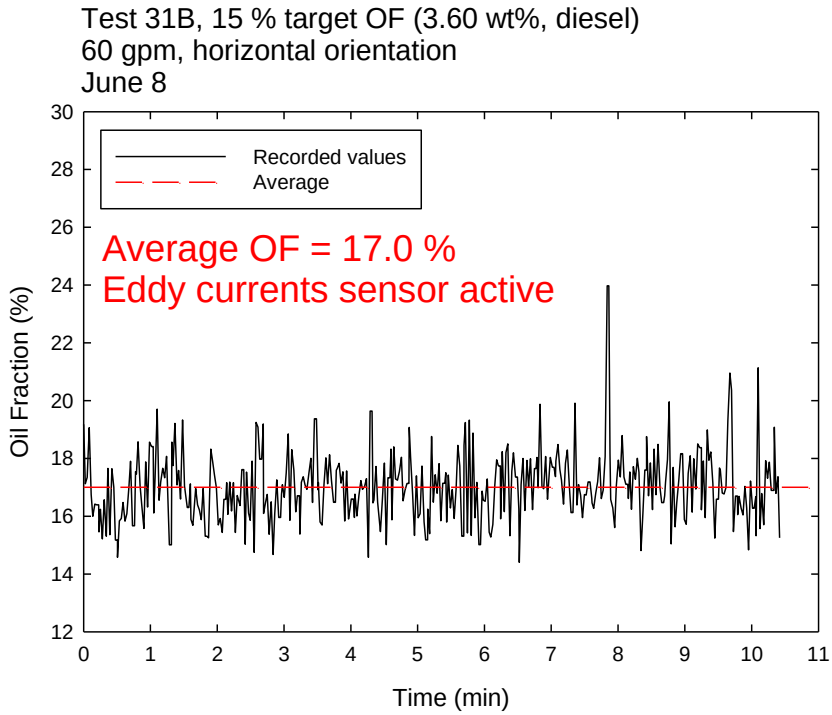

Figure 115. Test 31B - measured oil fraction as a function of time.

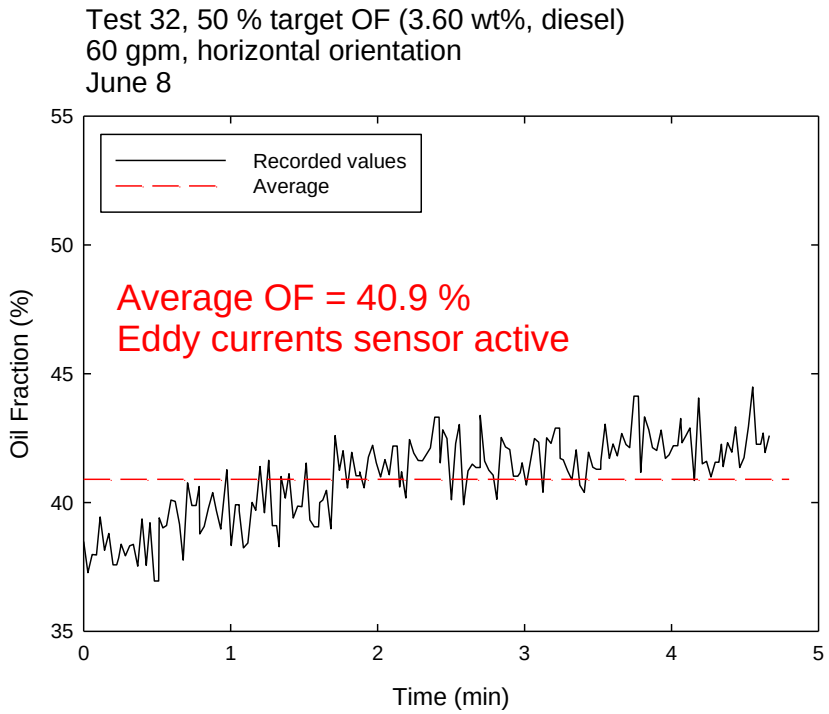

Figure 116. Test 32 - measured oil fraction as a function of time.

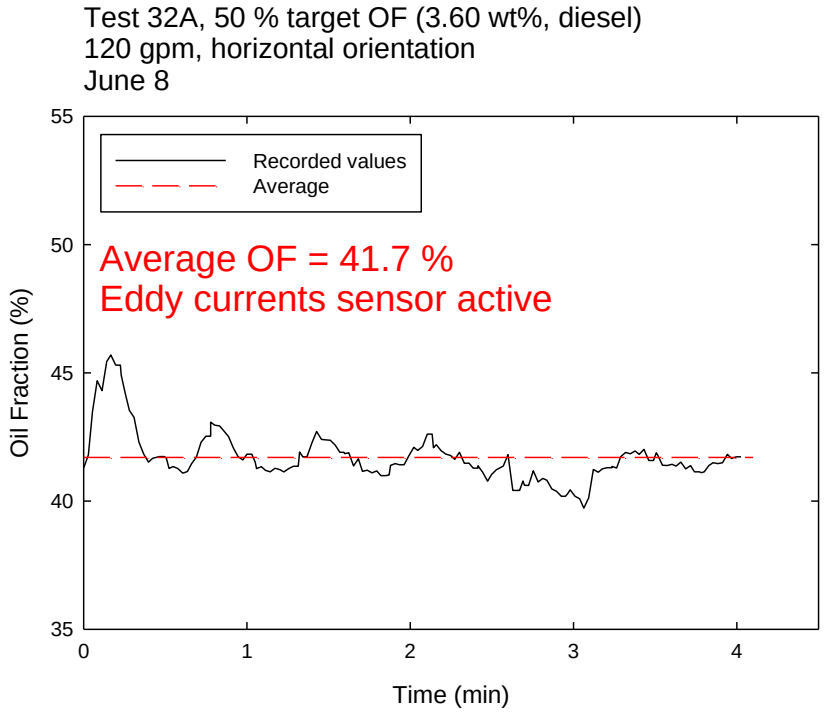

Figure 117. Test 32A - measured oil fraction as a function of time.

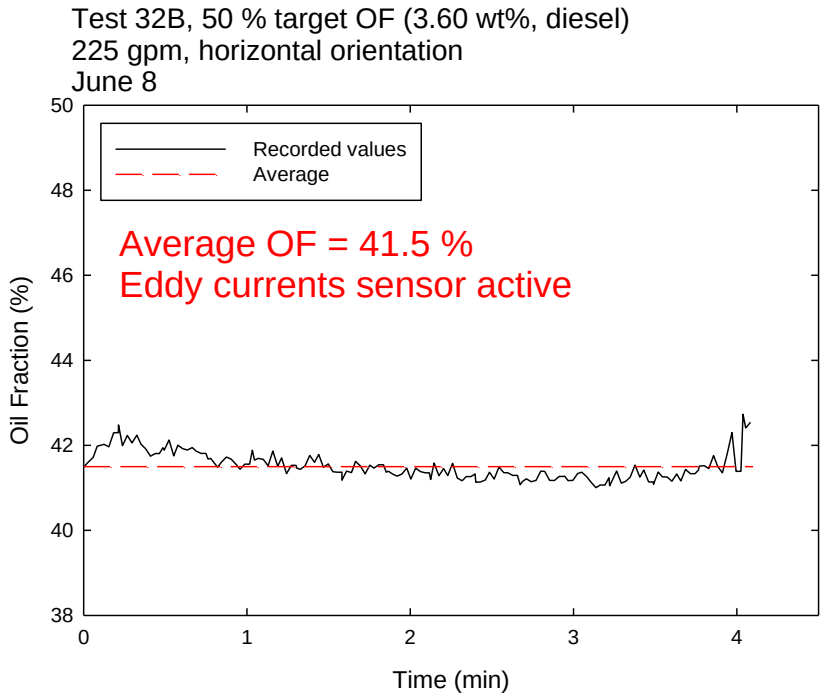

Figure 118. Test 32B - measured oil fraction as a function of time.

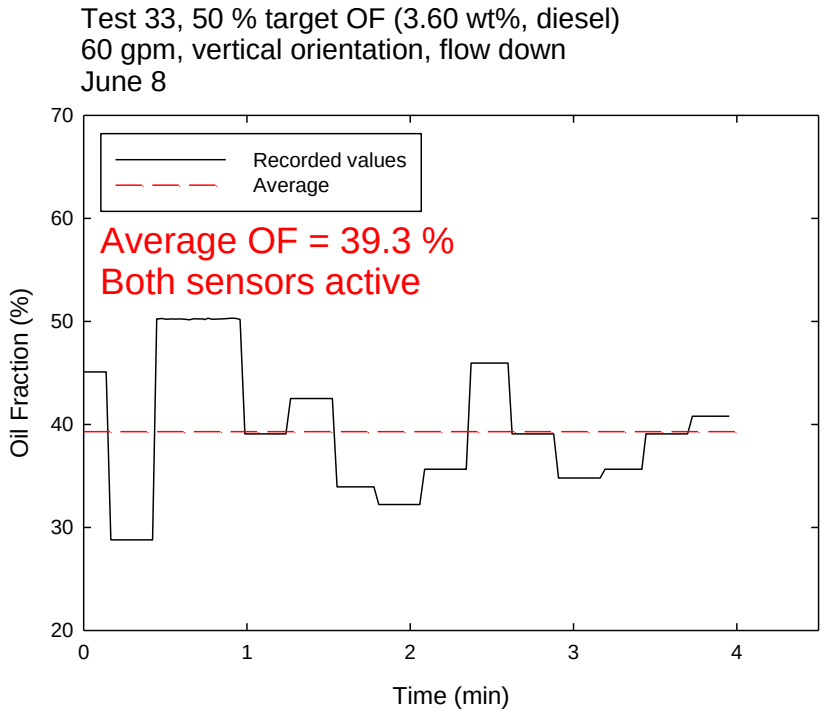

Figure 119. Test 33 - measured oil fraction as a function of time.

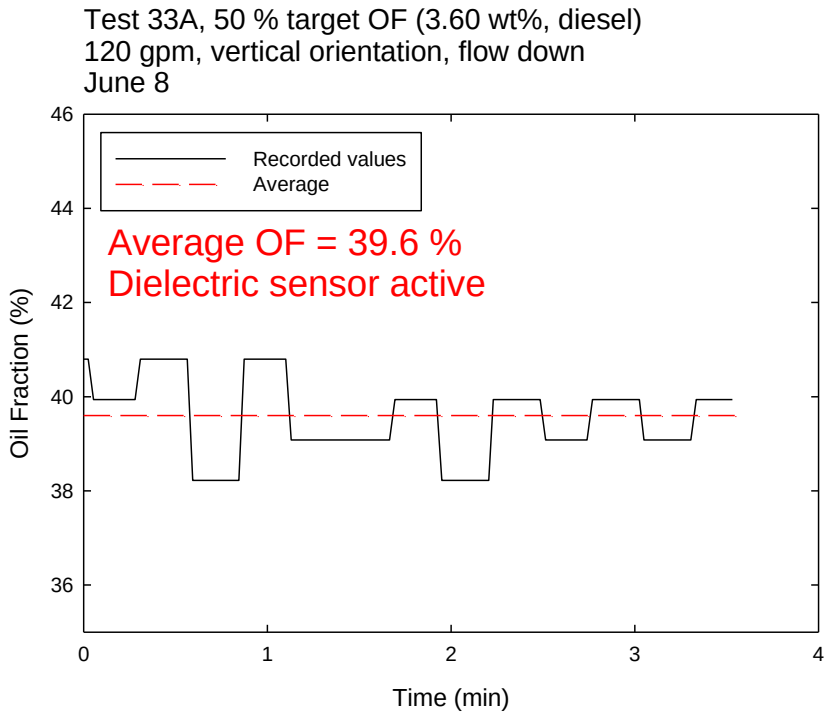

Figure 120. Test 33A - measured oil fraction as a function of time.

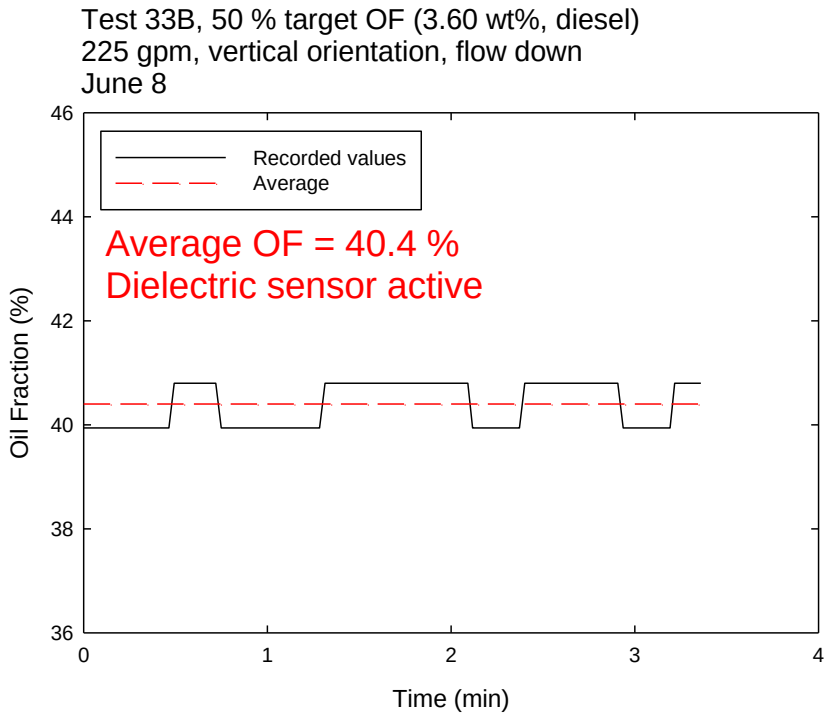

Figure 121. Test 33B - measured oil fraction as a function of time.

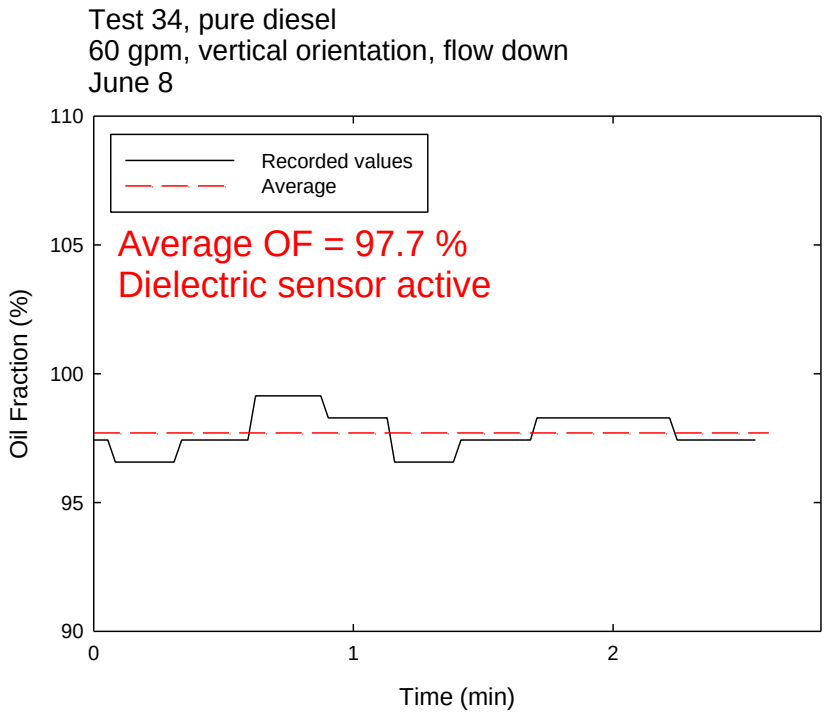

Figure 122. Test 34 - measured oil fraction as a function of time.

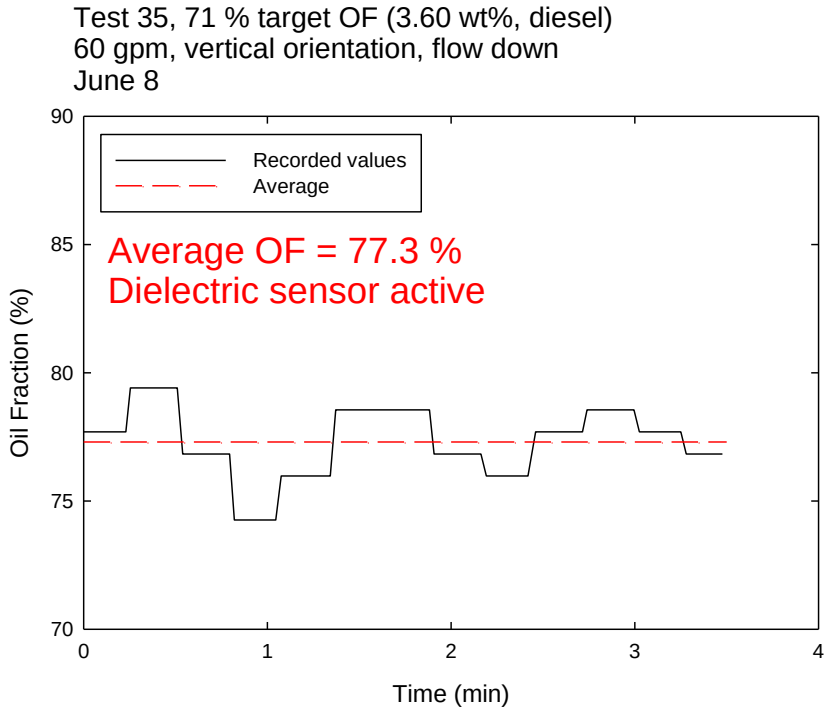

Figure 123. Test 35 - measured oil fraction as a function of time.

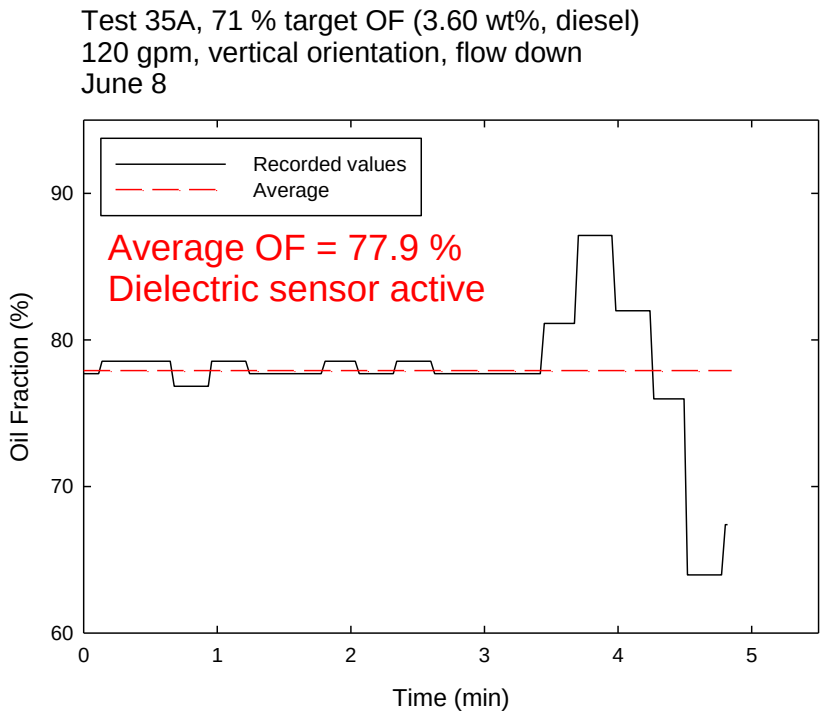

Figure 124. Test 35A - measured oil fraction as a function of time.

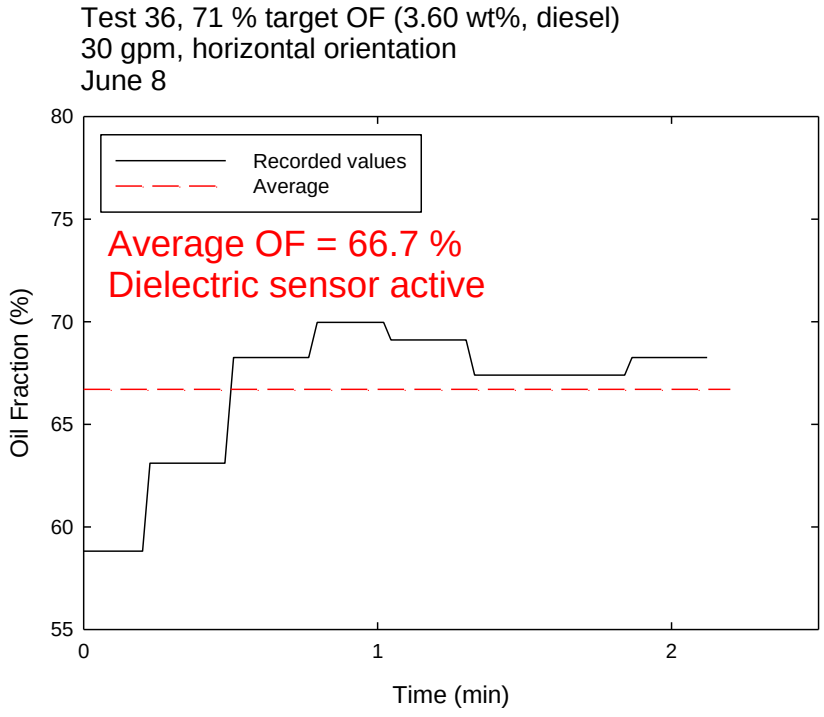

Figure 125. Test 36 - measured oil fraction as a function of time.

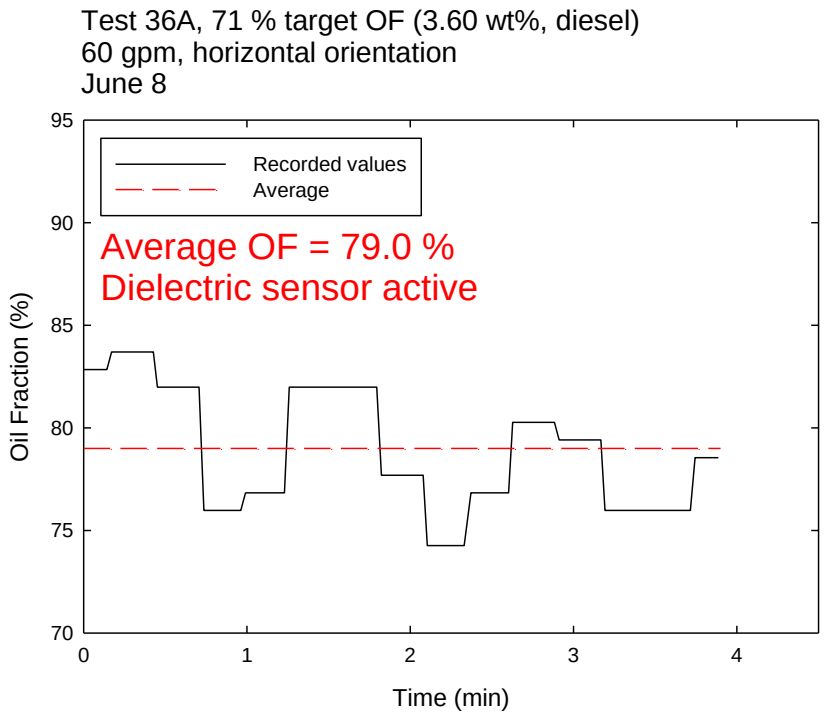

Figure 126. Test 36A - measured oil fraction as a function of time.

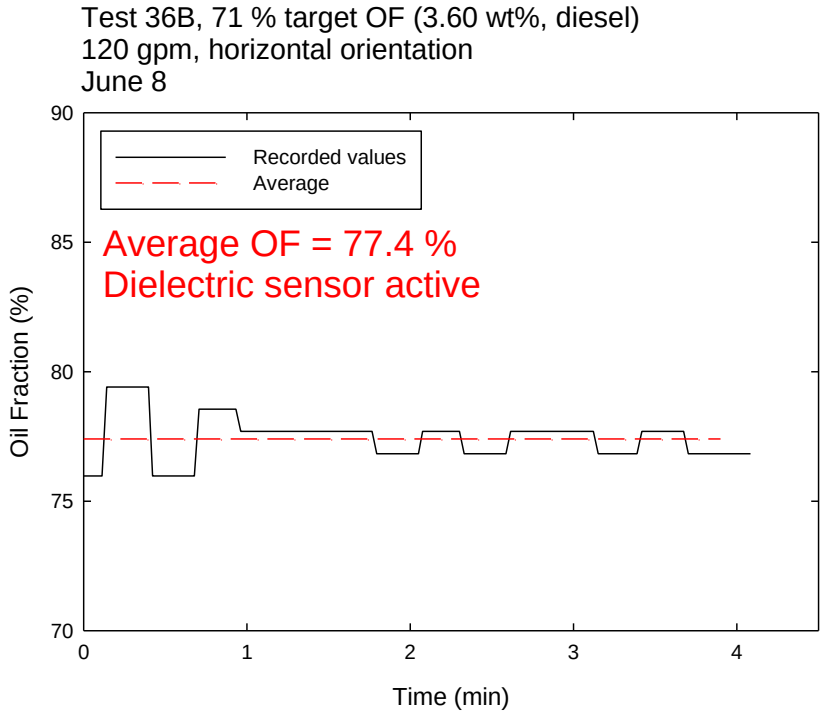

Figure 127. Test 36B - measured oil fraction as a function of time.

10.4.5 Tests where abnormal conditions were observed

In a course of several Ohmsett tests abnormal conditions were noticed. The most common problem entrapped air which was noticed during mixture sampling. One test used insufficient flow to disperse oil introduced into the testing loop. A couple of tests showed significant transient increase of measured oil contend during sample taking. Two tests, 3 and 31, had sufficient problems to justify their elimination from data analysis. Table 13 lists all the tests where abnormal conditions were observed.

Table 13: Tests where abnormal conditions were observed.

Test #	Observations
3	The flow of 60 gpm was not sufficient to disperse oil in the loop. The sensor reads ~ 0% oil. **This data point should be omitted from data analysis.**
9	Entrapped air was noticed dunning sample collection.
15	There was a transient jump of measured oil content from ~40% to ~55%. It coincided with the collection of sample indicating that some pockets of oil in the loop, likely at the bottom of liquid tank. This transient is visible on Figure 87.
31	Very large amount of entrapped air was noticed dunning sample collection. **This data point should be omitted from data analysis.**
31A	Again, large amount of air was noticed during sample collection. Sensor data are not collected during this run.
31B	Reduction of flow caused immediate reduction of measured oil fraction from ~30 % to ~ 16 %. Sensor data collected during this test.
36	Large amount of entrapped air was noticed dunning sample collection.

References

1. United States provisional patent application 62/678,407 filed on May 31, 2018.
2. Becher, P., *Encyclopedia of Emulsion Technology. Volume 1: Basic Theory*. Vol. 1. 1983: Marcel Dekker, Inc.
3. Lissant, K.J., *Demulsification Industrial Applications* 1983: Marcel Dekker, Inc.
4. Wakamatsu, H., *A Dielectric Spectrometer for Liquid Using the Electromagnetic Induction Method.* Hewlett-Packard Journal, 1997. **April 1997**: p. Article 8.
5. Li, Y., et al., *Gas/oil/water flow measurement by electrical capacitance tomography.* Meas. Sci. Technol., 2013. **24**: p. 074001 (12pp).
6. Demori, M., V. Ferrari, and D. Strazza, *A sensor system for oil fraction estimation in a two phase oil-water flow.* Procedia Chemistry, 2009. **1**: p. 1247-1250.
7. Jaworek, A. and A. Krupa, *Gas/liquid ratio measurements by rf resonance capacitance sensor.* Sensors and Actuators A, 2004. **113**: p. 133-139.
8. Jaworek, A. and A. Krupa, *Phase-shift detection for capacitance sensor measuring void fraction in two-phase flow.* Sensors and Actuators A: Physical, 2010. **160**: p. 78-86.
9. Foss, G.C., M.R. Tavares, and R.R. Basham, U.S. 7,201,068 B2, Water cut meter for measurement of water in crude oil. U.S. patent 7,201,068, 2007

10. *Wikipedia - List of bodies of water by salinity.*; Available from: https://en.wikipedia.org/wiki/List_of_bodies_of_water_by_salinity.
11. Ellison, W., et al., *New permittivity measurements of seawater.* Radio Science, 1998. **33**(3): p. 639-648.
12. Demori, M., V. Ferrari, D. Strazza, and P. Poesio, *A capacitive sensor system for the analysis of two-phase flows of oil and conductive water.* Sensors and Actuators A: Physical, 2010. **163**: p. 172-179.
13. Jaworek, A., A. Krupa, and M. Trela, *Capacitance sensor for void fraction measurement in water/steam flows.* Flow Measurement and Instrumentation, 2004. **15**: p. 317-324.

BATTELLE

It can be done